GROUNDBASED AND SPACECRAFT STUDIES OF JUPITER AT DECAMETER AND HECTOMETER WAVELENGTHS

By

MICHAEL DANIEL DESCH

A DISSERTATION PRESENTED TO THE GRADUATE COUNCIL
OF THE UNIVERSITY OF FLORIDA
IN PARTIAL FULFILLMENT OF THE REQUIREMENTS FOR THE
DEGREE OF DOCTOR OF PHILOSOPHY

UNIVERSITY OF FLORIDA
1976

To the family, of course.

ACKNOWLEDGMENTS

I WISH TO EXPRESS my deepest gratitude to Thomas D. Carr, my research advisor, for his guidance and patience and particularly for his having entrusted to me, time and again, the responsibilities of a research scholar. I have benefited in many ways as his student.

I am also grateful to Alex G. Smith, George R. Lebo, Kwan-Yu Chen, and Charles F. Hooper Jr. for having served as my Supervisory Committee and for offering instruction, advice, and council at various stages of my career. I appreciate the kindness with which Stephen T. Gottesman and Frank B. Wood also served in this capacity.

The hospitality shown by the Goddard Space Flight Center personnel during numerous visits to Greenbelt was very much appreciated. In particular, I owe much to Joseph K. Alexander and Michael L. Kaiser, whose scientific and technical expertise in managing the RAE satellite system was indispensable. Likewise, I am grateful for the technical assistance of members of the Astronomy staff of the University. Woody W. Richardson and Hans W. Schrader have helped in data handling and photography. The design and maintenance of the various groundbased installations

was masterfully conducted by Jorge Levy, Richard S. Flagg, and Wesley B. Greenman.

I have benefited, too, from interesting and informative discussions with Richard S. Flagg, Daniel P. McGuire, Michel A. Lynch, Andrew W. Seacord, Dolores S. Krausche, James R. Kennedy, Robert A. Smith, and Robert A. Brown.

I am indebted to Marcia L. Rackley for her thoughtful comments regarding the early manuscript and for her patience and care in reducing much of the RAE microfilm.

I will always be grateful to Denise Frank, both for having expanded my mental horizon and for even believing such a thing was possible.

The manuscript in final form was edited and typed by Roberta Solt. Her attention to detail and devotion to her craft have been a delight.

Financial support for this research has been provided by an NDEA Title IV fellowship, by a University of Florida Graduate School fellowship, by a grant from the National Science Foundation (Principal Investigator Alex G. Smith), and by a grant from the National Aeronautics and Space Administration (Principal Investigator Thomas D. Carr). Computing support was provided by the Goddard Space Flight Center computing facility and by the Northeast Regional Data Center of the State University System of Florida. The generous support of each of the above is gratefully acknowledged.

CONTENTS

Abstract of Dissertation Presented to the Graduate Council
of the University of Florida
in Partial Fulfillment of the Requirements for the
Requirements for the Degree of
Doctor of Philosophy

GROUNDBASED AND SPACECRAFT STUDIES OF JUPITER AT DECAMETER AND HECTOMETER WAVELENGTHS

By

MICHAEL DANIEL DESCH

August 1976

Chairman: Thomas D. Carr
Major Department: Physics and Astronomy

We present a study of the low-frequency Jovian emission. The investigation encompasses the frequency range between 450 kHz and 26.3 MHz and is unique in two respects: (i) At 26.3 MHz an array of 640 dipoles has provided information on a component of the Jovian emission which is three orders of magnitude weaker than that detected with conventional radiometer systems. (ii) Deployment of the earth-orbiting Radio Astronomy Explorer 1 (RAE-1) satellite has made available a window in the radio spectrum which is not generally accessible from the ground. Through refinements in the RAE-1 data-selection process, we have

succeeded in identifying Jovian activity at eight frequencies between 450 and 6550 kHz.

Both the groundbased (array) and spacecraft (RAE-1, V-antenna) systems are described, as are the procedures which were developed to obtain their absolute effective apertures and pointing directions.

Analysis of the data has led to three principal findings: (1) At 26.3 MHz a distinct intensity threshold exists below which statistical dependence of the activity on Io phase (γ_{Io}) disappears; by comparison, the System III (λ_{III}) behavior of the emission is well defined at all flux levels. (2) Io is seen to exert considerable control over the spacecraft-detected emission at frequencies as low as 2200 kHz. Modulation of the emission in the λ_{III} coordinate is insignificant at these frequencies, however, unless the data are intensity weighted. The λ_{III} morphology is thus seen to evolve markedly between 26 MHz and 6550 kHz, whereas Io control is invariant with respect to frequency. (3) Jupiter's power spectrum is found to peak at about 8 MHz with the low-frequency shoulder less sharply inclined than the high-frequency end. The shape of the occurrence probability spectrum of the emission is quite similar to that of the power spectrum.

The Io morphology documented in (1) and (2) is seen at once to challenge the widely held belief, based upon the analysis of data recorded with conventional radiometer systems, that

Io control is a pronounced function of frequency. Specifically, (1) is inconsistent with the distinct tendency for the high-frequency ($\upsilon \gtrsim 25$ MHz) emission to occur over only a very limited range of Io phase, and (2) is inconsistent with the low-frequency ($\upsilon \lesssim 15$ MHz) morphology which exhibits little dependence on γ_{Io}. Re-examination of conventionally recorded 18 and 10 MHz data has led to a uniquely compelling solution to this dilemma. We conclude that (1) and (2) are fundamentally correct, implying that Io control is independent of frequency, at least to first order, from 40 MHz down to 2200 kHz. Further we show that conventional recording of data leads to a specious correlation between Io control and frequency because of a selection effect resulting from a nonuniform intensity sampling of the emission.

The λ_{III} and γ_{Io} morphologies developed herein are examined within the framework of recent theoretical models, several aspects of which we refine in accordance with post-Pioneer concepts of the Jovian magnetosphere.

We conclude by exploring four specific areas of future interest in which theory and experiment may complement and reinforce one another. Relevant and definitive investigations are proposed involving the high-resolution dynamic spectra, Pioneer 10 and 11 data, and several of the experiments to be included onboard the MJS-77 spacecraft.

I

AN OVERVIEW

The solar system consists of the sun,
the planet Jupiter, and some debris.

--Isaac Asimov

IT HAS BEEN CALLED A RENAISSANCE. As grandiloquent as this statement appears, it is nonetheless undeniable that the astronomical community has been virtually transfigured by a large-scale resurgence in planetary studies. The concept of the solar system as a static and inert milieu has been supplanted by one in which the sun and its ever-attendant convoy interact dynamically on many scales in space and time. The solar system is now often thought of as both a microscale astrophysical *and* macroscale biological laboratory, a bubbling cauldron of wave-particle and molecule-molecule interplay. The astrophysical manifestations of these interactions are quite numerous, sometimes startling, and often inexplicable. On the other hand, exobiology has remained largely conjectural, but is no less exciting in its implications for mankind. Definitive *in vitro* experiments on Mars and Jupiter will radically alter its tentative status.

It is of interest to speculate as to the source of this reawakening. Certainly the original suggestions by Urey and subsequent experiments by Miller (1953) provided the foundation for the theoretical analysis of amino acid synthesis in reducing (proto-earth and Jovian) atmospheres. The ambitious Mars-Viking Project owes much to the groundwork established by Urey and Miller. In the physical domain, however, the existence of a single landmark occurrence, similar to that of Urey and Miller's experiments, is less evident. It may in fact be that a single cause is lacking; the present scenario has evolved somewhat slowly. Nevertheless, the development has no doubt been stimulated by various factors, among them the discovery of the Van Allen radiation belts (Van Allen *et al.* 1958), the first discussion of an open (*i.e.* interactive) magnetosphere (Dungey 1961), the verification of the solar wind by Mariner 2 (Neugebauer and Snyder 1962), and of course, the dawn of the space age itself (1957). The reader can no doubt supply several of his own historically significant catalysts depending upon personal bias.

A startling astronomical discovery occurred in 1955, however, which preceded all of the above events. Perhaps occupying that unique historical niche is the serendipitous discovery by Burke and Franklin (1955) of the intense radio emission from Jupiter. In contrast to the solar radio emission (Hey 1946) which had been anticipated as early as 1894 (Lodge 1894), the existence of

nonthermal planetary radiation was entirely unexpected. The accidental, and even belated, nature of the discovery is not at all surprising in view of the conceptual framework within which solar system astronomy was being applied at the time. That framework was shattered in 1955, and the distinction between star and planet had begun to blur.

Since the initial report by Burke and Franklin, the discovery and subsequent explication of many planetary and geophysical phenomena has taken place; but ironically, a completely successful understanding of the Jovian decametric phenomenon is lacking. In the present work various experimental studies have been conducted, both from the ground and via satellite. It is hoped that the convergence of the various emission models toward a single focus will be assisted by the interpretations presented here. Toward this end and in anticipation of the precise motivation of the present work, we present a brief summary of the rich phenomenology and morphology of the Jovian decametric radiation which has accumulated to date. Much more extensive treatments may be found in reviews published by Douglas (1964), Warwick (1967), and by Carr and Gulkis (1969). Carr and Desch (1976) and Smith (1976) have critically reviewed the current posture of the observations and emission models respectively; they have further complemented their discussions with the relevant Pioneer 10 and 11 results.

I-1. JOVIAN DECAMETRIC PHENOMENOLOGY[1]

Jovian "noise storms," as they are called, often last anywhere from a few minutes to several hours, with the storm intensity roughly proportional to the storm duration. Individual storms are separated by periods of time which are entirely devoid of activity; these interludes may last for only a few hours or they may persist, during unusually quiet conditions, for as long as several weeks. Noise storms will often commence and conclude rather abruptly, although the main storm is sometimes preceded by a brief, relatively feeble precursor. The storm intensity itself is always quite irregular, displaying radical amplitude fluctuations in times as short as a few milliseconds or as long as half a minute. The individual intensity fluctuations within a storm are termed bursts and, when ordered according to their durations, are generally observed to be of two distinct classes. The L bursts, which are decidedly the most common, usually vary with periods longer than a few tenths of a second. When monitored aurally, L bursts resemble the sound of waves breaking upon a beach. The S bursts are characterized by much shorter durations, typically between 1 and 50 msec each, creating an

---

[1] With the proper equipment, a single noise storm can reveal nearly all of the phenomenology to be discussed in this section. The "morphology" of the radiation, reviewed in Section I-2, requires the long-term accumulation of data and is thus of a more statistical nature.

unforgettable staccatolike chorus. Repeated transitions between L and S bursts within a single noise storm are not uncommon, and at such times the two types of bursts are sometimes recorded simultaneously.

The gross phenomenology of Jovian noise storms described by the foregoing can be, and indeed has been, gathered by the most modest of radio astronomical procedures. It is thus subject to a plethora of qualifications and refinements to be briefly sketched below. Nevertheless, it is worthwhile bearing in mind that the sporadic nature of Jupiter's noise storms and their inherent unpredictability are among the most characteristic features of the low-frequency radiation.

DYNAMIC SPECTRA

The phenomenology revealed by the dynamic-spectral studies is highly detailed. The early investigations at low resolution first uncovered the frequency drifting of the noise storm envelopes (Warwick 1963). Drift rates, either positive or negative, are usually less than about 1 MHz/min. The sign and to a certain extent the magnitude of the drift are determined predominantly by the Jovian longitude facing the earth at the time of emission (Dulk 1965). Noise storms have been observed to attain a frequency of 39.5 MHz, but then only rarely. As observed from the ground, activity is not usually recorded below about 10 MHz because of the absorbing effect of the earth's

ionosphere. At resolutions exceeding about 0.1 sec and 50 kHz, the structure of the L and S bursts themselves becomes apparent. The L burst emission envelopes, as they appear in the frequency-time plane, are often streaked by tilted, parallel bars which are nearly devoid of activity (Riihimaa 1970). These "modulation lanes" have varying slopes which are dependent upon Jovian longitude, indicating that they are either intrinsic to the emission process or are imposed on the envelopes during propagation through the planet's magnetosphere. On the other hand, as revealed by spaced-receiver studies, the envelopes themselves are apparently generated by drifting inhomogeneities in the solar wind plasma (Douglas and Smith 1967). The implication here is that at least a certain class of the L bursts is intrinsically long enduring, perhaps as long as several minutes, but with the characteristic 1- to 30-sec modulation imposed by interplanetary "obstructions." At still higher resolutions in frequency and time, the S bursts (Figure I-1) begin to display a wealth of structure and potentially a great deal of information. While they occur rather infrequently, the S bursts are of particular interest because they are believed to be manifestations of one of nature's more bizarre phenomena--the Io effect--to be discussed below. A possible hint as to the nature of the mechanism which couples Io to the source region near Jupiter follows from the observation (Ellis 1974) that keV electrons of a specific pitch-angle distribution may be responsible for

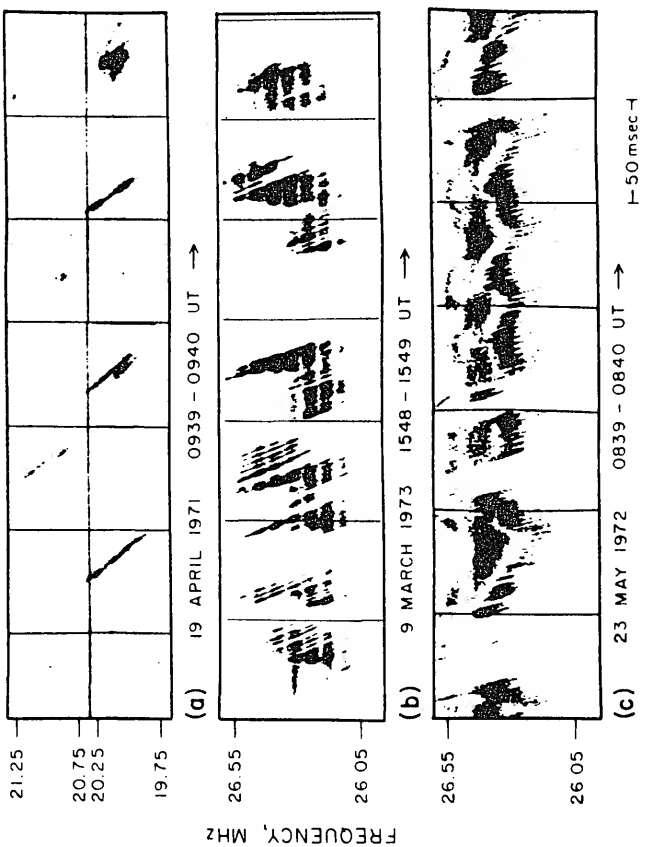

FIGURE I-1. High-Resolution Dynamic Spectra of Jovian S bursts (from Krausche *et al*. 1976).

the generation of the simplest of the S-burst classes (Figure I-1a). Proper interpretation of the more elaborate features displayed by some S bursts (Figure I-1b,c) is a more formidable problem which is just now being undertaken (Flagg *et al.* 1976). It is becoming clear now, however, that the separation of bursts into L and S classes, while appealing in its simplicity, is certainly inadequate.

POWER SPECTRUM OF THE EMISSION

The average power spectrum of the Jovian radio emission is illustrated in Figure I-2. In order to properly compare the sporadic decametric component with the continuous decimetric and thermal components as shown here, Carr *et al.* (1964) computed probability distribution functions for the peak flux densities occurring in consecutive 10-min intervals. In this way a mean power at each frequency in the interval between 10 and 27 MHz was attained. It is of considerable importance to note the extremely steep nature of the decametric portion of the spectrum. Radio emission occurring at 27.6 MHz is over two orders of magnitude less intense than that at 10 MHz. Moreover, if the peak (rather than the mean) flux densities at each frequency are compared, the behavior is quite similar; the spectrum is merely shifted upwards by three orders of magnitude. As will be discussed further in Section I-3, this aspect of the phenomenology is capable of imposing a selection effect upon the data which could improperly bias much of our understanding.

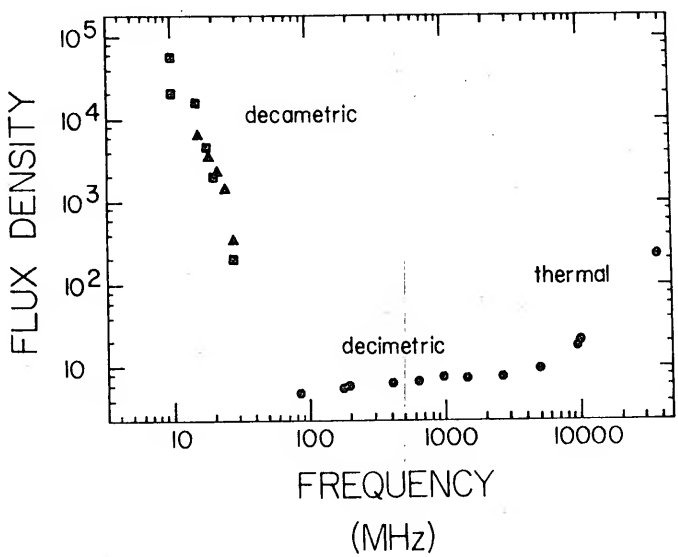

FIGURE I-2. Average Power Spectrum of the Radio Emission from Jupiter Showing the Decametric, Decimetric, and Thermal Components. Flux density is expressed in Jy (10^{-26} $Wm^{-2}Hz^{-1}$). Square points are from Carr *et al.* (1964), triangles from McCulloch and Ellis (1966), and circles from various sources, as quoted by Roberts (1965) and Warwick (1970).

SOURCE LOCATION AND SIZE

The precise location of the Jovian decameter source remains obscure to this day. That it is within the corotating portion of the planet's magnetosphere, that is within about 20 R_J, stems from the consistent repeatability of the dynamic spectral features and from the observed stability of the rotation period. In fact, there is evidence that the source is much closer still, say within 1 to 2 R_J of the planet's center. For example, an appeal for a source radiating at the local gyrofrequency ensues from the near coincidence of the maximum observed frequency of the noise storms (39.5 MHz) and the peak gyrofrequency at Jupiter's high-latitude cloud tops as derived from the *in situ* measurements of Pioneer 11. Gyrofrequency emission in the 10 to 40 MHz range, then, would all take place within a source region not exceeding a distance of about 1.7 R_J from the planet's center.

While the arguments for the source location are somewhat heuristic, limits on the size of the source itself have been obtained by more direct procedures, namely from the aforementioned S burst dynamic spectra and from very long baseline interferometry (Lynch 1972). Both methods have emphasized the imponderably small linear dimensions of the source, estimated between 50 and 300 km. This is particularly striking in view of the fact that the decametric radiation, while quite comparable to solar Type III activity both in character and intensity, originates from a source region three to four orders of magnitude

smaller in size than that of its solar counterpart! The extreme brightness temperature so imposed on this small emitting region implies that a highly efficient, induced (as opposed to spontaneous), coherent plasma process is taking place. This assumption has provided a conceptual basis upon which nearly all of the more recent decametric theories have evolved.

Besides requiring a coherent process, it has been common to assume further that the radiation is generated near the local gyrofrequency. Observations of the polarization characteristics of the waves have lent credence to this latter assumption.

POLARIZATION MEASUREMENTS

At frequencies above about 18 MHz the radiation is predominantly right-hand elliptically polarized. Careful examination of the magnetoionic theory of waves propagating in a magnetoplasma reveals that eliptical polarization is characteristic of radiation generated *near* the local electron gyrofrequency. How near depends to a large extent upon the ratio of the plasma density to the magnetic field strength at the point of emission. Strict limitations cannot be established at present; however, gyroemission appears to be a relatively safe working assumption in view of the near coincidence of the maximum observed frequency and the electron gyrofrequency corresponding to the field strength measurements. The predominance of the right-hand sense implies further that the radiation propagates in a

direction for which the field has a parallel rather than an antiparallel component, assuming the extraordinary base mode. The implication is that the source of the right-hand polarized radiation lies in Jupiter's northern hemisphere.

At frequencies below about 18 MHz the radiation can be left-hand or right-hand polarized, depending upon central meridian longitude, and can be circularly polarized (Kennedy 1969). Whether this is a propagation or emission dependent phenomenon has not been ascertained.

I-2. JOVIAN DECAMETRIC MORPHOLOGY

ROTATION PHASE AND IO PHASE DEPENDENCE

The long-term accumulation of Jupiter data has revealed that there are distinct occurrence probability increases during times when particular Jovian longitudes are facing the earth. It was observed (Douglas 1961) that the occurrence probability peaks were maximized when the activity was plotted as a function of the System III longitude (λ_{III}, 1957.0), corresponding to a rotation period of $9^h\ 55^m\ 29.^s37$; presumably this is approximately the rotation period of the magnetic field and hence, according to more recent theories, of the metallic hydrogen core of the planet. The discovery by Bigg (1964) that these specific longitude regions or "sources" are further enhanced, both with respect to the probability of their occurrence and overall intensity, when Jupiter's innermost Galilean Satellite, Io, is

in particular locations of its orbit, was one of the more important astrophysical discoveries of the past several decades. Order of magnitude increases in the occurrence probability are noted when γ_{Io} (departure of Io from superior geocentric conjunction) is equal to approximately 90^{o} or 240^{o}. A representative plot showing the locations and designations of these sources in the λ_{III}- γ_{Io} plane appears in Figure I-3. In addition to being classified as Io-related or non-Io-related, each source possesses distinguishing characteristics which are summarized in Table I-1. It is notable that the S burst activity discussed earlier is generally only associated with the Io-related sources.

LONG-TERM EFFECTS

Following a decade of continuous monitoring of the planet, it became evident that the position of Source A was drifting with respect to the System III longitude defined above. With the adoption of a revised rotation period (Gulkis and Carr 1966), this systematic drift of Source A toward higher longitudes was converted into a periodic oscillation of the source centroid about a mean value. The long-term drift had been removed. The period of the oscillation appeared to be more closely aligned with Jupiter's orbital period of 11.9 yr rather than with the approximate 11-yr semiperiod of the solar cycle. This orbital-period oscillation also manifests itself as a periodic

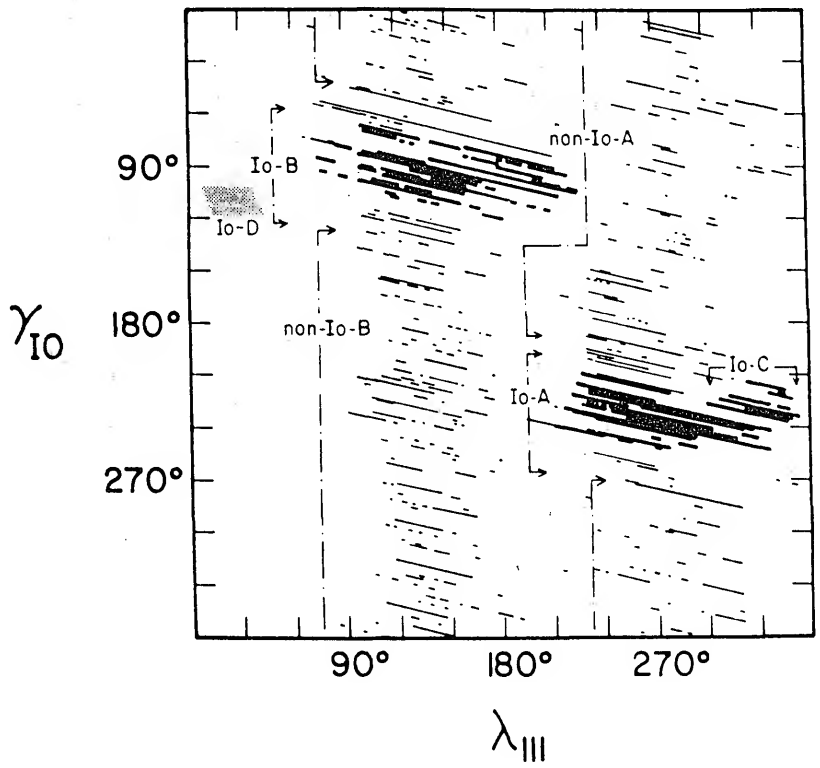

FIGURE I-3. Representative Plot in the $\lambda_{III} - \gamma_{Io}$ Plane of the Generally Recognized Jovian Sources. Each line traces the instantaneous $\gamma_{III} - \lambda_{Io}$ phase during a single storm. Heavy lines indicate activity exceeding 6 x 10^5 Jy.

TABLE I-1. Some Characteristics of the Jovian Source Regions at the Upper Frequencies.

Designation	λ_{III} (1965) Span[a] (Degrees)	γ_{Io} Span[a] (Degrees)	Frequency Range (MHz)	Predominant Polarization Sense	Other Characteristics
Io-A	195-285	220-260	14-36	RH	Often obscured by non-Io-A during years of positive D_E L bursts; S uncertain.
Non-Io-A	195-285	0-360	11-28	RH	Highest occurrence probability of all sources, for frequencies between 15 and 25 MHz and during years of positive D_E. Greatest change in source position, width, and occurrence probability with change in D_E. L bursts only.
Io-B	95-195	65-110	11-39.5	RH	Highest intensity bursts (both L and S). Principal S-burst source. Most predictable source. Bifurcation apparent in high-resolution histograms.
Non-Io-B	95-195	0-360	at least 16-26	Probably RH	Very weak, but relatively high occurrence probability. L bursts; S uncertain.
Io-C	285-5	220-260	11-26	LH (at least below 23 MHz)	Predictable. Other major S-burst source (also L bursts).
Non-Io-C	285-5	0-360	at least 16-26	Mixed	Moderately distinct from non-Io-A. Abundance of LH polarized emission relative to non-Io-A may be distinguishing characteristic. Probably L bursts only.

TABLE 1-1, continued:

Designation	λ_{III} (1965) Span[a] (Degrees)	γ_{Io} Span[a] (Degrees)	Frequency Range (MHz)	Predominant Polarization Sense	Other Characteristics
Io-D	20-95	95-115	11-18	LH	Very low occurrence probability. Characteristic dynamic spectrum and LH polarization sense important in identification.

[a]Between approximately 15 and 25 MHz.

variation in the overall occurrence probability of Source A. Both effects are in phase and are consistent with a model (Carr 1972) which depends upon the changing viewing geometry in the ecliptic plane between the earth and Jupiter. The parameter describing this geometry is called D_E (Jovicentric declination of the earth), and the maximum excursion in either direction north or south is only $3^{o}.5$. As remarkable as it seems that such a small angular deviation can have readily noticeable effects, it is perhaps to be expected in view of the narrow-beaming properties of coherently radiated emission.

Additional D_E-dependent phenomena have been found, notably the variations in source centroid positions with respect to the γ_{Io} coordinate (Conseil 1972; Lecacheux 1974; Thieman *et al.* 1975). It now appears that the Io-related source centroids vary both in the λ_{III} *and* γ_{Io} coordinates. One might anticipate that the λ_{III} and γ_{Io} variations would be related so as to effectively minimize any changes in the sub-Io longitude (λ_{Io}) on Jupiter which presumably stimulates the emission. This is not so. Surprisingly, source positions with respect to λ_{Io} change radically, increasing by as much as 15^{o} (for the Io-B source) as D_E changes from 0^{o} to 3.5^{o}. Even purely geometrical explanations of such viewing-angle phenomena are complicated by the magnetic field models of Jupiter's intricate surface field, now emerging from analyses of the Pioneer 11 data (Acuna and Ness 1975; Smith *et al.* 1975). Observations of the emission made by spacecraft

well out of the ecliptic plane will surely be revealing in this regard.

JUPITER'S ROTATION PERIOD

As implied by the above, if the apparition-by-apparition histograms are plotted in the old (Epoch 1957.0) System III, the observed drift of Source A may be used to calculate the rotation-rate error effecting the drift. This is applied as a correction to the old period to obtain a new rotation period which, as mentioned above, insures the absence of long-term drifts. In calculating the error, histograms are chosen which are separated by approximately 12 yr to remove any bias in the source centroids due to D_E modulations.

The Jovian rotation period may also be determined by using sophisticated power spectral techniques (Kaiser and Alexander 1972). Both methods, though, have resulted in similar values, the average of these and several other methods yielding an agreed-upon figure for the rotation rate of $870^{\circ}.536$ per ephemeris day. This figure, designated System III (Epoch 1965), will soon be adopted officially by the IAU. The corresponding rotation period is $9^h\ 55^m\ 29^s.71$, which should be used when analyzing data spanning more than a few years time if consistent results are desired. In the present work the old System III (1957.0) will be used, as detailed features in the λ_{III} coordinate will not be examined and the data do not span

long periods of time. Where confusion might arise, however, differences in source locations between the two systems will be specified. For example, comparisons between source locations as appearing in Table I-1 (Epoch 1965) and sources discussed in the present work (Epoch 1957.0) may be made through the simple application of the formula

$$\lambda_{III}\ (1965) = \lambda_{III}\ (1957.0) - 0.008284\ \Delta t \qquad \text{(I-1)}$$

where $\Delta t = \tau - 2438761.5$ and τ = epoch of date (JD).

I-3. PRINCIPAL MOTIVATIONS FOR CONDUCTING THIS STUDY

GROUNDBASED OBSERVATIONS

Nearly all of the observations of Jupiter's decametric emission have been made with low-gain Yagi antenna systems. The version of the Yagi monitoring system which consists of a two-element interferometer is probably the most sensitive Yagi radiometer currently being employed in the synoptic monitoring of the planet. Typical sensitivities (minimum flux density necessary for the positive identification of Jovian activity) have been quoted in the literature. Estimates range from 10^4 to 10^5 Jy (Jy = 10^{-26} Wm^{-2} Hz^{-1}) at frequencies in the 10 to 30 MHz range (Bozyan *et al.* 1972; Alexander *et al.* 1975*a*). Notwithstanding the fact that much of the Jovian emission which occurs is orders of magnitude more intense than this, one must consider

what morphological changes in the emission might become apparent under conditions of greatly increased sensitivity. Such high-gain monitoring should be carried out at a relatively high decametric frequency for a number of reasons. The large antenna arrays necessary for highly sensitive monitoring become prohibitively large and expensive as the frequency decreases; thus, the first reason for choosing a high decametric frequency is purely a pragmatic one. A more important justification, however, stems from the observation that the Jovian decametric flux spectrum falls off extremely sharply at frequencies above about 10 MHz (see Figure I-2). A uniform sampling of the radiation as a function of frequency would therefore demand conformity of the flux threshold of a given radiometer system with the flux spectrum of the emission itself. Hence, a statistically uniform sampling is assured only when, for example, monitoring at high frequencies is conducted with extremely high gain systems. This has not been the case. Synoptic monitoring has been carried out with antennas of relatively uniform sensitivity in comparison with the 2.5 order of magnitude decrease in the peak intensity of the radiation which prevails between 10 and 27 MHz.

Clearly, the elimination of the selection effects embodied in the synoptic monitoring heretofore is of vital importance. For this reason a program was established for the purpose of continuously monitoring the planet at 26.3 MHz using a highly

directive array. The phase and gain calibration of the radiometer system and the subsequent analysis of the data are described in this dissertation.

SPACECRAFT OBSERVATIONS

Because of the opacity of the earth's ionosphere, it becomes increasingly difficult to do radio astronomy as observations are extended to frequencies below about 10 MHz. This situation improved significantly after the launching into earth orbit of the Radio Astronomy Explorer (RAE-1) satellite in 1968. Operating in the frequency range between 0.5 and 9.2 MHz, the minimum frequency at which effective monitoring could take place had been reduced by at least several octaves. However, while the galactic background radiation and bursts of solar origin were studied intensively (Alexander and Novaco 1974; Fainberg and Stone 1974), the identification of the low-frequency Jovian emission remained elusive.

In order to establish the existence, or lack thereof, of Jovian emission over the RAE-1 frequency domain, we initiated a program designed, at the very least, to fix upper limits on the flux densities as a function of RAE-1 frequency. The study was anticipated to be of considerable value as many of the RAE-1 receiver channels covered frequencies at which Jupiter either had never been detected or had only been tentatively identified from the ground. The requisite elements of such a study

necessarily include (i) the optimum presentation of the satellite data for inspection and analysis, (ii) the isolation of periods of time relatively free from known sources of interference, (iii) the determination of radiometer sensitivity as a function of frequency, and (iv) either the establishment of the aforementioned upper limits or the presentation of the morphological features of the designated Jupiter activity. These elements are fully discussed in the following pages.

Although the experiments described here are being conducted at virtually opposite ends of Jupiter's low-frequency spectrum, we will examine the spacecraft-derived results in the framework of the morphology derived at 26.3 MHz to determine whether a self-consistent explanation of the various phenomena is possible.

II

THE INSTRUMENTATION

One reliable observation is worth a thousand models and a million speculations. --H. E. Landsberg

II-1. THE 26.3 MHz ARRAY

Located at the University of Florida Radio Observatory (UFRO) is one of the largest, filled aperture, low-frequency antenna arrays in the world. Approximately one half of the 640 half-wave dipoles comprising the array are visible in Figure II-1. It operates at a frequency of 26.3 MHz (λ = 11.4 m) and has an effective bandwidth of about 0.5 MHz. The individual dipoles are oriented east-west (ew), and they fill a rectangle, the major axis of which is oriented north-south (ns). The rectangular collecting area of the 26.3 MHz array (referred to hereafter as simply the "array") has an ew by ns extent of 16 by 40 dipoles. Since the dipoles are separated from one another by 0.6 λ in both the ew and ns directions, this corresponds to a perimeter of 9.0 λ by 23.4 λ. The principal lobe half-power beamwidth (HPBW) of the antenna is approximately $6\overset{\circ}{.}0$ ew by $2\overset{\circ}{.}5$ ns.

FIGURE II-1. A View Facing North of the 640-Element Dipole Array Located at the University of Florida Radio Observatory. The small white box is being opened by graduate assistants in order to make a coarse north-south (CNS) phase adjustment. The large white houses contain the Butler matrix networks.

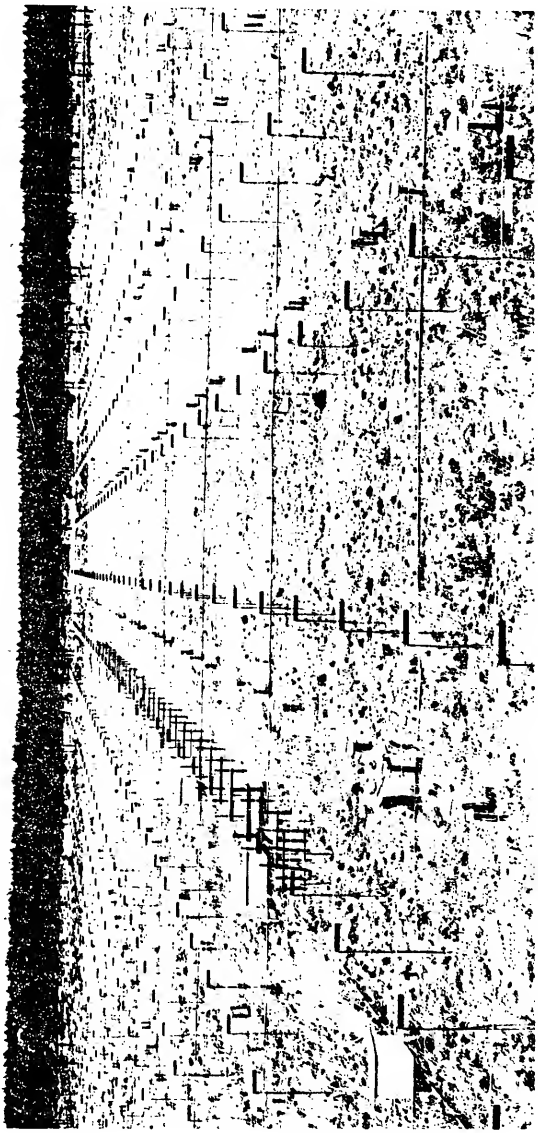

Tracking of sources across the sky is achieved by means of Butler matrix phasing (Butler 1966). The Butler matrix is a fairly complex network of hybrid rings which is capable of synthesizing a number of independent antenna beams equal (in the most efficient case) to the number of independent inputs. The 16-port (8 input, 8 output) Butler matrices employed in the array system (see Figure II-2) generate eight independent beams in the ew plane, each beam separated by 6^{o}. The beams intersect at the -4 db points. They are stepped through sequentially from east to west at approximately 26-min intervals as the source drifts across the sky. This permits about 3.4 hours of monitoring of a given source at one time.

A group of eight (2 ew by 4 ns) dipoles (see Figure II-3) is organized into a single subunit of phasing. Eight of these subunits, organized in the ew direction, supply the required eight inputs to the ew Butler matrix. The synthesis of these eight subunits by the Butler matrix results in a single main phasing unit comprised of 64 (16 ew by 4 ns) dipoles. A total of 10 ew Butler matrices (aligned ns) are required to control the array's complement of 640 dipoles.

A limited amount of adjustment of the position of the main beam in the ns plane is necessary during each step to a new ew Butler matrix output. This is accomplished by two (5 input, 8 output) ns Butler matrices, one for each ns half of the array. They are identical in design to the ew Butler matrices except

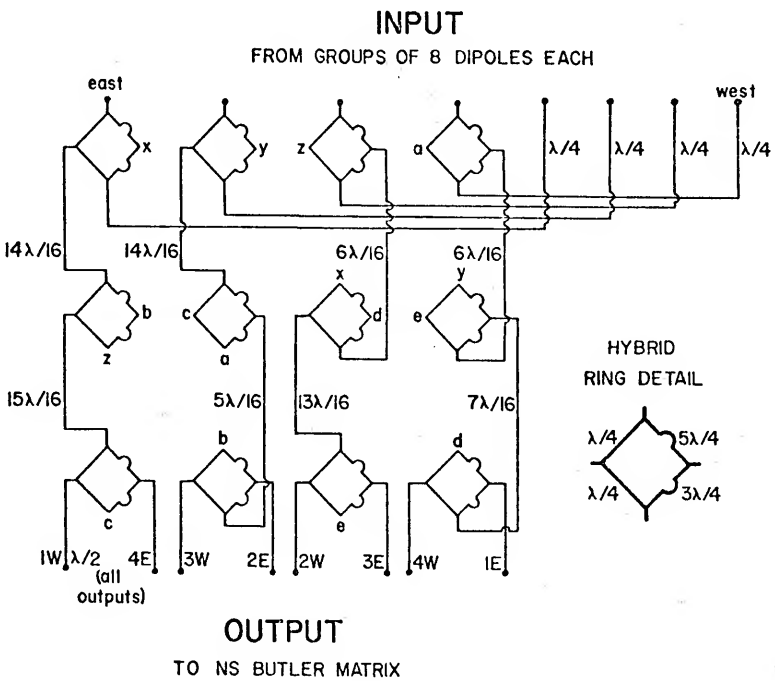

FIGURE II-2. Schematic of the Butler Matrix Circuitry. Similarly lettered junctions on the hybrid rings are connected directly together. The hybrid rings are constructed of 75 ohm, RG59 coaxial cable. The cables connecting the rings are 50 ohm, RG58. Each network, of which there are 10 for ew phasing and 2 for ns phasing, is enclosed in its own housing or "Butler matrix box." The control relays associated with the networks are also enclosed. In Figure II-1 the Butler matrix boxes are the dog-house sized structures running ns along the center of the array.

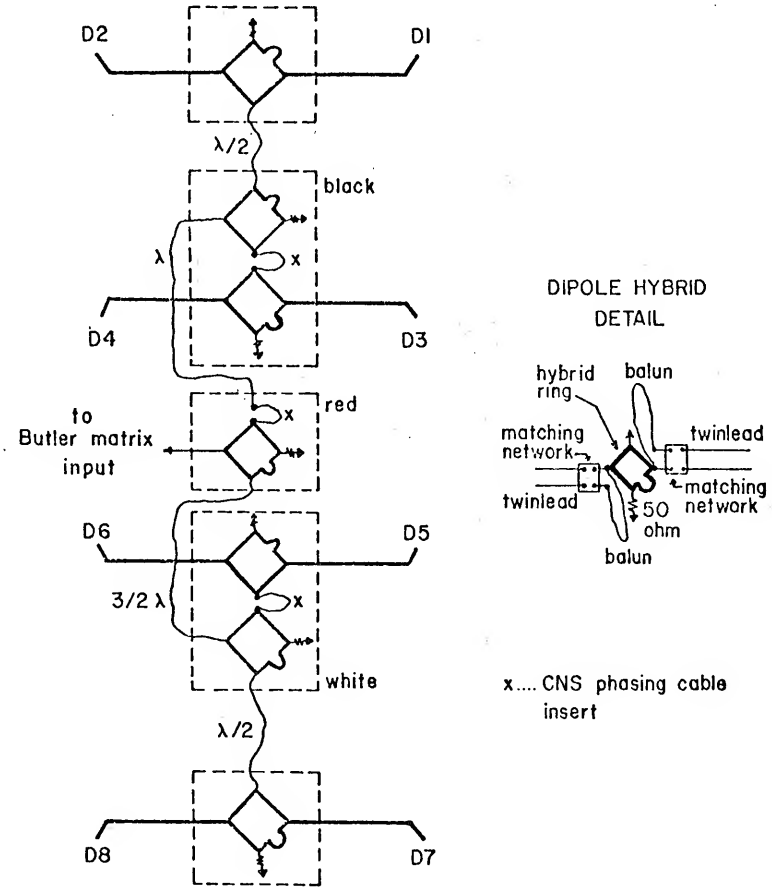

FIGURE III-3. Schematic of a Group of 8 Dipoles Constituting the Basic Subunit of Phasing of the Array. The dipoles, numbered D1 through D8, are not shown. The matching of two balanced, 78-ohm dipoles into the unbalanced, 50-ohm (RG58) coaxial cables (which connect the hybrid rings together) is accomplished by means of a matching network-balun-hybrid ring assembly (see detail in figure). Each assembly is enclosed in a small box, three of which are color coded for CNS phasing identification. The boxes are connected together by means of underground cable indicated in the figure by light wiggly lines.

that three of the inputs are terminated in 50-ohm loads. Three of the eight outputs of each ns Butler matrix are monitored at any given time. They are separated by about $2^{o}.6$ in the ns plane. The central beam is maintained on the source, and the two adjacent beams are used for the purpose of discriminating against interference. The signal from the entire array is finally arrived at by combining the outputs from the two ns Butler matrices through a hybrid ring unit containing a variable phase delay. There is one such unit for each of the three beams. The foregoing phasing hierarchy is illustrated schematically in Figure II-4.

While hour angle coverage is limited to within ± 1.75 hours of meridian transit, sky coverage is complete in terms of the declinations observable at $+30^{o}$ latitude (-60^{o} to $+90^{o}$). However, because the ns HPBW of a 64-dipole phasing unit is only about 24^{o}, sky coverage in the ns plane would be restricted to this narrow range if ns phasing between individual dipoles were not implemented. To obtain total sky coverage, then, the beam is phased in steps of about 12^{o} by means of manually inserted, plug-in phasing cables (see Figure II-2). This is referred to as coarse north-south (CNS) phasing and is required whenever a change in position of the beam by more than about 20^{o} in the ns plane is desired.

Combining the output of five ew Butler matrices at a ns Butler matrix results in a beam which is narrow enough in the

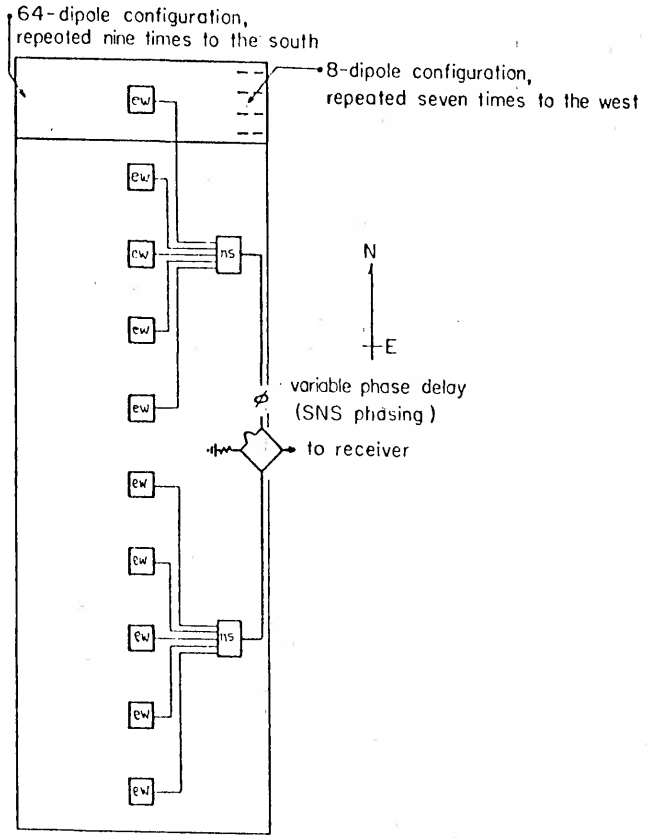

FIGURE II-4. The Array Phasing Hierarchy is Shown. Each ew Butler matrix (designated ew) is fed by the outputs from eight groups of 8 dipoles each. The two ns Butler matrices (designated ns) are each fed from the outputs of five groups of 64 dipoles each. The final signal is arrived at by combining the output from each ns Butler matrix through a single hybrid ring, whereupon the signal is amplified in the field and fed into the observatory receivers through aluminum coaxial cables (see Appendix A).

ns plane (5^{o} HPBW) that further phasing is required for each ew Butler matrix step, as mentioned previously. This fine north-south (FNS) phasing is performed automatically by the ns Butler matrices in 3^{o} increments. The final ns phasing adjustment (SNS) is made by the hybrid ring unit containing the variable phase delay mentioned above. SNS values must be converted to a rotary-switch-position (RSP) integer before being used. SNS increments are $0^{o}.6$ each. The proper delay lengths to be used for CNS, FNS, and SNS (RSP) phasing, which are each a function of source declination and ew beam position, are preselected by the observer, based on numbers tabulated in the "Phase Tracking Parameters" (PTP) booklet (Desch 1972), which is maintained at the observatory.

The signals from the three ns beams are amplified in the field by separate preamplifiers before being sent through 350 meters of shielded aluminum cable to the observatory. The noise temperature of the preamps is approximately 600 K. Because of the severe amount of loss in the shielded coaxial cables, comprising both the Butler matrices and all of the phasing and transmission paths, the galactic background temperature, as measured at the input to the field preamps, is comparable to the preamp noise temperature itself. Considerable enhancement in the signal to noise ratio is anticipated through the installation of ten additional preamps in order to increase the signal from the ew Butler matrix outputs. The present sensitivity

of the array is about 50 Jy for sources near the zenith. A factor of two improvement is expected.

In the observatory the signals from the three ns beams are total power, diode detected by identical 250 kHz bandwidth receivers. The integrated outputs are then recorded on paper or magnetic tape. Specifically, the Jupiter data taken in this analysis have been simultaneously recorded on both high and low dynamic range chart recorders. Individual events ranging from about 0.1 db (50 Jy) to nearly 27 db ($>10^6$ Jy) above the galactic background have been studied.

II-2. RECORDING AND PREPARATION OF ARRAY DATA FOR ANALYSIS

Conditions permitting, the array is operated and observations are made beginning about 2 hours before and extending for about 2 hours after each Jovian meridian transit. Because it has been possible to extend the monitoring program well into the daylight hours (during that portion of the apparition when Jupiter is near conjunction), a large fraction of each 13-month apparition is observable.

The receiver outputs are recorded on paper, using a post-detection time constant of 1 sec. The chart recorders are operated at speeds sufficient to specify listening and activity times to within $\pm$30 sec. Calibration steps are manually placed on the recordings before and after each observing session (see Appendix A). An observer is always present to aid in the aural

identification of suspected activity; however, the segregation of Jupiter activity from interference is ultimately made on the basis of the relative deflections in the three channels described in Section II-1. For example, because station and lightning interference generally propagate toward the ground from a large (larger than 10^{o} by 10^{o}) area of the sky, they will appear with approximately equal intensity in all three channels. On the other hand, Jupiter activity appears only in the main channel, that is the channel which monitors the source-centered antenna beam. Because much of the weaker activity is completely inaudible, the three-channel identifications are not only helpful but in fact indispensable. The accuracy with which the array's system of beams is pointed is discussed in Section III-1.

All data were reduced by the author, by noting the beginning and ending times of the observing and activity intervals. Periods of excessive interference were not counted as acceptable listening times. The actual beginning and ending times of Jupiter activity were recorded, as opposed to the conventional Florida method (Register 1968) of noting the presence or absence of activity in consecutive 5-min blocks. The single most intense segment of each uninterrupted activity interval was noted and scaled as to its peak and galactic-background calibration levels. These values were converted into flux density and normalized to a standard distance of 4 AU by means

of the gain-calibration results presented in Section III-2. Finally, a character figure was assigned to each interval of activity depending upon whether it displayed primarily S-, L-, or scintillation- (single bursts enduring for more than 30 sec) type emission. All of the foregoing information was stored on IBM cards. Approximately 500 cards (designated the raw data deck) were necessary to compile the above information for a single apparition. By means of Jupiter ephemeris data, the raw data were converted via the IBM 370 computer into an "intermediate" data deck (see Table II-1). The latter contains the radio longitudes (λ_{III}) and satellite positions for the beginning and ending times of the observing and activity periods. Also stored on the intermediate deck cards were the peak flux density and character figure for each storm. Resolution in both the λ_{III} and satellite coordinates is 1^{o}.

II-3. THE RAE-1 SATELLITE

The launching of the Radio Astronomy Explorer 1 satellite (Explorer 38) on 4 July 1968 marked the culmination of nearly a decade of investigation into the feasibility of making low-frequency radio astronomical observations from above the terrestrial ionosphere. The sounding rocket and satellite experiments which preceded the RAE contributed immensely to the development of a radiometer system which could function satisfactorily in an ionized medium and be mechanically stable in

TABLE II-1. Array Intermediate Deck Card.

IBM Card Space	*D a t a*
01-04	Station code 'F26A'
05-10	Year, month, day in format YYMDD
11-15	Julian date (Florida convention)
16-18	Begin listening λ_{III}, 1^{o} resolution
19-21	End listening λ_{III}, 1^{o} resolution
22-24	Begin activity λ_{III}, 1^{o} resolution
25-27	End activity λ_{III}, 1^{o} resolution
28-39	Same for Io (departure from superior conjunction)
40-51	Same for Europa
52-63	Same for Ganymede
64-66	Activity time in minutes
67-73	Peak flux density of activity interval in Jy
78	Character code: 1--S burst, 2--L burst, 3--scintillation
79	Credibility code: 1--certain, 2--probable, 3--possible
80	Coordinate system code: 0--geocentric, 1--heliocentric

spite of the antenna dimensions required for adequate spatial resolution at very long wavelengths. As such, RAE-1 became the first satellite devoted solely to radio astronomical studies. The following is a brief description of the orbital characteristics, radiometer system, and data managing technique incorporated in the final spacecraft design. The information has been derived primarily from Alexander (1970) and from Weber *et al.* (1971), who are members of the Goddard Space Flight Center staff and who have worked with the RAE design from its inception. Much of the information applies equally well to the RAE-2 satellite which is now in lunar orbit.

RAE-1 orbits in the retrograde sense at an altitude of 6,000 km (1.94 R_E from the earth's center). The orbit is nearly circular, having an eccentricity of less than 0.002 and a period of 224 min. It is inclined at an angle of 60^o to the equator and precesses at a rate of $0^o.52$ per day. The spacecraft altitude was confined to a certain range of values by the available launch vehicles. Within this range the altitude chosen was a compromise between the desirability of a relatively high altitude (low plasma density) orbit and a lower altitude orbit necessary for adequate stability of the antenna structure. This stability is derived from the gradient of the gravitational force across the 460 m extent of the satellite and is sufficient at 1.94 R_E to maintain the major axis of the antenna structure parallel to the local gravity vector. At the

altitude chosen, the *in situ* plasma frequencies range from about 200 to 600 kHz.

The traveling-wave V-antennas, shown in Figure II-5, constitute the primary antenna system on the RAE. Each boom is 229 m long with a 60^{o} apex angle. As mentioned, gravity gradient forces maintain the upper-V directed at the local zenith and the lower-V at the subsatellite point. The antennas were stored on motorized spools during launch and deployed in orbit. Analysis of pictures obtained from television cameras located on the satellite have verified the positioning of the booms and their relative freedom from oscillation ($\leq 3^{o}$). A 600-ohm resistor in each boom, located three fourths of the distance from the apex of the V, establishes the frequencies at which the antenna is correctly terminated to allow traveling waves to exist. This condition is satisfied at frequencies equal to 9.18, 6.55, 4.70, 3.93, 2.20, and 1.31 MHz, that is, when the section of the antenna beyond the resistor is an integral number of quarter wavelengths. At the frequencies for which the end section is an odd multiple of quarter wavelengths (6.55, 3.93, and 1.31 MHz), a front-to-back ratio exceeding 10 db is achieved. The calculated E- and H-plane antenna patterns for this ideal case are shown in Figure II-6. For the three satellite frequencies which are less than 1.31 MHz (0.90, 0.70, and 0.45 MHz) the antenna is shorter than one wavelength and hence has the isotropic reception pattern of a short dipole. The

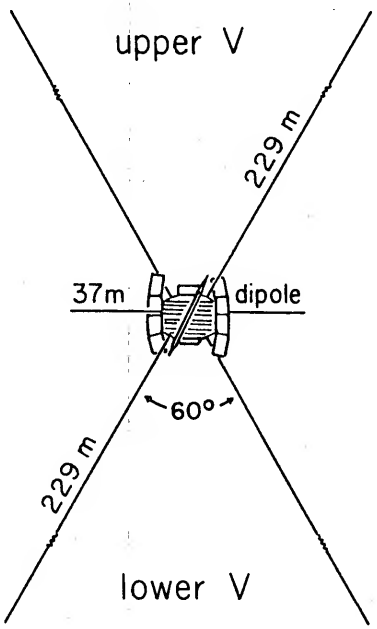

FIGURE II-5. A Drawing (Not to Scale) Showing the RAE Antenna Configuration. The dipole and V antennas all lie in the orbital plane of the satellite, with the 37 m dipole tangent to the satellite's instantaneous velocity vector.

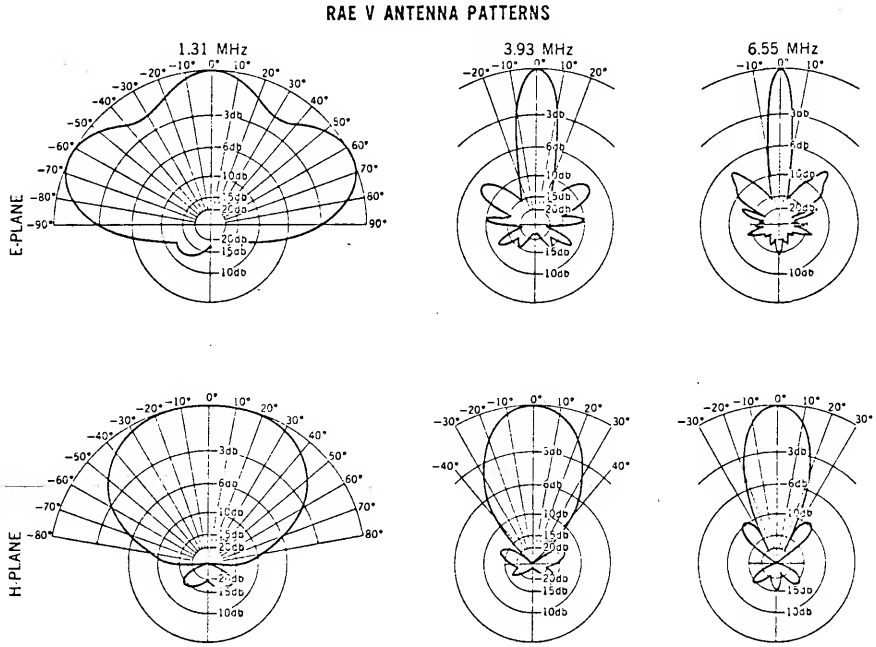

FIGURE II-6. The Calculated E- and H-Plane Antenna Patterns at Three Frequencies are Shown. (After Weber *et al.* 1971.) The E plane lies in the orbital plane of the satellite. The H plane is perpendicular to the E plane.

upper-V/lower-V antenna configuration permits discrimination between celestial and terrestrial noise since the signals from each are recorded separately. The orbital characteristics allow the upper-V to map the entire sky between $\pm 60^{o}$ declination in about one year.

Because of its relatively high directivity, the V-antenna is useful for detecting low intensity phenomena; however, the absolute gain of the system is not known to any great accuracy. For this reason, a 37-m dipole was included on the satellite since the radiation characteristics of the dipole antenna are well known. This allows for greater precision in terms of absolute flux density and brightness measurements. The dipole and V-antennas all lie in the orbital plane of the satellite.

Ryle-Vonberg (RV) receivers are connected to all three of the antenna systems mentioned above. The long-term stability and insensitivity to gain and bandwidth changes inherent in the RV radiometer was a determining factor in its selection as the principal receiver system. The effective bandwidth of the receiver is 40 kHz with a postdetection time constant of 0.1 sec. The preamplifier noise temperature is about three orders of magnitude less than the galactic background temperature of 10^{6} K. All nine frequency channels between 9.18 and 0.45 MHz are stepped through in 72 sec. Additional instrumentation exists in the form of a fast time response, total power receiver on the dipole and lower-V antennas. Designated "burst

radiometer" (BR), it is especially useful in generating dynamic spectra of the intense Type III solar bursts.

The spacecraft system was originally designed to record all data on magnetic tape to be played back to ground stations at a 25:1 speed-up. Because of a recorder malfunction after 2 months in orbit, however, data had to be telemetered to ground stations in real time. In spite of this, only 5% and 10% of the data were lost during the first and second years of operation, respectively. The raw data tapes are then edited by ground personnel and the recorded voltages are transformed into antenna temperatures by means of prelaunch calibration curves. The final tape recordings containing the antenna temperatures and all of the necessary orbital information are then ready for computer processing and analysis.

II-4. INITIAL SELECTION AND REDUCTION OF THE RAE-1 DATA

Although it was launched in July of 1968, the initial orbital characteristics of the RAE-1 were such that observations of Jupiter were not possible for the first 6 months of the satellite's operation. As indicated in Figure II-7, a single RAE-1 orbit permits the upper-V to view only a portion of the sky between $\pm 60^{\circ}$ declination. However, observations over the same declination range, but at successively increasing right ascensions, are achieved through precession of the orbital plane of the satellite at the rate of 2 min of right ascension

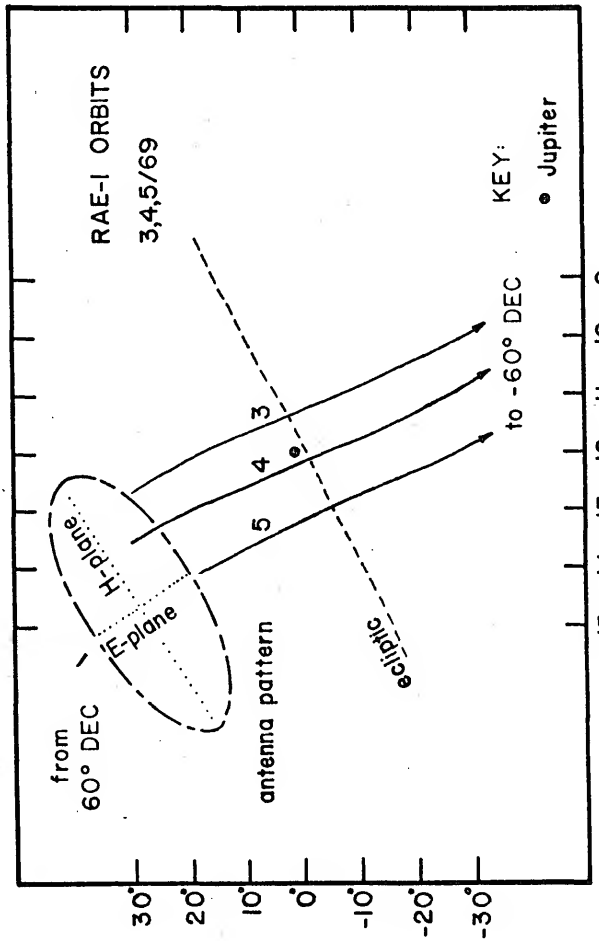

FIGURE II-7. Three Orbits of the RAE-1 Satellite on 1 Mar, 1 Apr, and 1 May 1969 Are Shown Projected onto a Portion of the Celestial Sphere. The 6550 kHz upper-V antenna pattern (to HPBW) is also illustrated as it would appear projected onto the sky. The eastward motion of the orbit is accomplished through the precession of the satellite's orbital plane.

($0^{o}.52$) per day. After one full year, all right ascensions between $\pm 60^{o}$ declination will have been sampled. Consequently, by January of 1969 the upper-V beam axis (projected upon the sky) was passing within about 45^{o} of Jupiter when the orbital phase[1] of the satellite was 0^{o}. Beginning at this time and continuing for about 6 months, detection of emission from the planet was considered feasible; that is, Jupiter was within the V-antenna pattern at all frequencies for some fraction of each orbit. By July of 1969 the angle at closest approach between Jupiter and the projected upper-V beam axis began to exceed 45^{o}, having passed through 0^{o} on 24 Mar 69. This period of time, from 1 Jan 69 to 1 Jul 69, defined the interval over which the RAE-1 data tapes were to be processed and examined for indications of Jovian emission.

It was decided to process the magnetic tape data by reducing it to a format which permitted visual identification of Jovian activity. In addition, the large volume of data available (over 1,000 orbits at each of 9 frequencies in 1969 alone) required that the visual inspection of the records be carried out at the University of Florida and, therefore, that the records be easily portable. Both requirements were satisfied

---

[1] In this study the satellite's orbital phase was arbitrarily set equal to 0^{o} when the angle between Jupiter and the projection of the beam axis of the upper-V antenna upon the sky was a minimum. Orbital phase increases as this angle increases, and the time between successive 0^{o} transits is one orbital period (224 min).

through the generation of 16-mm microfilm plots of the appropriate RAE-1 data.

An additional constraint on the observing interval, more rigorous than that determined by the V-antenna power pattern, was the angle between Jupiter and the sun when the upper-V beam was scanning Jupiter. This parameter is important because solar Type III bursts were found to be a major source of interference. Clearly, it was desirable that the Jupiter-sun angle approach 180^{o} so that the upper-V/lower-V antenna configuration might be utilized. Fortunately, Jovian opposition (24 Mar 69) occurred precisely in the middle of the 6-month observing period chosen for processing of the data tapes, as described above. A 3-month interval of time, approximately centered on the time of Jovian opposition, was chosen as the most favorable period over which the microfilm search was initially conducted. The technique of discriminating between solar and Jovian emissions based upon the comparison of simultaneous upper-V and lower-V deflections was then optimized.

Similar considerations to those outlined above were applied to the remaining RAE-1 data which were available during the 1970 and 1971 apparitions of Jupiter. The following table lists the periods of time during 1969, 1970, and 1971 over which the data tapes were processed. All of the frequencies between 450 and 9180 kHz were transferred onto microfilm. Also tabulated are the time intervals and frequencies at which the resultant microfilm has been read.

TABLE II-2.

RAE Data Tapes Processed	*Microfilm Read*	*Frequency*
13 Jan 69-03 Jul 69	26 Feb 69-12 May 69	450-6550
06 Feb 70-07 Jul 70	06 Mar 70-09 Jun 70	1300;6550
01 May 71-12 Aug 71	1 May 71-12 Aug 71	6550

Processing of the data tapes was performed via the IBM 360/91 and the Univac 1108 computers at NASA-GSFC, Greenbelt, Maryland. An outline of the microfilm production scheme is illustrated in Figure II-8. Each magnetic tape contained 16 days of RAE-1 data in digital form. The data on the tapes were organized into units known as data sets, each set containing twenty-three words. Besides upper-V and lower-V antenna temperatures, each data set also contained the instantaneous satellite pointing direction in right ascension and declination, impedance probe information, thermal probe information for calibration purposes, and elapsed time in msec from 1 Jan 68. All of this information, excepting the impedance and calibration probe data, was necessary for the generation of the microfilm plots. Only the Ryle-Vonberg coarse signals (word numbers 12, 13, 15, and 16 on each data set) were used.

A Fortran IV program (MPLOT) was written to control the processing of the microfilm on a production basis. MPLOT ordered the data such that individual satellite orbits were displayed on each frame of the microfilm. In addition, knowledge of the

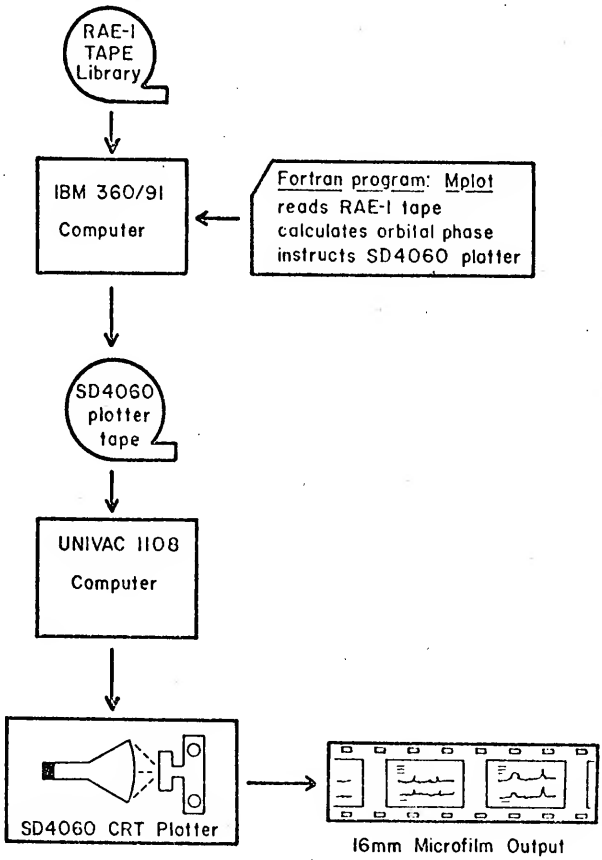

FIGURE II-8. Schematic Outline of the Microfilm Processing. The facilities of NASA-GSFC were used throughout. The SD (Stromberg Datagraphix) 4060 CRT plotter is a fast-plotting accessory of the Univac 1108 computer.

position of Jupiter and of the instantaneous pointing direction of the upper-V antenna permitted the calculation of the instant of Jupiter beam transit during each orbit. Based upon this calculation, MPLOT adjusted the time of beam transit (defined as the 0^{o} orbital phase point) such that it occurred in the middle of each frame. For ease in reading the microfilm, however, the orbital phase was shifted by 100^{o} so that negative numbers would not appear. As the probability of positively identifying, or even detecting, Jovian emission decreases rapidly as the angle from the E-plane beam axis increases, only 56% (200^{o}) of each orbit was actually plotted. Each frame of the resultant microfilm presents data at a single RV frequency. An example of two such frames is illustrated in Figure II-9.

FIGURE II-9. Two Consecutive Frames of the 16-mm Microfilm Are Shown. Each frame plots the upper-V and lower-V antenna temperatures as a function of satellite orbital phase at a single RV frequency. The instant of time coinciding with 0^{o} orbital phase appears on each frame in the format YYMMDD and HHMM at the top and bottom respectively. Jupiter beam transit occurs at 100^{o} orbital phase. An intense Jupiter storm is apparent at 3930 kHz between 100^{o} and 106^{o} orbital phase.

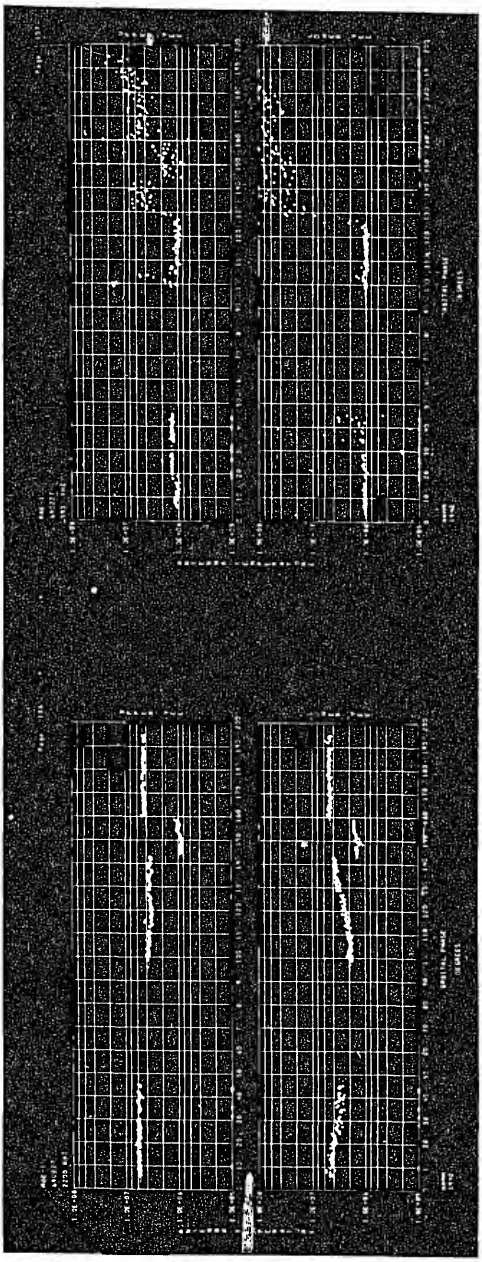

III

THE CALIBRATION OF THE 26.3 MHz ARRAY

One ring to rule them all,
One ring to find them,
One ring to bring them all,
And in the Darkness bind them . . .

--J. R. R. Tolkien

IN EVALUATING THE PERFORMANCE of an antenna system, there are two major considerations: (1) The alignment of the antenna's main beam must be known to within a suitable fraction of the beamwidth depending upon user requirements; (2) The absolute gain of the antenna and its variations with azimuth and altitude must be known in order to make quantitative measurements of radio source flux densities.

The determination of beam alignment and absolute gain becomes far more critical and time consuming as the antenna system increases in size. Small antennas, such as the Yagi, lend themselves to suitably accurate beam alignment through simple bore-sighting. Absolute gain may be determined by way of calculation alone. Unfortunately, these generally straightforward techniques become more open to question as the system complexity

increases. However, the greater directivity of a large antenna system makes possible the detection of radio sources whose positions and absolute intensities are sufficiently well known that they may be used to map the antenna pattern precisely and to determine its absolute gain. The technique of calibration by means of standard radio sources has been chosen for evaluating the performance of the 26.3 MHz array.

The detection system used in making the observations at 26.3 MHz is of fundamental design. The signals were recorded in the total-power mode by means of single-conversion superheterodyne receivers. Each receiver (one for each of three channels) has an IF bandpass of 250 kHz, with a diode detector and a postdetection time constant of 1 sec. The receivers were designed and constructed by Mr. Jorge Levy and Mr. Richard Flagg. Three different models of chart recorders were used (not simultaneously) at various times during development of the system to record data: a dual-channel (PDP) Texas Instruments chart recorder, a Honeywell three-channel Electronik 16, and a Rikadenki three-channel chart recorder. The latter instrument was found to be the most versatile and reliable. The scintillation events for the phase calibration of the array and the radio source drift scans for the gain calibration were recorded at 20 cm/hr and 6 cm/hr respectively. The calibration methods are described in the following sections.

III-1. PHASING ACCURACY

The beam alignment of the array is determined by a complex network of electronically and manually inserted phase delay lines between its 640 dipole elements. Beam alignment is therefore equivalent to phasing and will be referred to as such. The following is a presentation of the results of the phase calibration of the array.

Upon completion of the north half of the antenna (320 elements) a complete phasing unit was established. That is, a test of the resultant beam positioning represented an evaluation of the fine (Butler matrix) and coarse (plug-in phasing cables) phase adjustments which would be incorporated into the entire array. The Butler matrices and the manually inserted phasing cables would be required to be working properly in order for the tests to be successful. During the tests made at this time, there were five Butler matrices controlling east-west (ew) phasing and one controlling north-south (ns) phasing.

The method used for testing the ew phasing accuracy was simply to allow a strong radio source to drift through each of the eight ew antenna beams in turn. Because the radio sources chosen for these tests were effectively point sources relative to the 6^{o} ew HPBW, the resultant drift scans were a true representation of the actual power pattern of the array, after the application of receiver calibration data. The normalized field pattern for a linear (ew) array of n dipoles is given by Kraus (1950):

$$E = \frac{1}{n} E_1 \cos \Psi_1/2 \frac{\sin n\Psi_2/2}{\sin \Psi_2/2} \qquad \text{(III-1)}$$

where n = number of elements in array factor = 8, E_1 = ew field pattern of a single half-wave dipole, $\Psi_1 = \beta d_1 \sin \phi$, $\Psi_2 = \beta d_2 \sin \phi$, $\beta = 2\pi/\lambda$, $d_1 = 0.6\ \lambda$, $d_2 = 1.2\ \lambda$, ϕ = angle (ew) from beam transit plane. An additional factor contributing to the field pattern, $\sin(\pi/2 \cos \phi)$, is due to the combined effect of a reflecting ground screen and the surface of the ground, each located $\lambda/4$ below the dipoles. The variation in this term is insignificant over the extent of the main beam, however, and has been neglected here.

In Figure III-1 are shown the results of two such drift-scan analyses using 3C274 (Virgo A) and 3C218 (Hydra A) taken during times when there was little ionospheric scintillation to mar the records. It is clear that the observed drift scans conform very well to the shape of the theoretically expected power pattern. Additionally, the expected time of beam transit is correct to within $\pm$1 min. Visual inspection of similar drift scans through the remaining beam positions led to the same conclusion: the ew phasing is quite accurate.

Testing the phasing accuracy in the ns direction is somewhat more complicated. The method utilized takes advantage of the fact that there are three slightly overlapping ns beams during normal operation of the array, corresponding to the three

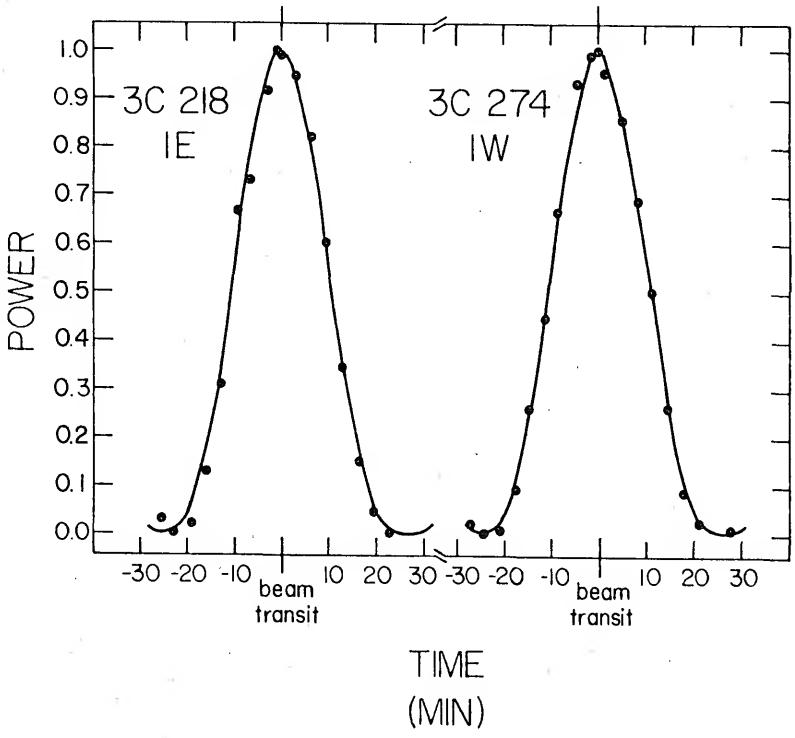

FIGURE III-1. Comparison of the Theoretical, Normalized ew Power Pattern of the Array (Solid Curve) with the Experimentally Derived Signal Powers (Solid Circles).

recording channels. The three beams were separated by 3^{o} and intersected at the -1.5 db point when only half of the array was used (with the full array, these quantities are different). Hence in general, a source will appear simultaneously in two of the beams during a drift scan, with the signal power in each beam being determined by the position of the two beams relative to the source. Assuming that the position of the beams is known precisely and by comparing the deflections occurring simultaneously in the two channels, one may determine the position in declination of an unknown source. Conversely, if the position of the source is already known, one may use the experimentally derived power ratios to determine the error in the beam alignment of the antenna. The latter approach has been used to establish the ns phasing accuracy of each of the eight ew beams by comparing the true position of the source with the position as deduced from the multiple-beam method. The normalized field pattern profile of the beams in the ns plane is given by

$$E = \frac{1}{n_1 n_2} \frac{\sin n_1 \Psi_1/2}{\sin \Psi_1/2} \frac{\sin n_2 \Psi_2/2}{\sin \Psi_2/2} \qquad \text{(III-2)}$$

where $n_1 = 4$ and $n_2 = 5$. Ψ_1 and Ψ_2 are defined as in Equation III-1 with ϕ = angle (ns) from beam axis, $d_1 = 0.60\ \lambda$, and $d_2 = 2.40\ \lambda$. Subscript-1 quantities refer to a ns row of four dipoles in a group of eight, and subscript-2 quantities to the

array factor formed by the center of the five groups of sixty-four dipoles each. It was found that a strongly scintillating source was the best suited for this type of analysis.

The results of analyzing 225 scintillation "events" using 3C144 (Taurus A) are shown in Figure III-2. Each scintillation event lasts for about 30 sec to a minute, and on the average, about ten events during a given 25-min drift scan are of sufficient magnitude for scaling. In addition, a limited number of events (15) were studied using the radio source 3C218 (Hydra A). This was done to uncover possible variations in phasing accuracy with zenith angle. The zenith angles at meridian transit for 3C144 and 3C218 were 8^{o} south and 42^{o} south respectively.

The ns phasing error for each ew beam position may be obtained from Figure III-2. The dotted line represents the true declination of 3C144 and 3C218. The plotted points represent the positions of the sources as deduced from the foregoing procedure. The mean phasing error is $0^{o}.34$ north, with the error tending to increase away from meridian transit. The maximum deviation (4W beam) is $0^{o}.60$ north. Although the data sampled at -12^{o} declination (3C218) are incomplete, there does not appear to be any indication of increased phasing error at negative declinations. Ionospheric refraction, which is expected to contribute insignificantly to the phasing error at 26.3 MHz (Viner 1975), has been neglected.

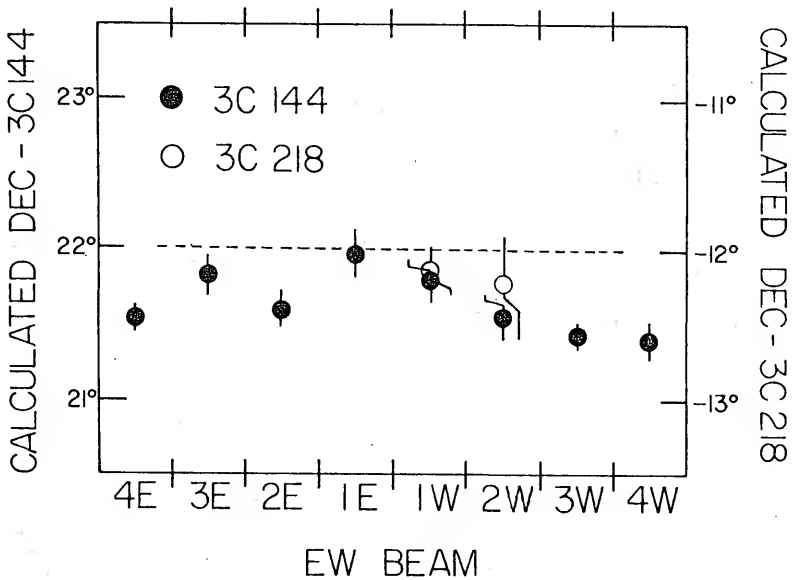

FIGURE III-2. The Declinations of 3C144 and 3C218 As Deduced from the Method Described in the Text Are Plotted for Each ew Beam Position. The dotted line represents the true declination of the sources. The ns phasing error for each ew beam position is given by the difference between the true and calculated declination.

In view of the results presented here, one may expect to be able to point the main beam of the array to within a probable error of about $0^{\circ}.6$ in the ns plane. This is in fact the angle between the ns beam positions when the entire array is operating. From a practical standpoint this means that the values tabulated in the PTP booklet (Desch 1972) will be correct to within $\pm$ one digit in the SNS number. Extensive monitoring of radio sources over a wide range of zenith angles for the purpose of gain calibration (see next section) has further substantiated this result. In addition, the monitoring of very weak Jupiter bursts over a period of 3 years has been eminently successful (Desch *et al.* 1975). It was found that the radio bursts could be distinguished from interference in three-channel recordings (one channel for each ns beam) based solely upon the signal power ratios predicted from the theoretically expected beam positions. The system phasing appears to be stable over time scales of at least several years.

III-2. ABSOLUTE GAIN CALIBRATION

The absolute gain of the array has been established over approximately 60° of zenith angle through drift scan analyses of thirteen radio sources. Table III-1 tabulates the sources chosen along with their positions, flux densities in Jy at 26.3 MHz, alternate names, and specific comments concerning certain of the sources which posed special problems. The flux

TABLE III-1. Standard Calibration Sources.

Source Number[a] (1)	Source Name (2)	R.A. 1950 h m (3)	Dec 1950 o ' (4)	Flux Density 26.3 MHz Jy (5)	Alternate Names (6)	Comments[b] (7)
1	PKS 0213-13.2	02 13	-13 13	110± 10	MSH 02-105	a
2	MSH 02-07	02 18	-02 12	120± 20	3C 63	b
3	MSH 03-301	03 19	-37 18	3,100± 300	Fornax A, PKS 0320-37	c
4	3C 89	03 32	-01 23	160± 30	MSH 03-03, PKS 0331-01	
5	3C 144	05 31	21 58	2,500± 100	Taurus A	
6	3C 181	07 25	14 45	60± 10	PKS 0725+14	d
7	3C 190	07 59	14 27	63± 10	PKS 0748+14	
8	MSH 08-404	08 20	-42 48	1,650± 100	Puppis A	e
9	3C 218	09 16	-11 53	1,800± 150	Hydra A, MSH 09-104	
10	3C 225	09 39	14 17	140± 30	PKS 0939+14	
11	3C 274	12 28	12 40	4,500± 300	Virgo A	
12	MSH 13-402	13 22	-42 46	20,000±3,000	Centaurus A	f
13	MSH 22-17	22 12	-17 17	400± 100	PKS 2211-17, 3C 444	

[a]Source numbers are keyed to Figure III-8.

[b]Key to comments: (a) confusing source PKS 0213-13.5, (b) confusing source MSH 02-012; (c) extended source, integrated flux is tabulated, (d) confusing source 4C+15.2, (e) confusing source MSH 08-405, (f) extended source, integrated flux tabulated.

densities and uncertainties quoted have been obtained from the spectra presented in Figures III-3 through III-7. In each case the uncertainty in the flux density at 26.3 MHz is arrived at after making a reasonable estimate of the variation in the flux density curve because of the scatter in the published points. This scatter is seen to be greatest at the lower frequencies. The higher frequency data points (>26 MHz) have been obtained from figures published by Dixon (1970). The flux densities at decameter wavelengths were obtained from various sources, namely Erickson and Cronyn (1965) at 26.3 MHz; Roger *et al.* (1969) at 22.25 MHz; Bridle and Purton (1968) at 10.03 MHz; Braude *et al.* (1969) at 12.6, 14.7, 16.7, 20.0, and 25.0 MHz; Bazelyan *et al.* (1965) at 20.0, 25.0, 34.0, and 38.5 MHz; Guidice (1966) at 22.3, 26.7, 33.45, and 38.7 MHz; and Shain (1958) at 19.7 MHz.

Once the standard radio sources have been chosen, the procedure for establishing antenna gain is relatively straightforward. In Table III-2 are presented the results of the drift-scan analyses, along with the dates that the records were taken and the phasing parameters used in locating the sources. The following are the steps used in making a single determination of the antenna gain at a particular zenith angle.

1. A drift scan is made of one of the sources tabulated in Table III-1 using the phasing parameters appearing in Columns 3 through 6 of Table III-2.

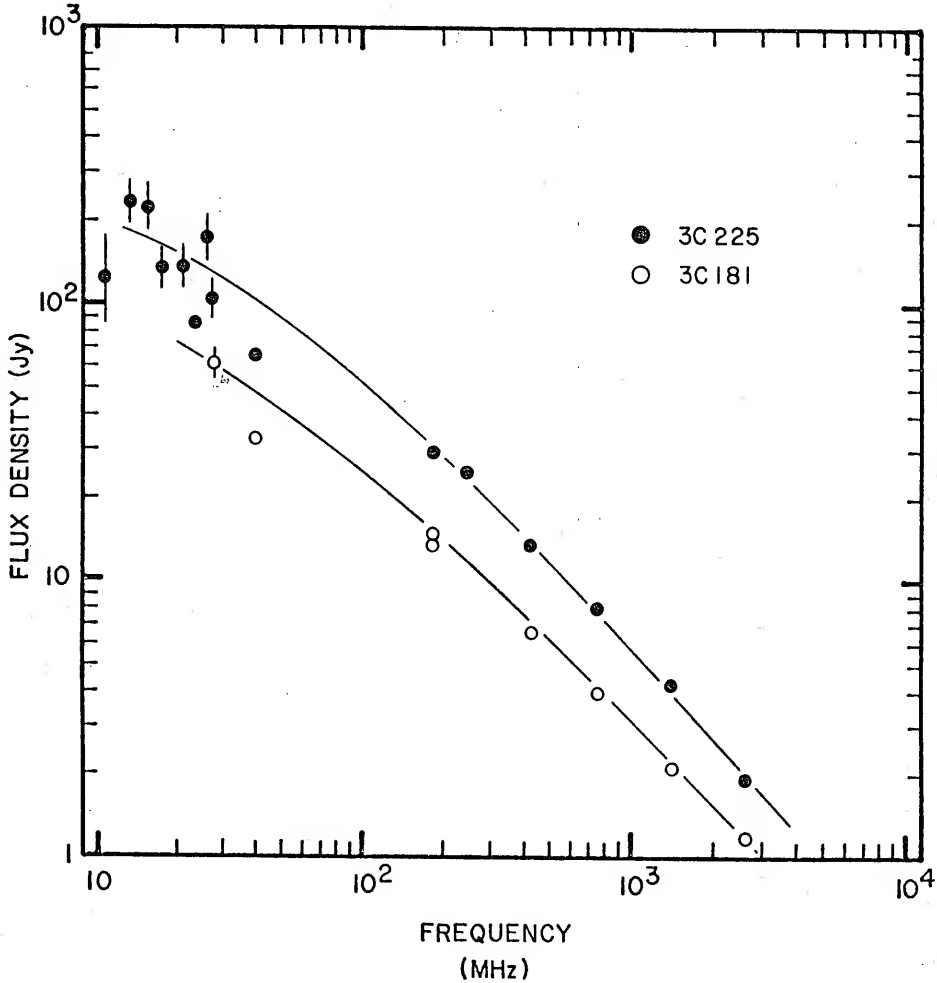

FIGURE III-3. Flux Density Spectra of 3C225 and 3C181. See text for references.

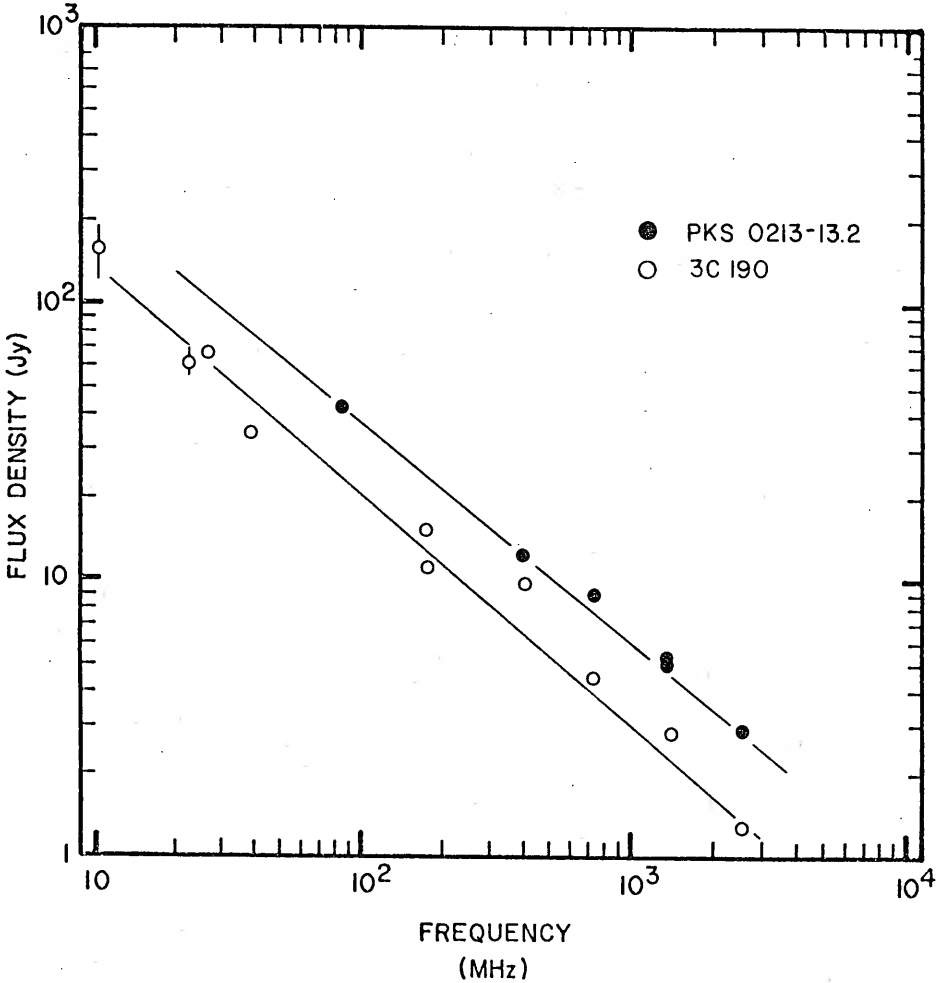

FIGURE III-4. Flux Density Spectra of PKS 0213-13.2 and 3C190. See text for references.

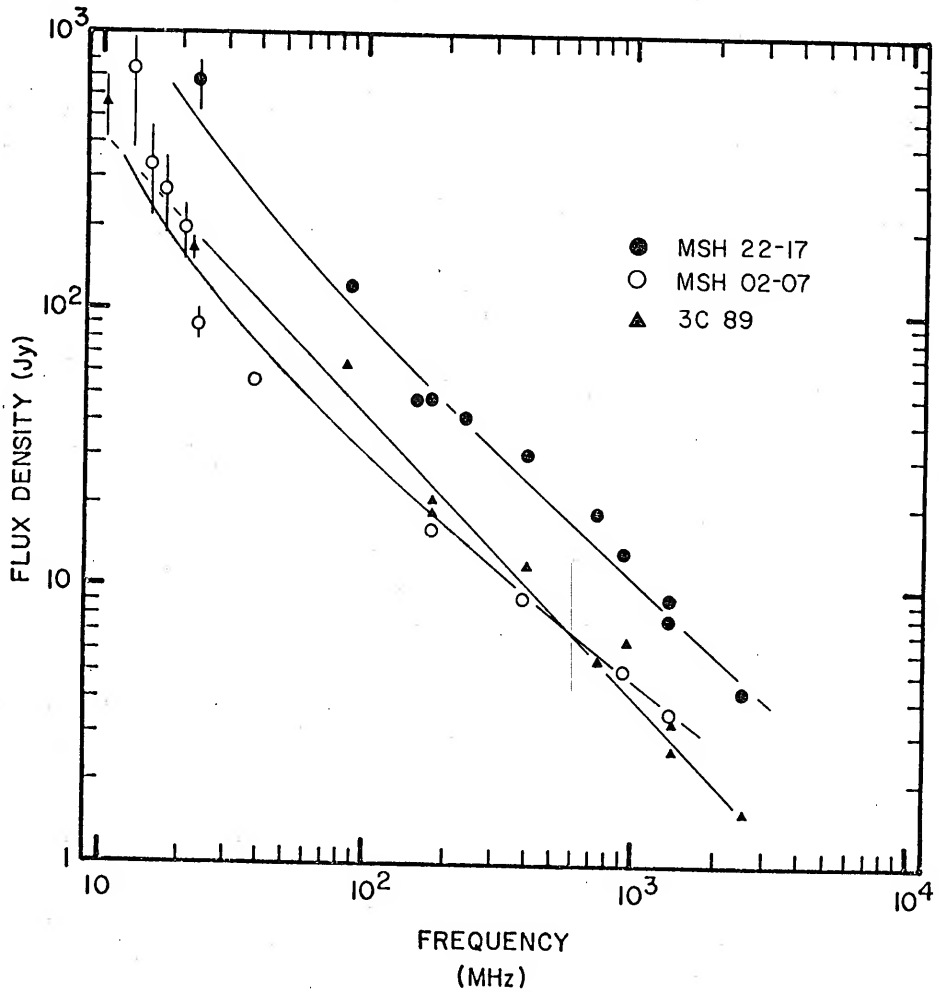

FIGURE III-5. Flux Density Spectra of MSH 22-17, MSH 02-07, and 3C89. See text for references.

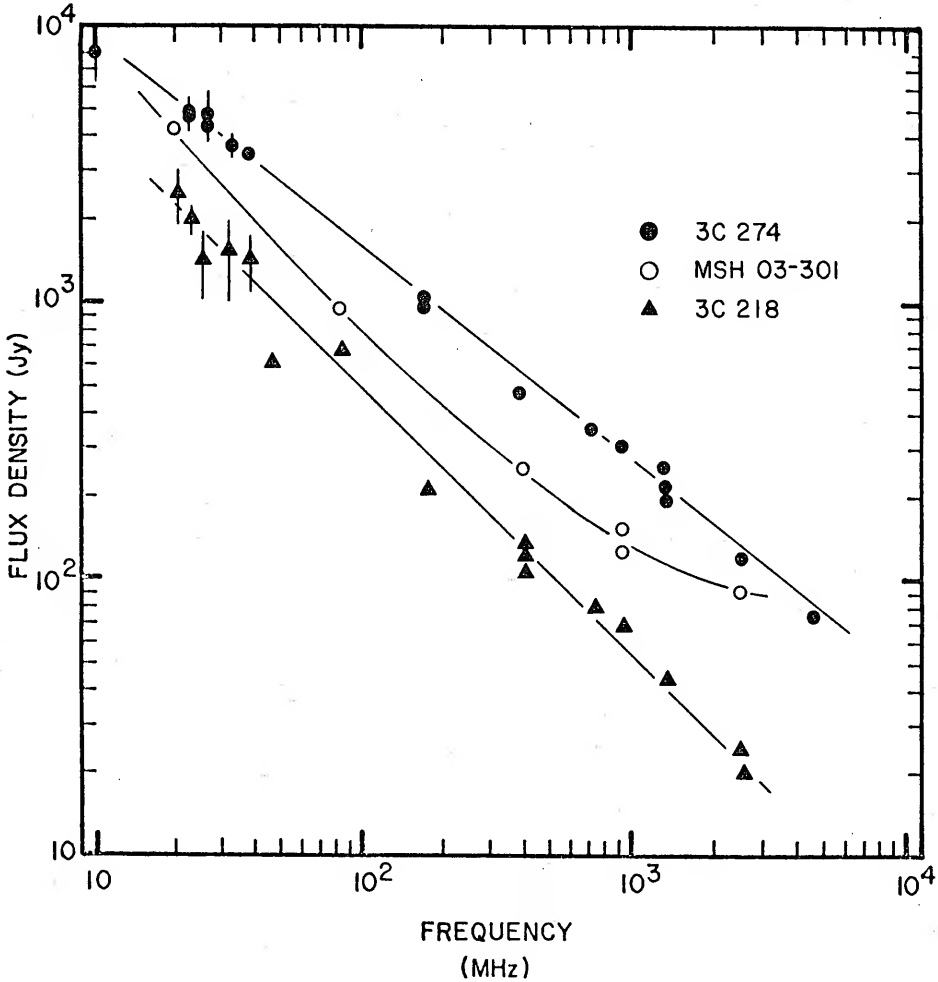

FIGURE III-6. Flux Density Spectra of 3C274, MSH 03-301, and 3C218. See text for references.

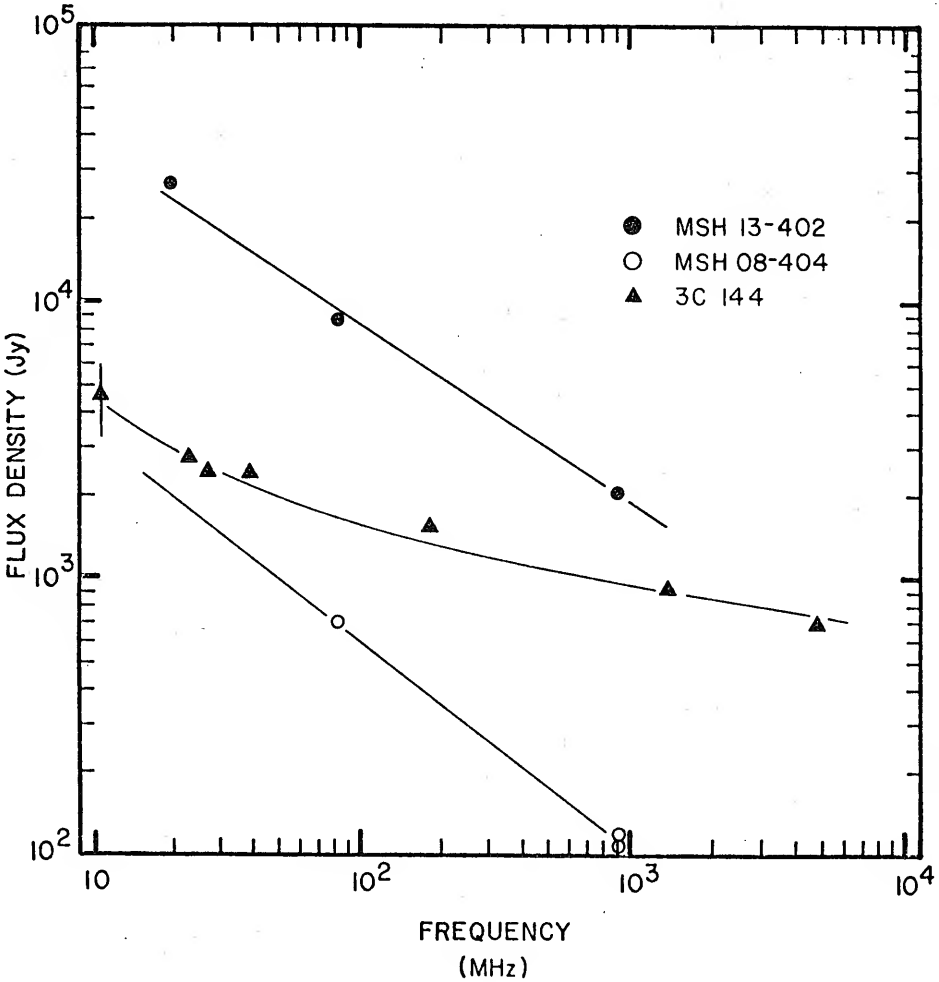

FIGURE III-7. Flux Density Spectra of MSH 13-402, MSH 08-404, and 3C144. See text for references.

TABLE III-2. Results of Array Gain Calibration

Source (1)	Date (2)	Phasing Parameters CNS (3)	FNS (4)	RSP (5)	EW (6)	p_1 (7)	p_2 (8)	T_A (K) (9)	T_A^* (K) (10)	A_e^* (K/Jy) (11)
PKS 0213-13.2	17 Jan 75	+3	5	2	1E	0.69	1.39	17± 3	18± 2	0.16±.02
	18 Jan 75	+3	5	2	1W	0.69	1.39	22± 4	23± 4	0.21±.04
	25 Jan 75	+3	5	2	1W	0.69	1.39	24± 7	25± 6	0.23±.06
MSH 02-07	16 Nov 73	+3	3	3	1W	0.63	1.23	28± 9	37±12	0.31±.11
MSH 03-301	21 Apr 73	+4	6	1	1W	0.85	0.79	119±11	177±16	0.06±.01
3C 89	21 Nov 73	+3	2	3	1W	0.61		36± 6	59±10	0.37±.09
	23 Nov 73	+3	2	3	1E	0.61		36± 4	59± 7	0.37±.08
	12 Nov 74	+3	2	3	1E	0.61		29± 5	47± 8	0.29±.07
	6 Jan 75	+3	2	3	1E	0.61		22± 4	36± 7	0.22±.06
	17 Jan 75	+3	2	3	1W	0.61		30± 5	49± 8	0.30±.07
	19 Jan 75	+3	2	2	1E	0.68		28± 8	41±12	0.26±.09
3C 144	25 Dec 72	+1	3	6	1E	0.86		568±51	661±59	0.26±.03
	5 Apr 73	+1	3	6	1W	0.86		675±48	786±56	0.31±.02
3C 181	29 Mar 73	+1	5	2	1W	0.75	1.49	33± 5	29± 5	0.48±.12
	5 Apr 73	+1	5	2	1W	0.75	1.49	26± 5	23± 5	0.38±.11
3C 190	16 Dec 72	+1	5	2	1W	0.68		19± 7	28±10	0.44±.17
	29 Mar 73	+1	5	2	1W	0.68		14± 4	21± 6	0.33±.11
	5 Apr 73	+1	5	2	1W	0.68		22± 4	32± 6	0.51±.13
MSH 08-404	20 Apr 73	+4	7	5	1W	0.68	1.82	165± 5	156± 5	0.09±.01
	21 Apr 73	+4	7	4	1W	0.70	1.82	205± 5	190± 5	0.12±.01
3C 218	14 Nov 73	+3	5	1	1E	0.89		273± 9	308±10	0.17±.02
	17 Nov 74	+3	5	1	1W	0.89		232±40	262±45	0.15±.03
	24 Nov 74	+3	5	1	1W	0.89		225±24	254±27	0.14±.02
	25 Jan 75	+3	5	1	1W	0.89		256±31	289±35	0.16±.02
	26 Jan 75	+3	5	1	1E	0.89		243±32	274±36	0.15±.02
3C 225	5 Apr 73	+1	6	3	1W	0.69		31± 5	45± 7	0.32±.08

TABLE III-2, continued:

Source (1)	Date (2)	Phasing Parameters CNS (3)	FNS (4)	RSP (5)	EW (6)	p_1 (7)	p_2 (8)	T_A (K) (9)	T_A^* (K) (10)	A_e^* (K/Jy) (11)
3C 274	26 Feb 74	+1	6	5	1W	0.86		1,277±78	1,480±90	0.33±.03
	22 Apr 74	+1	6	5	1E	0.86		1,287±75	1,491±87	0.33±.03
MSH 13-402	14 Apr 73	+4	7	5	1W	0.69	0.45	404±24	1,309±78	0.07±.01
	15 Apr 73	+4	7	5	1W	0.69	0.45	338±19	1,096±62	0.05±.01
	17 Apr 73	+4	7	5	1E	0.69	0.45	406± 6	1,316±20	0.07±.01
	20 Apr 73	+4	7	4	1E	0.70	0.45	425± 6	1,344±18	0.07±.01
	21 Apr 73	+4	7	4	1W	0.70	0.45	494±17	1,564±53	0.01±.01
MSH 22-17	10 Jul 73	+4	2	7	1W	0.61		30± 9	45±15	0.12±.05

NOTE: Key to Table III-2: (1) name of calibration source, (2) date of observation, (3-5) phase-tracking parameters used in making observations, as derived from PTP booklet, (6) EW beam through which drift scan occurred, (7) normalized power pattern of antenna in direction of source, applied to T_A as a correction, (8) correction applied to T_A due to presence of confusing source, or due to a source having a finite extent relative to main beam; blank column--no correction necessary, (9) measured, uncorrected antenna temperature due to source alone, (10) corrected antenna temperature, (11) final effective area of antenna from Equation III-5.

2. The antenna temperature Tn due to the combined effects of the galactic background and the source is calibrated against a secondary noise standard at 5- to 10-min intervals as detailed in Appendix A.

3. Usable records (~25%) are those which are relatively free of large antenna temperature fluctuations caused by ionosopheric scintillation. The remaining 75% are not used. Occasionally the calibration will exhibit a constant drift. That is, because of ambient temperature changes at the field preamplifier (see Appendix A), a given calibration level will record at different levels on the chart recorder. This thermal drift is always subtracted out of each drift scan before proceeding.

4. The antenna Temperature T_A due to the source alone is determined by subtracting the galactic background from the temperature due to the source and background combined. The temperatures used are those which occur at beam transit when the source deflection is greatest. The galactic background temperature at beam transit is obtained by drawing a straight line between the values for the antenna temperature obtained at the antenna pattern nulls which occur approximately 25 min before and after beam transit (see Figure III-1).

5a. This value for T_A must then be corrected by a factor p_1, which is the value of the antenna's normalized power pattern in the direction of the source. This factor is always less than 1.0 because in general a source will never pass through the beam axes of each of the modulating power pattern envelopes of the array simultaneously. In all, three ns envelopes and two ew envelopes combine as factors to generate a final product p_1, which is different for each source and set of phasing parameters used. In calculating p_1, Equations III-1, III-2, and the principle of pattern multiplication are used (Kraus 1950). The corrected figure $T_A^* = T_A/p_1$ is thus the value for the antenna temperature normalized to beam axis conditions.

5b. In the case of four of the radio sources (PKS 0213-13.2, MSH 02-07, 3C181, MSH 08-404), an additional correction p_2 is necessary because of the presence of confusing sources as noted in Column 7 of Table III-1. The confusing sources were close enough to the standard radio sources that their contributions to the antenna temperatures were not negligible. In these four special cases the final corrected figure T_A^* is given by $T_A/p_1 p_2$.

5C. A further correction was applied to two of the sources (MSH 03-301, MSH 13-402) due to their finite extent relative to the main beam of the antenna. This correction is necessary if the angular diameter of the source exceeds about one fifth of the antenna half-power beamwidth (Guidice and Castelli 1968). At decameter wavelengths the ns by ew extents of MSH 03-301 and MSH 13-402 are approximately $1^{\circ}.2$ by $1^{\circ}.75$ and $4^{\circ}.5$ by $2^{\circ}.0$ respectively (Shain 1958). Given the ns and ew antenna half-power beamwidths, one may then calculate the correction factor to be used for each source (Baars *et al.* 1965). The values so derived are tabulated under p_2 in Column 8 of Table III-2.

6. The absolute gain of the antenna is now directly expressable in terms of quantities which are tabulated in Tables III-1 and III-2. From Kraus (1966) the effective area of an antenna is given by

$$A_e = \frac{2kT_A \cdot 10^{26}}{S} \qquad \text{(III-3)}$$

where A_e = effective area in m^2, k = Boltzman's constant = 1.38×10^{-23} joules/K, S = true flux density of source in Jy, T_A = antenna temperature K due to source of flux density S, = T_A^*. It has been decided to express the absolute gain in terms of K/Jy which are the most practical dimensions, both from the standpoint of quantities derived by the foregoing procedure and application to future observations. Collecting constants, one can see Equation III-3

$$A_e = 2.76 \cdot 10^3 \, A_e^* \qquad \text{(III-4)}$$

where A^* = effective area of antenna in working units of K/Jy. As mentioned, A_e^* may be obtained directly from quantities already derived in the gain calibration procedure, namely the flux density S and the adjusted antenna temperature T_A^*. That is, A_e^* is given by

$$A_e^* = T_A^*/S \qquad \text{(III-5)}$$

This quantity is tabulated for each of the drift scans listed in Table III-2.

The errors quoted in A_e^* are due to two effects. The uncertainty in scaling the chart recordings, primarily as a result of scintillation effects, contributed about 50% to the final error. Another 50% is due to the uncertainty in the assumed flux density values as mentioned previously. Uncertainties because of phasing errors (calculation of p_1), calibration of the secondary noise standard (Appendix A), and changes in the calibrator line attenuation with ambient temperature fluctuations have been neglected. These rather small effects are not expected to contribute more than 10 to 15% to the errors already quoted in A_e^*. Ionospheric absorption, which is rarely greater than 2% for nighttime propagation conditions at 26.3 MHz (Viner 1975), has also been neglected. All of the observations reported on in this chapter were made between 1800 and 0600 local time.

In Figure III-8 are plotted the weighted mean values of A_e^* as a function of zenith angle and declination. There is a general trend in that the absolute gain of the antenna is seen to decrease with increasing zenith angle z, as expected. The data points do not, however, obey a simple cos (z) sin [π/2 cos (z)] fall-off as might be expected from the combined effects of foreshortening (cosine factor) and reduced ground reflection (sine factor). This may be due to variations in impedance matching with phase which have not been evaluated. In addition, the value obtained for A_e^* using 3C144 appears to be too low, since one would expect the gain to peak at 0^o zenith angle. In any event, a greater number of measurements are needed at declinations exceeding 10^o.

The procedure used here in deriving the absolute gain of the antenna is considered to be a compromise between that necessary for precise monitoring of weak, unknown radio sources and that necessary for determining the flux density of Jupiter radio bursts, for which precise calibration is unnecessary. The procedure is well suited for determining relative changes in array performance over long periods of time in order to diagnose the possible damaging effects of lightning or the gradual deterioration of electrical elements with age. Conversely, monitoring radio sources for intensity fluctuations on time scales greater than a few days is also possible, especially if a nearby comparison source is used. The reproduceability of drift scans

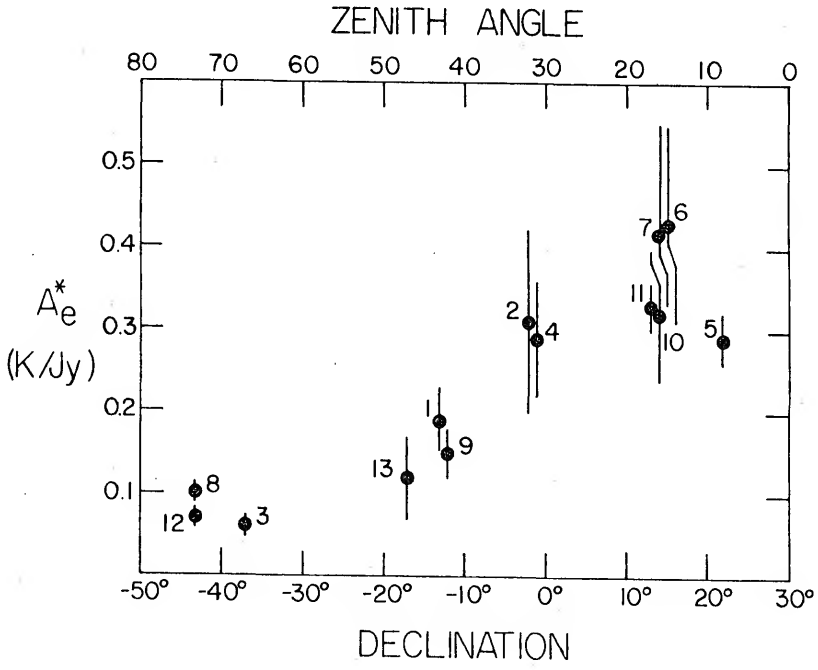

FIGURE III-8. The Effective Area of the Array in K/Jy Is Plotted As a Function of Source Declination and Zenith Angle. The source numbers are keyed to Table III-1.

from standard sources over a period of about 2 years indicates that about a 10% variation in collecting area or source intensity could be recognized following the procedures outlined here.

IV

THE CALIBRATION OF THE V-ANTENNA SYSTEM ON THE RAE-1

One man's magic is another man's engineering.

--Robert Heinlein

SINCE JUPITER ACTIVITY HAD NOT BEEN IDENTIFIED via satellite prior to this study, it was considered appropriate that the V-antenna power pattern and its attitude relative to the local gravity vector (*i.e.* the nominal upper-V pointing direction) be investigated as carefully as possible prior to undertaking an intensive campaign. Using the sun as a source of powerful Type-III bursts, a method was devised to verify the pointing accuracy in the E-plane and subsequently to confirm the existence of low-frequency Jovian activity. Further, by superposing the Jovian activity recorded over many orbital scans, it was possible to synthesize E-plane antenna patterns at a number of the higher RV frequencies and thus complement similarly directed theoretical studies. This preliminary investigation is described in this section.

IV-1. ORBITAL PHASE CALIBRATION

The orbital superposition technique is applicable only at frequencies exceeding 1310 kHz. Above this frequency, the probability of detecting emission from the sun or Jupiter is a clearly defined function of satellite orbital phase, after the easily recognizable terrestrial interference has been deleted (below this frequency the terrestrial interference is excessive). That is, as is evident from Figure II-7, there is a direct relationship between orbital phase and the pointing direction of the upper V in the E plane relative to a given source direction. Consequently, as the upper-V antenna is swept across a source the resulting antenna temperature will be directly proportional to the E-plane antenna power pattern or equivalently to the satellite's orbital phase. Clearly, the orbital phase variation will become more evident at the higher frequencies as the E-plane power patterns become increasingly directive. Because of the precession of the orbital plane of the satellite, the precise response function is also modulated somewhat by the H-plane pattern, but over relatively short periods of time ($\leq$ 3 months) this effect is negligible.

In using a source whose activity is unpredictable, such as the sun, the data collected over many orbital scans must be superposed until a smooth antenna pattern begins to emerge. In practice, the entire observing period in 1969 (26 Feb-12 May) was used in confirming both the upper-V attitude and the existence of the Jovian emission.

In order to insure that this initial study be as objective as possible, the microfilm versions of the data were temporarily abandoned and the computer was instructed to search the original RAE-1 magnetic tapes for "upper-V only" events, that is those which were supposedly of celestial origin. The program simultaneously compared the upper-V and lower-V radiometer channels at 3930 and 4700 kHz, with "upper-V only" events being counted when the signal from the upper V was found to be at least 3 db greater than the lower-V signal. Superposing 500 orbital epochs, the probability of occurrence of "upper-V only" events was plotted as a function of the orbital phase in Figure IV-1. Here the 0^{o} orbital-phase point in each orbit occurred at the time of Jupiter beam transit. As Jupiter was at or close to opposition during the period, the sun was always near 180^{o} orbital phase. As Figure IV-1 clearly indicates, the two significant peaks at both frequencies occurred at 0^{o} and 180^{o} orbital phase, corresponding respectively to the positions of Jupiter and the sun as seen by the upper-V antenna. This result firmly established not only the existence of the Jovian activity, but also the pointing accuracy of the upper-V antenna in the E plane.

Not all data were as well behaved as the 3930- and 4700-kHz radiometer channels. At 2,200 kHz, erratic drifts of the upper-V or lower-V background levels would sometimes result in the computer counting as "upper-V only" events those which by visual inspection were obviously not Jovian. At 6550 kHz the

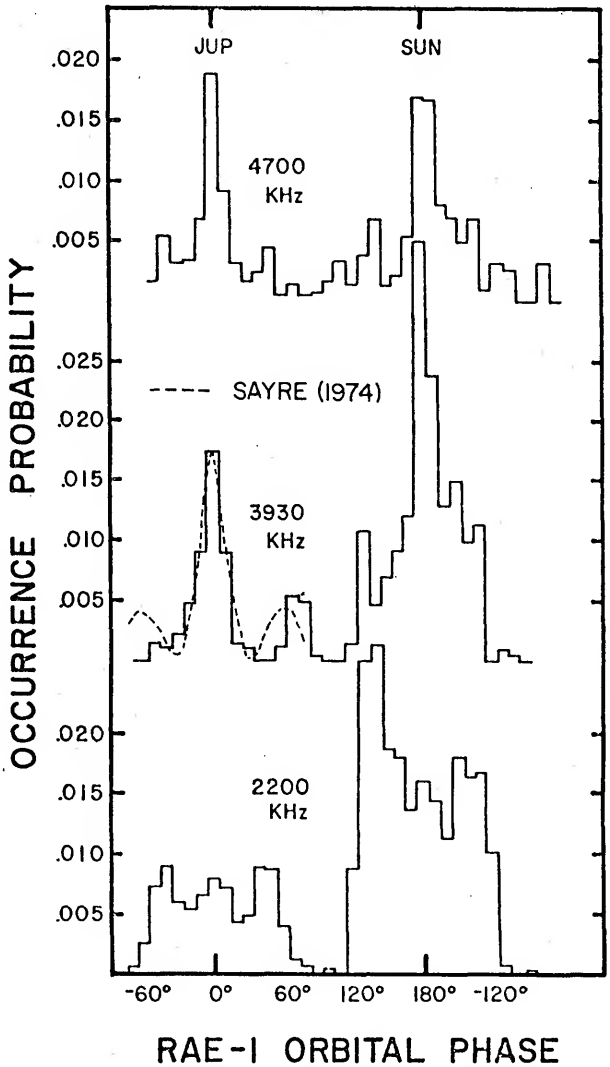

FIGURE IV-1. Occurrence Probability of "Upper-V Only" Events As a Function of RAE-1 Orbital Phase. Contributions from both Jupiter and the sun are clearly visible. The theoretical (50^{o} apex angle) calculation of Sayre (1974) is included for comparison at 3930 kHz.

common occurrence of terrestrial ground interference ("ionospheric breakthrough") often resulted in similar misidentifications. Hence, at these two frequencies the microfilm versions of the data were examined with the resulting phase variations appearing quite similar to those found at 3930 and 4700 kHz. At 6550 kHz, however, only the data within about $\pm 50^{o}$ of Jupiter beam transit were read (see Figure IV-2).

Besides verifying the existence of celestial activity at 0^{o} orbital phase, it was also possible at 3930 and 6650 kHz to compare the experimentally derived antenna patterns with the theoretical calculations for E-plane response made by Sayre (1974). In both cases, the theoretical pattern shown is that for the ideal in-orbit case; that is, the V antenna is assumed to have a 50^{o} apex angle. At 6550 kHz the agreement is remarkably good, especially considering that one is plotting the occurrence of sporadic events over a 3-month interval. At 3930 kHz, the 50^{o} apex-angle profile appears somewhat narrower than the pattern derived from the orbital superposition of activity, suggesting that the 35^{o} apex-angle calculation of Sayre, which results in a less directional main beam, might be more applicable. The data do not permit a definitive judgment, however.

The first sidelobe, at $+60^{o}$ orbital phase, is also evident at 3930 kHz, although it is displaced somewhat relative to that predicted by the 50^{o} apex-angle model. The sidelobe at -60^{o}

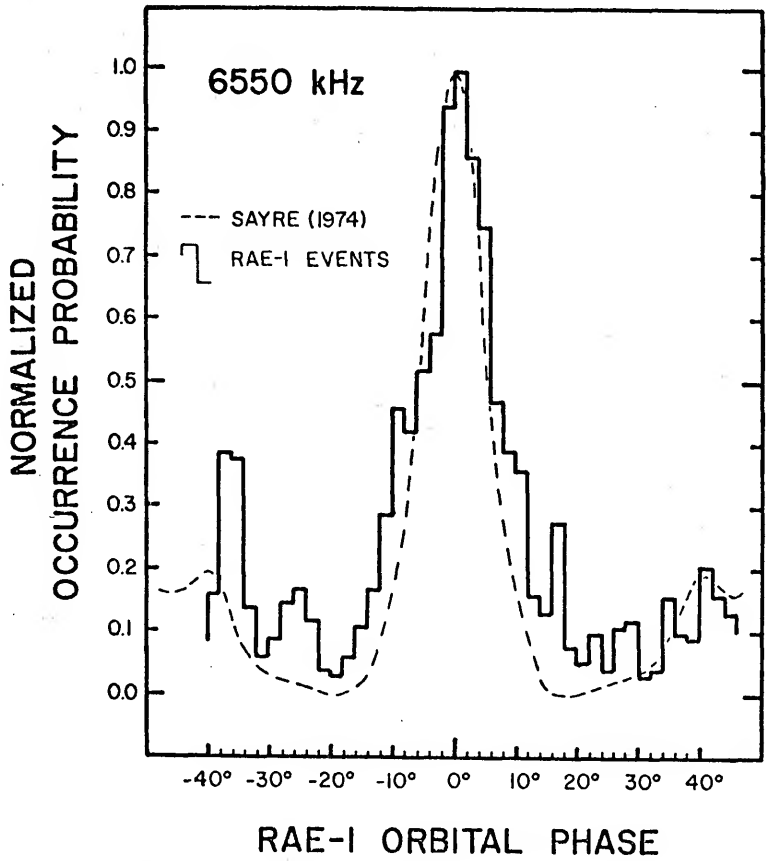

FIGURE IV-2. Normalized Occurrence Probability of "Upper-V Only" Events As a Function of Orbital Phase at 6550 kHz. The theoretical (50^{o} apex angle) calculation of Sayre (1974) for the E-plane antenna power pattern is included for comparison.

orbital phase does not appear at all, probably because of the masking effect of the ionospheric breakthrough which frequently occurred over this range of orbital phase.

Further comparison of the patterns in Figures IV-1 and IV-2 reveals a broadening with decreasing RV frequency. This is to be expected, of course, because of the decrease in directivity of the V antenna with increasing wavelength. The antenna patterns at 180^{o} phase are also broader than the 0^{o}-phase profiles occurring at the same frequency. This is due to the fact that the sun did not remain precisely at 180^{o} with respect to Jupiter during the 3-month interval under study.

The results presented in this section have demonstrated the usefulness of both computer reading of the RAE-1 tapes and visual examination of the microfilm transcriptions in identifying Jovian activity. The remainder of the data has been reduced via the microfilm-inspection method for reasons explained in Section II-4. In the following section, some of the results obtained in the foregoing analysis are used to assist in deriving values for the absolute gain of the V antenna at frequencies between 450 and 6550 kHz.

IV-2. ABSOLUTE GAIN CALIBRATION

The calibration method employed at 26.3 MHz, which depended upon the detection of standard radio sources, was not applicable in the case of the RAE system. No continuously emitting "point"

sources have been identified using the RAE-1 satellite, even at the higher frequencies where the antenna directivity is greatest (Alexander, personal communication). As a result, the V-antenna effective areas were determined by an indirect method (Kraus 1966) which is outlined below. The method requires a knowledge of the antenna's power pattern and also a knowledge of the loss factor involved in the matching of the antenna to the RV receiver. The former is known to some extent both theoretically and experimentally as discussed in the previous section. The latter depends upon the absolute measurement of the temperature of some sky source--thus permitting the direct comparison of V-antenna-derived source temperatures with the "true" source temperatures. In the present analysis, the true source temperatures have been determined from the absolute brightness measurements of the galactic background made by Brown (1973) and by Alexander *et al.* (1969). They are tabulated in Column 2 of Table IV-1 for each of the RAE frequencies. Hence the loss factor k_o is established at each frequency by forming the ratio of T_v (background temperature measured by the V-antenna) over T_s (known brightness temperature of the galactic background). These figures are tabulated in Columns 3 through 5 of Table IV-1.

The absolute brightness measurements of the galactic background are critically dependent upon an understanding of the radiation characteristics of the dipole antennas employed by the above authors. Fortunately, studies of the dipole antenna

TABLE IV-1. V-Antenna Calibration Parameters.

Freq *kHz* *(1)*	*B* 10^{-20} *(2)*	*T* 10^{6} *(3)*	T_s 10^{6} *(4)*	k_o *(5)*	ε_M *(6)*	Θ^o_{HP} *(7)*	ϕ^o_{HP} *(8)*	A_e^* *(9)*
6550	1.20±18%	0.91	0.4 ±10%	0.44 ±20%	0.72	14 ±10%	60 ±25%	2600 ±33%
4700	1.22±18%	1.80	1.0 ±10%	0.55 ±20%	0.73	30 ±20%	62 ±25%	2900 ±38%
3930	1.30±18%	2.70	1.0 ±10%	0.37 ±20%	0.80	38 ±20%	64 ±25%	2300 ±38%
2200	1.10±12%	7.40	4.0 ±10%	0.54 ±16%	0.95	60 ±25%	100 ±25%	5200 ±39%
1310	0.73±10%	14.00	4.0[a]±10%	0.29[a]±14%	0.95	180 ±25%	120 ±25%	2200[a]±38%
900	0.49±10%	20.00	4.0[a]±10%	0.20[a]±14%	--[b]	--[b]±	--[b]±	2600[a]±14%
700	0.35±11%	23.00	2.0[a]±10%	0.09[a]±15%	--[b]	--[b]±	--[b]±	2000[a]±15%
450	0.10±14%	16.00	1.0[a]±10%	0.06[a]±17%	--[b]	--[b]±	--[b]±	3200[a]±17%

[a]Only nominal values are tabulated (see text).

[b]Antenna pattern effectively that of a short dipole.

NOTE: Key to Table IV-1: (1) RAE-1 frequency in kHz, (2) galactic background brightness in units of $Wm^{-2}Hz^{-1}sr^{-1}$, (3) brightness temperature (K) from (2), (4) brightness temperature (K) from RAE-1, V-antenna measurements, (5) loss factor (dimensionless), (6) main-beam efficiency, (7) E-plane HPBW in degrees, (8) H-plane HPBW in degrees, (9) V-antenna effective area in m^2.

have been quite exhaustive, and its behavior in the plasma environment of the earth's magnetosphere is well documented. Nonetheless, it is well to keep in mind that the method employed here to calibrate the V-antenna gain is not as reliable as that used in calibrating the effective area of the 26.3 MHz array, primarily because of its ultimate dependence upon measurements made by a secondary antenna system.

The following is a derivation of the equations used in determining the effective area of the V-antenna at a given frequency. Kraus (1966) has shown that

$$A_e = \lambda^2 / \Omega_A \qquad \text{(IV-1)}$$

where A_e = antenna effective area as determined solely from the antenna pattern and Ω_A = beam solid angle in sr (sr = steradian = radian^2). In the ideal case, when ohmic and mismatch losses are negligible, Equation IV-1 is correct as stated. However, in general an ohmic loss factor k_o must be included. Equation IV-1 then becomes

$$A_e^* = k_o \lambda^2 / \Omega_A \qquad \text{(IV-2)}$$

where A_e^* = true effective area, k_o = loss factor because of impedance mismatching, resistance, etc., and in general, $0 \leq k_o \leq 1.0$.

In the present analysis, k_o is given by the ratio T_v/T_s, as explained previously. The beam solid angle may be expressed as

$$\Omega_A = \Omega_M/\epsilon_M \qquad \text{(IV-3)}$$

where Ω_M = main beam solid angle and ϵ_M = main beam efficiency. Furthermore, the main beam solid angle may be expressed as

$$\Omega_M = k_p \ \Theta_{HP} \ \phi_{HP} \qquad \text{(IV-4)}$$

where k_p = pattern shape factor = $1.05 \pm .05$, Θ_{HP} = HPBW in radians in the Θ direction (E plane), and ϕ_{HP} = HPBW in radians in the ϕ direction (H plane). Because k_p varies over so narrow a range as compared to the relative uncertainty involved in determining the other factors in this analysis, we shall set k_p equal to 1.0. Then, by combining the above equations and converting from radians to degrees and from wavelength to frequency, we obtain the final form:

$$A_e^* = \frac{29.5 \times 10^7 \epsilon_M \ k_o}{\Theta^o_{HP} \ \phi^o_{HP} \ \nu^2} \qquad \text{(IV-5)}$$

where Θ^o_{HP} = E-plane HPBW in degrees, ϕ^o_{HP} = H-plane HPBW in degrees, ν = frequency in MHz, and A_e^* = true effective area in m^2.

Equation IV-5 has been used to calculate the effective area of the V-antenna at frequencies between 6550 and 1310 kHz inclusive. At the lower frequencies the V-antenna power pattern is essentially that of a short dipole. Hence, the effective area at 900, 700, and 450 kHz has been calculated from the expression

$$A_e^* = 0.119 k_o \lambda^2 \qquad \text{(IV-6)}$$

which is the equation for evaluating the effective area of a short dipole (Kraus 1950). Using Equations IV-5 and IV-6 we have tabulated the true effective areas in Column 9 of Table IV-1. The remainder of this section will be devoted to describing how the parameters used in evaluating A_e^* and appearing in Table IV-1 were obtained.

The brightness spectrum of the galactic background derived by Brown (1973) has been used for the frequencies between 2200 and 450 kHz because the uncertainties quoted were less than those of Alexander *et al.* (1969). Hence, the error limits appearing in Table IV-1 at these frequencies were those obtained by Brown. His investigation, which employed the 91-m dipole on the IMP-6, did not extend above 2600 kHz however. Thus, between 6550 and 3930 kHz, the figures derived by Alexander *et al.* have been used. Using the 37-m dipole on the RAE-1, Alexander *et al.* have formally calculated an error in each

brightness measurement of ±18%. They estimated that the absolute determination of their brightness values might have been in doubt by as much as ±25%, however, because of systematic or random errors not accounted for. The formal error (±18%) has been chosen here as representative of the uncertainty since the lower frequency extension of the RAE-1 curve merges so well with the Imp-6 spectrum obtained by Brown. The brightness temperatures were obtained directly from the brightness measurements themselves by means of the equation

$$T_s = 0.5\lambda^2 \, B/k \qquad \text{(IV-7)}$$

where B = galactic background brightness ($Wm^{-2}Hz^{-1}sr^{-1}$) and k = Boltzmann's constant. The percentage errors associated with T_s (not explicitly shown) are thus the same as those associated with B.

The galactic background temperatures T_v measured with the V-antenna system on the RAE-1 were read directly from the microfilm plots of the upper-V antenna temperatures (see Figure II-9). They are subject to an uncertainty of about ±10% at each RV frequency. This value has been derived by Alexander and Novaco (1974), based upon an analysis of the errors inherent in the RV-radiometer measurements. The individual factors contributing to the total uncertainty were (i) receiver noise, (ii) internal satellite temperature uncertainties, (iii) finite digitization

steps involved in telemetry, (iv) errors in the radiometer calibration, (v) gain shifts in the radiometer, and (vi) variations in antenna impedance because of *in situ* plasma density changes and V-antenna boom motions. Hence, combining the errors associated with T_s and T_v, we obtain the uncertainty in k_o which, depending upon frequency, is seen to vary between $\pm$14% and $\pm$20%.

Changes in the galactic background level because of Factor vi are quite often apparent and should be discussed here in greater detail. The phenomenon manifests itself as a background level oscillation occurring with a period of about 224 min (one orbital period). During this time the mean plasma density will vary by a factor of about three, thus changing the degree to which the V-antenna is matched to the RV receiver system. This effect is minimal at frequencies above about 4000 kHz (Alexander and Novaco 1974). Often superimposed on this drift is a shorter-period variation in the background temperature because of changes in solar insolation on the V-antenna booms. The thermal stress on the booms during times of solar shadowing establishes a physical oscillation with a period of 50 min which also changes the effective impedance match. Because of these effects, only the nominal values of T_v, k_o, and hence, A_e^* appear in Table IV-1 at frequencies below 2200 kHz. In general, the variations were observed to decrease with increasing frequency and were not apparent above 1310 kHz.

The main beam efficiencies, tabulated in Column 6 of Table IV-1, have been estimated from the published theoretical V-antenna power patterns (Weber *et al.* 1971; Sayre 1974). The main-beam efficiency is the fraction of the total power incident over 4π sr which is intercepted by the antenna's main beam. Since the numbers are only estimates and do not involve experimentally derived data, no uncertainties have been attached to them.

Where possible, HPBW's have been derived from the orbital superposition data presented in Section IV-1. Hence, the E-plane values (Column 7, Table IV-1) quoted at 6550, 4700, and 3930 kHz are the experimentally derived figures. It is of interest to compare these values with the theoretical predictions of Sayre (1974). As pointed out in the previous section, the 6550-kHz pattern derived from the stacking of Jupiter bursts agreed exceptionally well with Sayre's analysis for the 50^{o} apex-angle case. The 3930-kHz value is approximately midway between the 50^{o} and 35^{o} apex-angle calculation of Sayre. No theoretical 4700-kHz antenna patterns have been calculated as yet. The H-plane HPBW's at 6550 and 3930 kHz were taken from Sayre's 35^{o} apex-angle calculation. The average of these two values was used at 4700 kHz. The greater uncertainty in choosing the proper H-plane value is reflected in the generally larger errors associated with them. At 2200 and 1310 kHz the figures quoted are from Alexander (personal communication).

Below 1310 kHz, power pattern information was not necessary for determining effective area.

As a final note, it is evident that the uncertainties in A_e^* are rather large. It should be clear from the discussion, however, that the figures are not rigorous determinations of the errors but rather merely representative of the general degree of certainty which may be attached to each figure.

V

THE GROUNDBASED RESULTS AT 26.3 MHz

It has always seemed to me that the most difficult part of building a bridge would be the start.
--Robert Benchley

SYNOPTIC OBSERVATIONS OF JUPITER at 26.3 MHz have been conducted from 16 April 1973 to the present. The monitoring has not been carried out entirely without interruption, however, as observations are normally suspended for a 2- to 3-month interval centered on Jovian conjunction. Additionally, during the regular season, the program may be interrupted for several days at a time for special experiments which require rephasing (*e.g.* lunar occultation, VLBI, or QSO monitoring). Unscheduled interruptions such as those due to severe lightning conditions or equipment failure have generally been a minor source of difficulty, although summer atmospheric conditions can reduce operations by as much as 20 to 25%. Nevertheless, the gross statistics derived from the uncontaminated Jupiter data (Table V-1) are impressive, especially in view of the fact that observations are possible for only about 3.4 out of every 24 hours.

TABLE V-1. Gross Statistics at 26.3 MHz.

Apparition	*Observing Dates*	*Interference-Free Observing*	*Jupiter Activity*	*Occurrence Probability*
1973/74	16 Apr 73-11 Feb 74	564.7 hr	74.6 hr	13.2%
1974/75	10 May 74-1 Mar 75	432.4 hr	76.9 hr	17.8%

Much of the discussion in this chapter has been reported by Desch *et al.* (1975) based upon the data gathered during the 1973/74 apparition. However, except where noted, the results presented herein are derived from both the 1973/74 and 1974/75 apparitions. As a consequence of the improved data base (and additional reflection), the treatment has been expanded in many places.

V-1. THE DEPENDENCE OF THE OCCURRENCE PROBABILITY ON FREQUENCY

As pointed out in Section II-1, the minimum flux density of the bursts detected in this study was about 50 Jy. After correcting for antenna phase and normalizing all flux densities to 4 AU (minimum earth-Jupiter distance), a representative figure for the threshold sensitivity maintained throughout the observing program is attained. It is approximately 100 to 150 Jy, which represents a two to three order of magnitude improvement over the most directive Yagi radiometer systems currently in use. It is thus of interest to examine the overall

flux density distribution of the Jovian activity, with special regard to the very low-level activity.

The number-intensity behavior and duration-intensity behavior of the Jupiter storms[1] recorded during the 1973/74 apparition are shown in Figure V-1. The arrow in the figure indicates the approximate sensitivity limit (6×10^4 Jy) of a five-element Yagi antenna operating at this frequency. The number of storms occurring below this limit rises sharply as the flux density is reduced (note log scale on ordinate). In fact, over 75% (by number) of the storms occurred at flux levels below 6×10^4 Jy. The duration-intensity behavior was quite the reverse, however. The mean duration of the storms suffered a pronounced decline as their peak flux density decreased so that as a result the low-intensity component (peak flux not exceeding 6×10^4 Jy) accounted for only about 50% of the total activity time at 26.3 MHz. As we shall now see, these circumstances have direct bearing upon the widely accepted notion of the dependence of the decametric occurrence probability on frequency.

---

[1] Because of the character of the weak activity recorded in this study, the definition of Jupiter "storm" necessarily differs somewhat from that implied in previous works. The low-level activity was generally observed to persist for only very short intervals (t) at a time, relative to the fully developed storms (t > 30 min) normally observed. However, weak activity preceding or following the longer, more intense storms were not counted as independent storms.

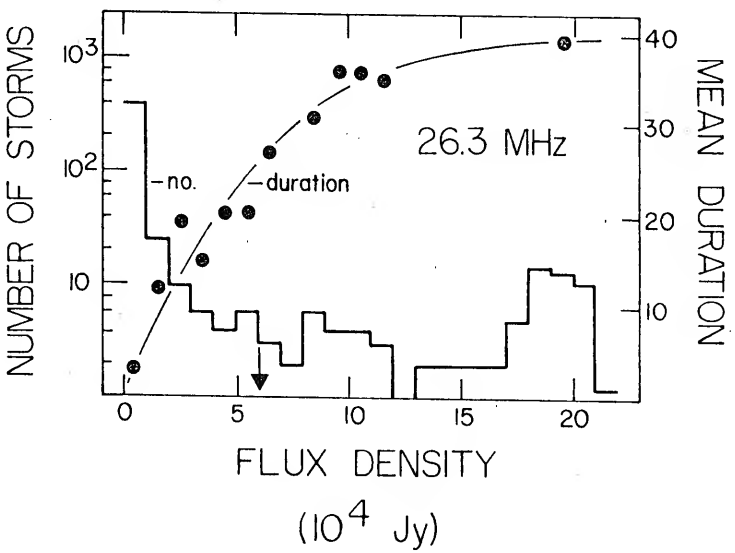

FIGURE V-1. The Number and Mean Duration (in Minutes) of Jupiter Storms Are Plotted As a Function of the Peak Flux Density Measured for Each Storm. The arrow indicates the approximate sensitivity limit of a five-element Yagi antenna at this frequency.

It is most remarkable that despite the vast improvement in sensitivity which has been achieved, no overwhelming increase in overall occurrence probability was observed. This result is in contrast to the conditions noted by Dulk and Clark (1966) in an 8-month study conducted during the 1964/65 apparition. Using a moderately directive interferometer system to positively identify the Jovian activity, they observed nearly continuous radio emission at 8.9 and 10 MHz, at flux levels exceeding approximately 4×10^3 and 2×10^4 Jy respectively.[2] The probability levels were a striking 95% at 8.9 MHz and 75% at 10 MHz. While it is recognized that the overall occurrence probability of Jovian emission decreases rapidly at the higher frequencies, one might nevertheless have expected the present study to yield a probability level comparable to that found by Dulk and Clark, owing simply to the highly directive nature of the array system. For example, although the peak flux density of the radiation at 27 MHz is about two orders of magnitude less than that at 10 MHz (Carr *et al.* 1964), the threshold sensitivities achieved in the present study and by Dulk and Clark are also very nearly in the ratio of 100 to 1. Additionally,

---

[2] Although Dulk and Clark did not analyze their 8.9 MHz data on an absolute flux scale, I have calculated the above threshold figure (4×10^3 Jy) based upon the system parameters quoted by them. The figure is within a factor of four of the sensitivity limit they realized at 10 MHz using a system of comparable size.

the value of D_E, which is recognized as a factor in controlling probability levels, was positive during both studies, differing during the 1974/75 and 1964/65 apparitions by less than 1^o. Hence, both in terms of the viewing geometry and the relative intensity levels, the sampling of the radiation was nearly identical in both investigations.

As it stands, the foregoing discussion strongly suggests that the occurrence probability of Jovian activity is indeed a pronounced function of frequency. Of course, this character of the morphology was immediately apparent to the early investigators (*e.g.* Burke and Franklin 1955); nonetheless, one must be cautioned against blindly identifying the intrinsic behavior of the emission with the observed character for--recalling the discussion of Section I-3--the occurrence probabilities as derived from the Yagi-monitoring programs are no doubt strongly biased by the steep flux density spectrum of the emission (Figure I-2). However, as has been explained above, the probability levels observed at 26.3 MHz ($\sim$0.15) and at 8.9 MHz ($\sim$0.95) are decidedly not subject to the selection effect caused by Jupiter's steep spectrum. The sampling was equal in both studies. Consequently, the elimination of any possible bias would appear to have finally confirmed the frequency-dependent nature of the occurrence probability. This conclusion is subject to the following important qualification, however.

In their investigation, Dulk and Clark appear to have observed for the first time a lower limit to the flux density of the radiation. That is, they failed (except on one occasion) to detect any bursts at 10 MHz below a certain flux density threshold (5×10^3 Jy), even though they could have detected radiation as weak as 1×10^3 Jy. This would imply that they succeeded at 10 MHz, and probably also at 8.9 MHz, in sampling the entire range of intensity levels and, hence, all possible events. In principle, we may assume that they observed the maximum possible probability level. This was not the case in the present study. We failed to detect any threshold below which radiation did not occur. Bursts were detected down to the limit of the instrument itself (50 Jy). It can be argued, then, that there is a significant volume of activity which has not yet been detected at 26.3 MHz which, if added to the probability level already realized, could conceivably raise it to the level observed by Dulk and Clark. This probability appears unlikely, though, as one may interpret the mean-duration curve in Figure V-1 to imply that there is an insignificant volume of activity remaining below the detection threshold of the array. That is, in extrapolating the curve toward lower flux levels, one quickly reaches a point at which the mean duration of the storms is zero. This situation is further amplified in Figure V-2 where the low intensity end of the curve is illustrated in detail. It appears that if even an order of magnitude improvement in the

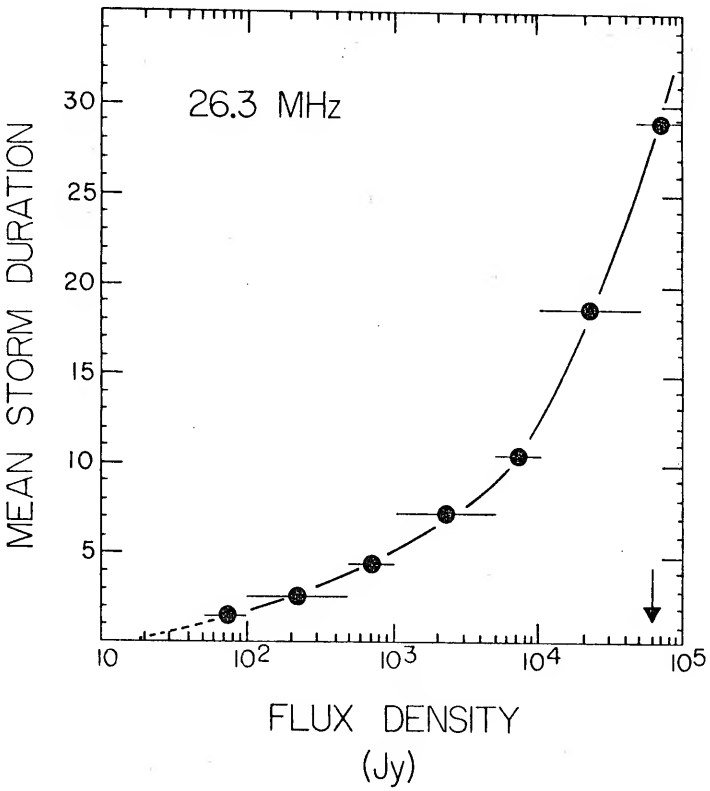

FIGURE V-2. The Mean Duration of the Storms in Minutes Is Plotted As a Function of Their Peak Flux Density in Jy. Data from both the 1973/74 and 1974/75 apparitions are used. The arrow indicates the approximate detection threshold for a Yagi-radiometer system at this frequency. The error bars indicate the range of flux densities over which the storms were averaged.

array sensitivity were realized (5 to 10 Jy detection threshold), the increase in occurrence probability would be marginal. It could surely not increase to the quasi-continuous level observed by Dulk and Clark.

In summary, although we cannot make an unqualified statement concerning the absence of considerable low-level activity, the results seem to support the contention that the bulk of the 26.3 MHz activity has now been detected. A representative figure for the maximum attainable occurrence probability at this frequency is probably about 25%, depending upon the value of D_E. We conclude that the frequency-dependent nature of the occurrence probability is substantially confirmed.

V-2. ROTATION-PHASE AND IO-PHASE MODULATIONS

The following two sections are devoted to a study of the rotation phase (λ_{III}, 1957.0) and Io phase (γ_{Io}) modulations of the 26.3 MHz activity. In the spirit of the present investigation, we will examine the dependence of the histogram profiles on intensity. More specifically, by dividing the data approximately in half so that one data set contains a low intensity component and the other a high intensity component, any dependence upon the flux density will become apparent immediately. When conducted in this fashion, the analysis can be particularly revealing, for as mentioned in Section II-1, the 26.3 MHz activity has been recorded over a dynamic range spanning nearly six orders

of magnitude. This is to be compared with the three-decade range typically realized in synoptic monitoring programs carried out heretofore. Additionally, examining the intensity dependence of the λ_{III} and γ_{Io} modulations is of importance with regard to the selection effect discussed in Section I-3. In particular, if the λ_{III} or γ_{Io} profiles exhibit markedly different signatures depending upon the intensity level which is sampled, then a very real source of bias can exist in data recorded with low gain systems. Mindful of these preliminary remarks, we proceed to examine further the data gathered by the array.

Figure V-3 illustrates the variations in planetary activity with respect to the λ_{III} and γ_{Io} coordinates. The occurrence probabilities have been calculated in the usual manner by accumulating the amount of activity time and interference-free listening time which occurs in each 10^{o} zone and dividing the former by the latter. As mentioned, the data have been further divided into low intensity and high intensity components. The low intensity component is comprised of all storms whose peak intensity did not exceed a certain flux density. Storms whose peak flux density exceeded this threshold formed the high intensity component. The particular threshold value assigned (2×10^{4} Jy) has not been chosen arbitrarily as will become clear in Chapter VII.

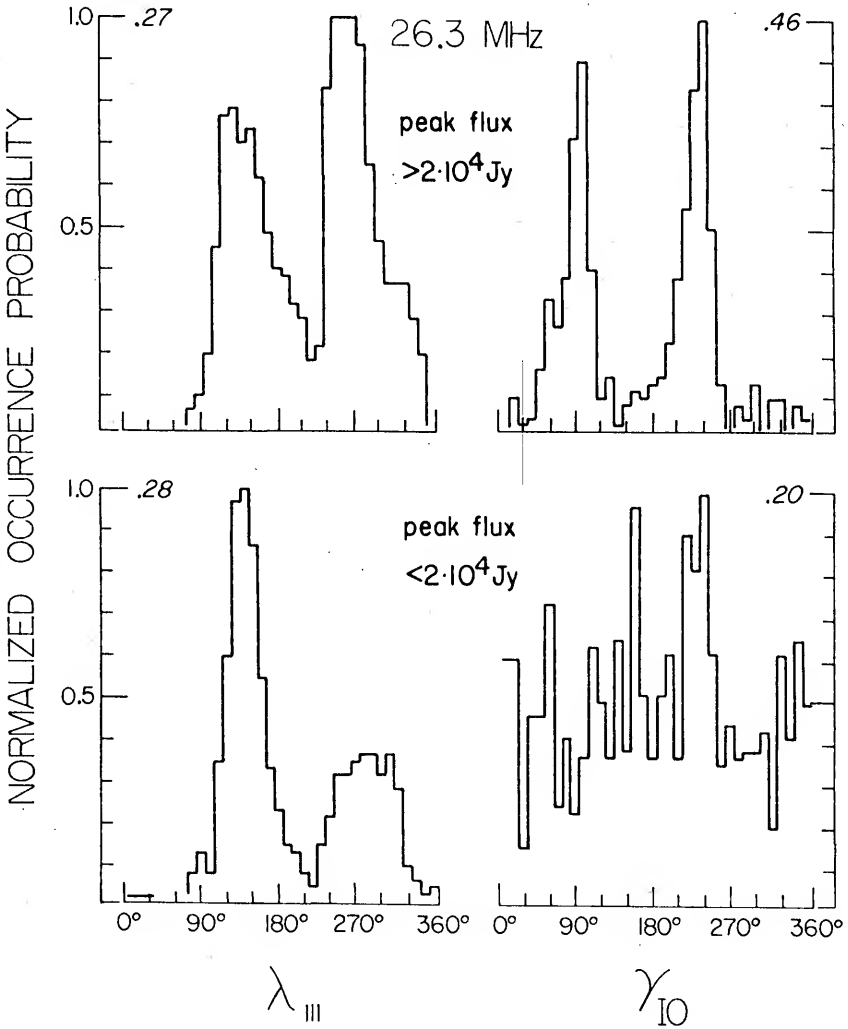

FIGURE V-3. The Variation in Jupiter Activity Is Plotted As a Function of λ_{III} and γ_{Io}. The upper two profiles are derived from the high intensity component and the lower two from the low intensity component. The scaling factors for conversion between normalized and absolute occurrence probabilities appear at the top of each ordinate grid. Data from both the 1973/74 and 1974/75 apparitions are included.

Examining first the rotation phase histograms, it is evident that Source B ($90^{o} \leq \lambda_{III} \leq 210^{o}$) and Source A ($230^{o} \leq \lambda_{III} \leq 310^{o}$) are very well defined in both the high intensity and low intensity plots. It is significant that there are only minor differences between the signatures of the two major Jovian sources. With regard to these differences we note that at low flux levels Source B accounts for a greater portion of the total activity, whereas Source A dominates the high intensity component. Source C ($310^{o} \leq \lambda_{III} \leq 30^{o}$) is not evident as a distinct source in either plot, which agrees with most studies indicating an upper limit to C emission in the neighborhood of 26 MHz (Wilson *et al.* 1968). In addition, even with the sensitivity achieved in this study, the "null" region ($0^{o} \leq \lambda_{III} \leq 70^{o}$) is nearly devoid of activity. Only a few events, never exceeding about 1,000 Jy, have been recorded. Stone *et al.* (1964) failed to detect any activity in the null region exceeding a system threshold of about 500 Jy.

It is evident from Figure V-3 that the Io phase histograms are strikingly different. The high intensity profile yields significant Io modulations at 90^{o} and 240^{o} γ_{Io}. As expected, this is quite similar to previous studies made at 27 MHz (*e.g.* Register 1968; Leacock 1971). The signature of the low intensity component appears quite random however. In fact, there are no statistically significant enhancements present; the highest peak exceeds the mean activity level by only 1.5 σ. Clearly,

limited to this body of data alone it would be rather impossible to identify the otherwise unmistakable Io effect.

This result concerning the γ_{Io} intensity behavior might have been anticipated based upon a not too unreasonable extrapolation of certain previous investigations. Flux density studies conducted at frequencies where non-Io emission is more abundant (Dulk and Clark 1966; Miller and Smith 1973) have consistently shown the Io-related activity to be the more intense. Nonetheless, the mere existence of such a large proportion ($\sim$50%) of Io-independent activity at 26.3 MHz was most surprising in view of the fact that Io-related storms have previously been observed to constitute nearly all the high frequency decametric emission (*e.g.* McCulloch and Ellis 1966; Wilson *et al.* 1968). Viewed within the latter framework, the results prompted a re-examination of the nature of Io and non-Io-related emission, in particular the dependence of Io control on frequency. Accordingly, after first examining the credibility of the important low intensity data, the consequences of the array results will be explored in greater detail.

There might be some cause for concern that the lack of Io-control exhibited at low flux levels is due either to insufficient sampling or to misidentification of the weak activity. Either case could result in an apparent dilution of the observed Io modulation. Neither condition applies however. With regard to the size of each body of data, the high and low

intensity components contained 55% and 45% of all of the recorded activity, respectively. Thus, they each carry nearly equal statistical weights. Regarding the second possible problem, consistent misidentification of the weak emission would affect not only the γ_{Io} profile, but also the λ_{III} profile. Yet remarkably the Jovian sources clearly retain their identities (or lack thereof in the case of C and null) at both intensity levels. Therefore, confident as to the reliability of the λ_{III} and γ_{Io} morphology, the implications of the observed behavior will be discussed.

It was noted initially that the rotation phase profiles are independent of flux density, at least to first order. The leading edges and centroids of the sources exhibit only minor variations at widely separated intensity levels. This tendency for the λ_{III} signatures to persist practically unchanged over so wide a range of intensities strongly implies that the rotation phase modulation may be of primary importance in determining the emission mechanism. This point is stressed because of the emphasis in the past several years which has been placed on explaining Io's role in the radiation process. Notwithstanding the intriguing aspects of the various Io-related phenomena, the fixed behavior of the rotation phase modulation suggests that it is of a more fundamental nature. Conceptualizing the problem in this way is especially compelling, particularly in view of of the Jovianlike nature of the terrestrial

kilometric radiation (Gurnett 1974) which, we note, occurs entirely without the benefit of any satellite interaction.

Before plunging into the consequences of the γ_{Io} morphology, we note in passing that the flux-independent character of the λ_{III} modulation is also of interest regarding System III rotation period (τ_{III}) measurements. Specifically, we consider the case in which the period is determined through the comparison of histograms made approximately 12 yr apart (Section I-1). The method should be highly tolerant of long-term systematic gain variations since the rotation phase profiles are independent of the flux density levels being sampled. As the longitude profiles are highly dependent upon observing frequency, this point further encourages the use of single-frequency data in determining τ_{III}, as opposed to the multifrequency approach which is sometimes used.

In contrast to the nearly unalterable λ_{III} modulation, the modulation of the radiation by Io is observed to be a rather pronounced function of the intensity level which is sampled. Control by Io is rather conspicuous for its absence at low flux levels. Herein lies the source of bias anticipated both in Section I-3 and in the preface to this section. Namely, the degree of Io modulation assigned to a particular set of data will depend to a large measure upon the threshold sensitivity of the radiometer system being employed. Thus, if the radiometer sensitivities are relatively uniform over the decameter range

(as they are), then one concludes that the degree of Io modulation apparent at a particular frequency will be free of bias, and should then represent a statistically and physically significant parameter of the emission. This happy situation prevails subject to one important qualification: the flux density spectrum of the emission must also be uniform. As has been discussed (Section I-1 and Figure I-2), Jupiter's decametric power spectrum is anything but uniform. Hence the selection effect, and hence the source of the statistical biasing of the data. The following hypothetical situation illustrates the major thrust of the argument.

A radiometer operating at 30 MHz, having a threshold sensitivity characteristic of those usually employed in the synoptic monitoring programs, will record significantly less radiation than a similar system operating at, say, 10 MHz. Indeed, the 30 MHz system will detect only the most intense bursts, precisely the emission which is most closely associated with Io. On the other hand, the 10 MHz system is capable of detecting a much greater proportion of the weaker, non-Io-related radiation, simply owing to the nature of the power spectrum of the emission. Consequently, in agreement with observations, a high degree of Io-control is observed at 30 MHz and relatively little Io modulation appears at 10 MHz. These observations have led to the conclusion that Io-control of the radiation diminishes with decreasing wave frequency, a conclusion which

we suggest is due primarily to a selection effect resulting in strong statistical biasing of the data.

The possibility of statistical bias entering into deductions regarding the frequency-dependent nature of the Io effect is of more than incidental concern. No fewer than three major theories of the decametric emission (Goldreich and Lynden-Bell 1969; Goertz 1973*b*; Smith 1973) have incorporated within their framework mechanisms accounting for the apparent effect. If the observations were shown to stem entirely from a selection-effect phenomenon such as the one described here, then a long-accepted constraint on the emission mechanism will have been relaxed.

Of course it is still entirely possible that the abundance of non-Io-related emission observed at low decametric frequencies (10-15 MHz) is due to a genuine relinquishing of control by Io. The hypothetical situation described above is merely a plausible--not a proven--exposé because in creating a situation in which a statistical bias is operating, we have *a priori* attributed to the low frequency radiation the same morphology found to be in effect at 26.3 MHz. Specifically, it has been assumed that the intensity-dependent dichotomy between Io- and non-Io-modulated radiation applies equally well over the entire decametric spectrum. This assumption is in fact no less than a necessary and sufficient condition for eventually attributing the observed frequency dependence of Io-control to

a selection effect. Consequently, further development of the argument must await determination of the extent to which the 26.3 MHz morphology prevails at other decametric frequencies. In addition, it is clear that RAE-1 measurements of the degree of Io modulation appearing at frequencies well below 10 MHz should be timely and indeed crucial. Hence we will postpone the quantitative evaluation of the parameters necessary for establishing the selection-effect hypothesis until after the RAE-1 results have been presented in Chapter VI. For the time being, we continue our analysis of the 26.3 MHz data.

V-3. TWO-DIMENSIONAL ANALYSIS

In Figure V-3 it was apparent that there is considerable low intensity radiation associated with Source B. We can further deduce that nearly all of this radiation must be non-Io related because the data set from which the low intensity λ_{III} profile was generated was the same body of data used to generate the Io-independent histogram. A two dimensional analysis of the activity showing the explicit dependence on the λ_{III} and γ_{Io} coordinates will further clarify this situation.

The occurrence of listening and activity periods in the λ_{III} - γ_{Io} plane are shown in Figure V-4. The "time-line" format has been chosen for displaying the data.[3] Monitoring of the

---

[3] Since each time-line traces the instantaneous λ_{III} - γ_{Io} phase from beginning to end of a single observing or activity

FIGURE V-4. Time-Line Plots of the Observing (Top) and Activity (Bottom) Intervals As a Function of Rotation Phase (λ_{III}) and Io Phase (γ_{Io}). All 26.3 MHz data from the 1973/74 and 1974/75 apparitions are included.

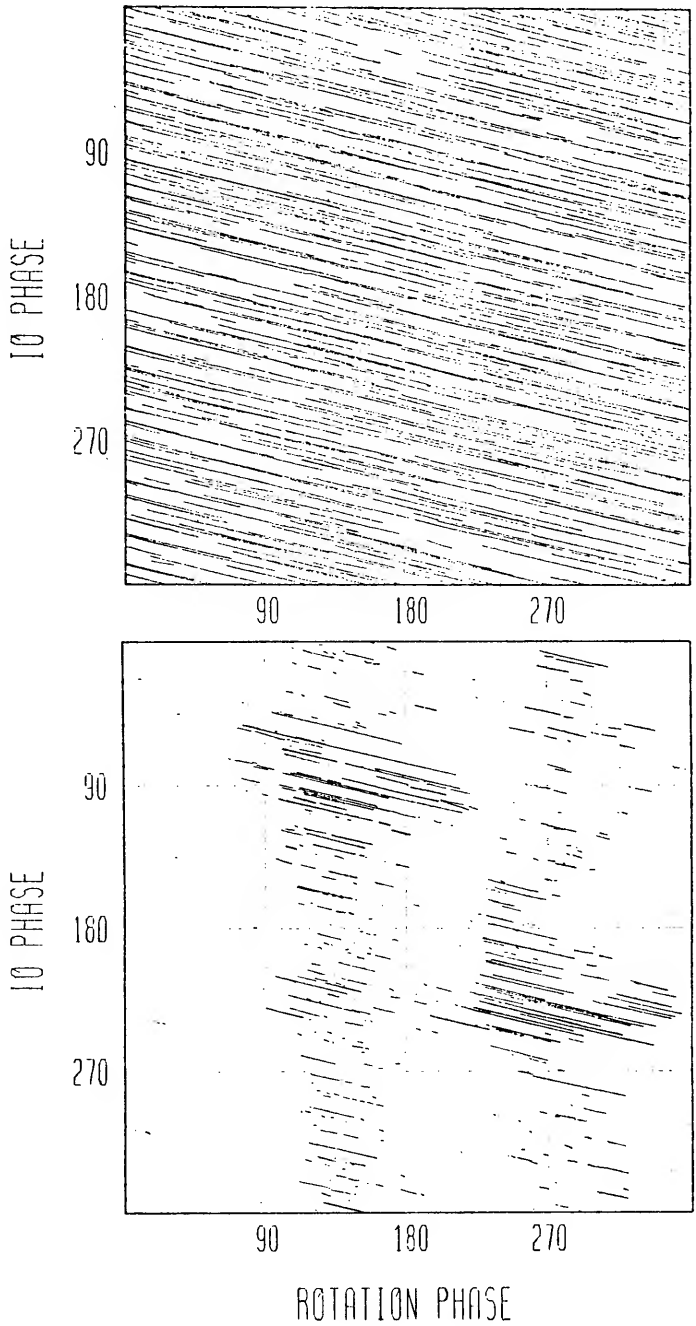
IO PHASE
90
180
270
90
180
270
IO PHASE
90
180
270
90
180
270
ROTATION PHASE

λ_{III} - γ_{Io} plane has been fairly uniform, as is evident from the listening plot (upper part of Figure V-4). It is certainly adequate for noting, as we shall, the coarse-grain behavior of the emission (lower plot). The most striking feature displayed, as first reported by Desch *et al.* (1975), is the extent of Source B along the Io coordinate. This result is to be anticipated, of course, following the above discussion; nevertheless the appearance of the non-Io-B emission was a totally unexpected product of this investigation for the following reason. While Source A is well known to possess what are generally regarded as individual Io- and non-Io-related components, Source B at the higher decametric frequencies rarely if ever occurs outside the range $\gamma_{Io} = 90^{o} \pm 30^{o}$. Indeed, not until very recently (Bozyan and Douglas 1976) has non-Io-B been recognized as a distinct source even at the lower decametric frequencies where non-Io-emission is generally more abundant. It now appears that the non-Io-B emission is well established over a frequency range extending from at least 16 to 26 MHz.

One might well be impelled to ask whether the Io-C source has a non-Io counterpart as do A and B. In fact, Bozyan and Douglas also isolated non-Io-C as a source relatively distinct

---

interval, it most nearly represents the true behavior of the emission. More sophisticated averaging and contour plotting of the data are not necessary until the time lines have begun to overlap and obscure previous intervals of activity.

from non-Io-A at frequencies near 16 MHz. Commenting on their results, Carr and Desch (1976) noted further that non-Io-C is especially distinguishable from non-Io-A based upon the polarization characteristics of the two sources. It appears then that each Io-related source has its non-Io counterpart. Moreover, the rotation phase centroids of each pair are nearly identical; the Io-related member simply manifests the well-recognized tendency to radiate at a higher overall flux density. Although greatly oversimplified, this description of the Jovian source morphology seems to lend itself to a working model in which the satellite Io, at the properly assigned γ_{Io} position, simply acts to further stimulate emission from the appropriate non-Io source region. Io thus acts to supply an additional source of free energy to encourage the growth of the required plasma instability.[4]

While the details of an "Io enhancement" model are lacking at present, it appears to be a reasonably attractive and sound organizing postulate worthy of further consideration. Caution must be exercised at the outset however. For example, Smith (1976) has noted that if a single emission mechanism (*i.e.* one

---

[4] In what follows we consider the Jovian L-bursts only. As revealed by the high-resolution dynamic spectra (Section I-1 and Figure I-1), the millisecond bursts are of a distinctly different character, and thus they are assumed to be generated in a unique fashion.

which does not involve beaming) is invoked to generate both the Io and non-Io components, then the Io enhancement hypothesis establishes an absolute reference frame (namely that of the observer) with respect to the γ_{Io} coordinate. This is described as a physically preposterous situation, which of course it is. However, by proposing separate mechanisms for each Io and non-Io component, the strong beaming of the Io-controlled emission can be reintroduced. The problem of an observer-defined morphology is then eliminated. The perplexing question then arises as to how the two mechanisms are coupled so as to explain the coincidence of the source-pair positions in the λ_{III} coordinate. While not treating this specific question directly, Cavaliere and Speranza (1971) proposed a model which retained the spirit of an Io enhancement mechanism, but which avoided the problem of an observer-defined morphology. Unfortunately, the model does fail at a key juncture, as will be demonstrated. In so doing, another singularly difficult aspect of the Io enhancement hypothesis is revealed.

Based on data obtained below about 25 MHz, the model of Cavaliere and Speranza associates two Jovian "surface anomalies" with the λ_{III} centroids of Sources A and B. In addition to being capable of radiating independently of Io, each source is subject to considerable enhancement when it sweeps past the foot of Io's magnetic flux tube (IFT). Accordingly, the model requires that the sub-Io longitude (λ_{Io}) during Io-controlled A

and B storms be equal to the System III longitudes of Sources B and A respectively. For example, Io-B activity is presumed to occur when the surface anomaly associated with Source A sweeps past the IFT. This predicts that the active sub-Io longitude ($\lambda_{Io} = \lambda_{III} - \gamma_{Io} + 180^{o}$) is equal to approximately 270^{o}, that is, equal to the λ_{III} centroid of Source A (Figure V-3). Io-A emission then occurs when the Source B anomaly sweeps past the IFT, giving $\lambda_{Io} = 140^{o}$. If the 26.3 MHz Io-related data is plotted as a function of λ_{Io}, these predictions are immediately subject to a test. There should be two peaks in the histogram: one corresponding to the Source-A sweep ($270^{o}\lambda_{Io}$) and the other to the Source-B sweep (140^{o} λ_{Io}). That these predictions fail is evident from Figure V-5. There is primarily only a single active sub-Io longitude (due to the superposition of the Io-related Sources A and B), located at 225^{o} λ_{Io}. This longitude, which is between the two predicted by Cavaliere and Speranza, is more closely associated with the meridian toward which Jupiter's north magnetic pole is tipped.

Clearly, the observed morphology does not lend support to the rather direct interaction scheme envisioned by Cavaliere and Speranza. Hypothesizing that the non-Io source regions are coupled to Io through the IFT appears to be untenable. Moreover, even if a clever geometry were devised to explain the observed morphology at one frequency, it would fail at any other frequency because, as we mentioned somewhat earlier, the λ_{III}

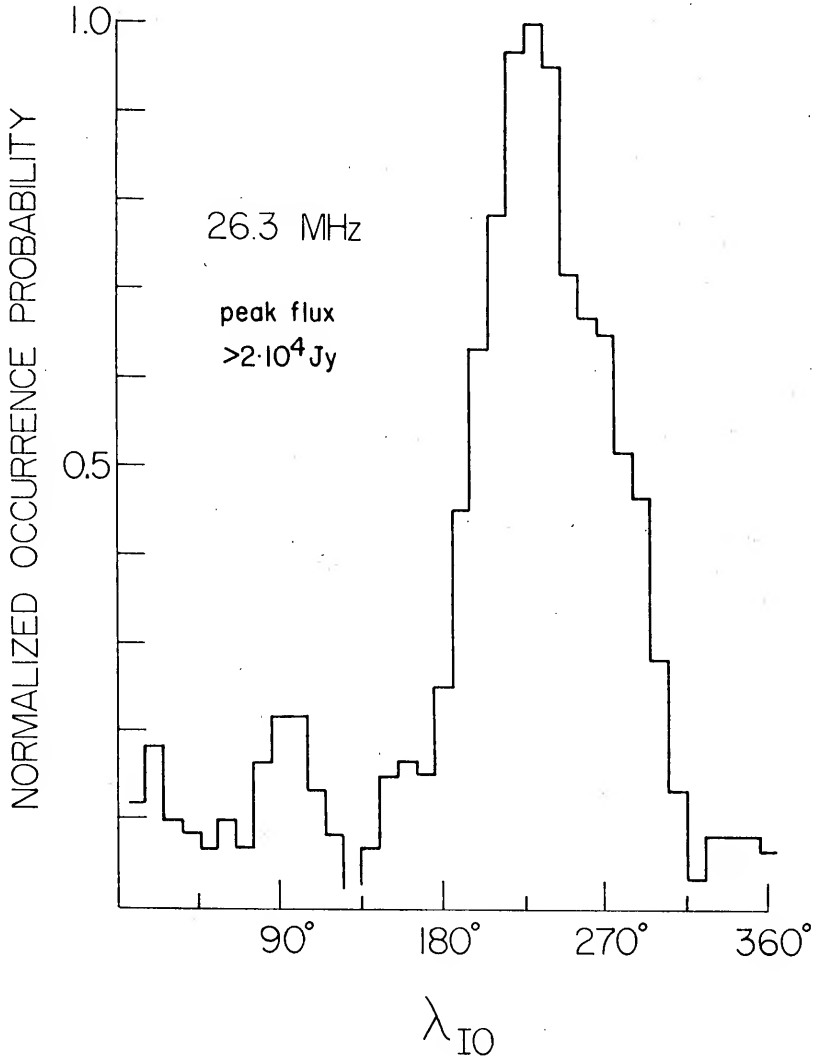

FIGURE V-5. The Variation in the Io-Related Component (Peak Flux Exceeding 2 x 10^4 Jy) of Jovian Activity Is Plotted As a Function of the Sub-Io Longitude λ_{Io}.

centroids are highly frequency dependent. It is important, then, in considering any prospective model of the decametric radiation, to examine the changes in the morphology that occur with frequency. To this end, the RAE-1 results obtained at frequencies below 8 MHz are presented in the next chapter.

VI

THE RAE-1 OBSERVATIONS

Science is built up with facts, as a house is with stones. But a collection of facts is no more a science than a heap of stones is a house.
--Jules Henri Poincare

THE RESULTS PRESENTED in this chapter have been obtained by means of the data-processing methods described in Chapter IV. However, the computer identification of "upper-V-only" events has not been used because it was found to be unreliable at the lower frequencies. All of the data has now been reduced in a uniform fashion using only the visual identification of Jupiter activity. Additionally, the original body of data (26 Feb 69 to 12 May 69) has been supplemented at frequencies between 1310 kHz and 6550 kHz inclusive. This was achieved through the analysis of microfilm covering the periods extending 44 days before and 9 days after the initial 3-month interval of study. No useful information was obtained from the microfilm which covered the period from 22 May 69 to 3 July 69 because the RV receivers were locked in the calibration mode. This new data set is thus larger

than that used in Chapter IV to establish the pointing accuracy of the upper-V antenna, and it is also larger than that originally reported on by Desch and Carr (1974; their Table 1). Table VI-1 summarizes the overall observing and activity statistics. It is from this body of data that the observations presented in this chapter have been drawn.

With reference to Table VI-1, the number of hours of observing and activity from 4700 to 1310 kHz differ from those reported by Desch and Carr. This is due to the expanded observing period and also due to the transformation from computer to visual analysis of the data. The latter modification has resulted in an overall reduction in the total observing time at 3930 and 4700 kHz relative to that reported by Desch and Carr because the computer was generally less critical than the human reader with regard to the appraisal of what constituted interference-free observing time. Otherwise, the statistics at 900 kHz and below are unchanged. Of interest is the occurrence probability of activity reported in the last two columns of Table VI-1. A general trend in the probabilities as a function of frequency is immediately apparent and will be discussed more fully in the next section.

VI-1. THE OCCURRENCE PROBABILITY SPECTRUM

The probability of detecting Jovian emission at any given frequency is a function of radiometer sensitivity. Hence, a statistically meaningful comparison of the occurrence probabilities

TABLE VI-1. Overall RAE-1 Statistics.

Freq kHz	*Observing Interval 1969*	*Observing Hours*	*Activity Hours*	*Occurrence Overall*	*Probability Above 7 x 10^5 Jy*
6550	13 Jan to 21 May	111.0	5.8	0.053	0.044
4700	13 Jan to 21 May	206.1	9.7	0.047	0.029
3930	13 Jan to 21 May	276.1	11.5	0.042	0.024
2200	13 Jan to 21 May	712.6	12.2	0.017	0.010
1310	13 Jan to 21 May	684.3	21.2	0.031	0.009
900	26 Feb to 12 May	389.4	10.5	0.027	0.005
700	26 Feb to 12 May	285.1	6.3	0.022	0.016
450	26 Feb to 12 May	62.9	1.2	0.020	0.004

at two or more frequencies can be made only if the results are referred to some standard threshold flux density level. On this basis, the first determination of the probability spectrum of Jovian emission at low frequencies has been made. A flux-density threshold was chosen based upon the sensitivities at each of the RAE-1 channels as derived from the calculated values of A_e^* (Chapter IV). Obviously, the threshold must be large enough that each radiometer channel is capable of detecting radiation at that level. For this reason, a value of 7×10^5 Jy was chosen, as this figure is at or above the detection threshold of every RAE-1 channel.

The occurrence probabilities as calculated in the above manner are illustrated in Figure VI-1. Groundbased (Florida) data available during the 1969 apparition have been included for comparison; the same flux density threshold of 7×10^5 Jy was applied. It is perhaps not surprising that the groundbased probability points appear to behave in much the same manner as the peak flux density spectrum (Figure I-2). This could be expected to occur because if a single threshold is used, then the resulting occurrence probabilities reflect the already-known fact that high-intensity activity is much less abundant at the higher decametric frequencies. Hence, we may expect that the RAE-1 probability curve, which exhibits a pronounced decline with decreasing frequency, offers a clue as to the behavior of the low-frequency extension of the flux-density spectrum.

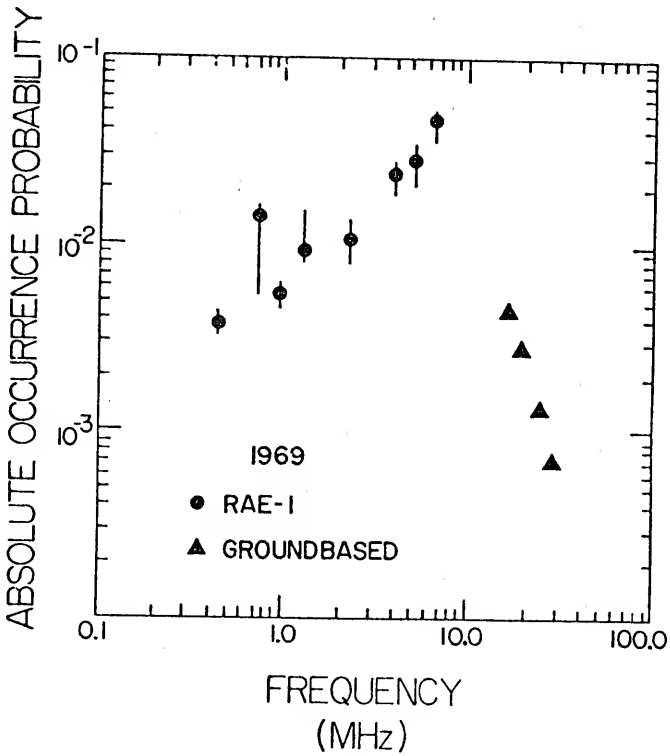

FIGURE VI-1. The Absolute Occurrence Probability of Jovian Emission Exceeding a Threshold Intensity of 7×10^5 Jy Is Plotted As a Function of Frequency. The ground-based data are derived from University of Florida observations made in 1969 at frequencies of 15, 18, 22, and 27 MHz. Error limits on the spacecraft observations are due to uncertainties in assigning absolute flux densities to the RAE-1 events.

Unfortunately, the RAE-1 occurrence probabilities could not be examined in the same manner that the 26.3, 10, and 8.9 MHz data were (Section V-1). This is due to the fact that the RAE-1 detection thresholds exhibited rather extreme variability relative to the peak flux density values appearing at each frequency. For example, while the minimum detectable flux densities at 8.9, 10, and 26.3 MHz were each approximately three orders of magnitude below their respective peak flux densities, the RAE-1 detection thresholds varied between approximately a factor of 2 and a factor of 100 below the peak intensities. This extreme range of flux-density sampling clearly discourages the sort of analysis described in Section V-1. Consequently, one must caution that the occurrence probabilities shown in Figure VI-1 only reflect the behavior of activity exceeding 7×10^5 Jy. Given sufficiently sensitive observations in the hectometer range, the occurrence probabilities might be expected to approach the near-continuous level observed by Dulk and Clark (1966) at 10 MHz.

VI-2. THE FLUX DENSITY SPECTRUM OF THE EMISSION

For many years one of the major questions concerning Jupiter's decametric radiation has been the behavior of the power spectrum at frequencies below 10 MHz. Above 10 MHz, the mean and peak flux-density spectra were established by Carr *et al.* (1964) based upon extensive analysis of groundbased measurements (Figure I-2). These important observations have already been discussed,

particularly with reference to the possibility of a selection effect resulting from the steep nature of the spectrum. In attempting to extend the measurements below 10 MHz, Carr *et al.* reported a tentative value of 1.8×10^7 Jy for the peak flux density of 5 MHz radiation. This figure indicated a possible turning over of the spectrum, suggesting a peak in the curve somewhere between 5 and 10 MHz. However, in disagreement with the report of Carr *et al.*, observations made by McCulloch and Ellis (1966) at 4.7 MHz indicated that the spectrum continued to increase at frequencies below 10 MHz. This behavior was rendered even more plausible by the work of Slysh (1966). Using the Zond 3 and Venera 2 earth-orbiting spacecraft, Slysh reported the detection of continuous emission from Jupiter at 200 kHz. The measured flux density was in excess of 2×10^8 Jy. If true, this would imply that the groundbased observations represented only a small fraction of the total radiated power of the planet.

The RAE-1 observations marked the first attempt to identify Jovian emission from a satellite possessing a directive antenna. Motivated by Slysh's account of extremely intense, continuous radiation from Jupiter at 200 kHz, Weber and Stone (1970) attempted to distinguish between the planet and background noise by examining RAE-1 records at a time when Jupiter was being occulted by the moon. Clearly, if Jupiter were a continuously radiating source, the disappearance and reappearance of that source would provide a convenient method of establishing power

levels at all RAE-1 frequencies. Unaccountably, no indication of an occultation event appeared. It had become evident that (i) either Jupiter was emitting radiation sporadically (as at the higher frequencies), or (ii) the emission was not nearly as intense as the results of Slysh had indicated, or (iii) both. That condition (iii) actually obtained was finally shown to be the case by Desch and Carr (1974).[1]

Figure VI-2 illustrates the power spectrum as derived by Desch and Carr at frequencies between 450 and 4700 kHz and by Carr *et al.* at the higher frequencies; the 6550 kHz point was established later as reported by Carr and Desch (1976). Using the antenna-gain figures derived in Chapter IV, the peak flux density of each Jupiter storm was calculated and the flux densities of the three most intense storms at each frequency were averaged to obtain the peak-power spectrum shown in the figure. Also included for comparison is the spectrum derived by Brown (1974) using IMP-6 data. Brown's result confirmed the general spectral behavior reported by Desch and Carr, but the spectrum also showed an occasional tendency for a second peak in the emission

---

[1] The rather conspicuous problem of accounting for the 200-kHz measurement of Slysh was resolved shortly after the lunar-occultation study of Weber and Stone. Based upon additional satellite measurements, Grigoreva and Slysh (1970) showed that the radiation was probably of terrestrial origin, that is, terrestrial kilometric radiation.

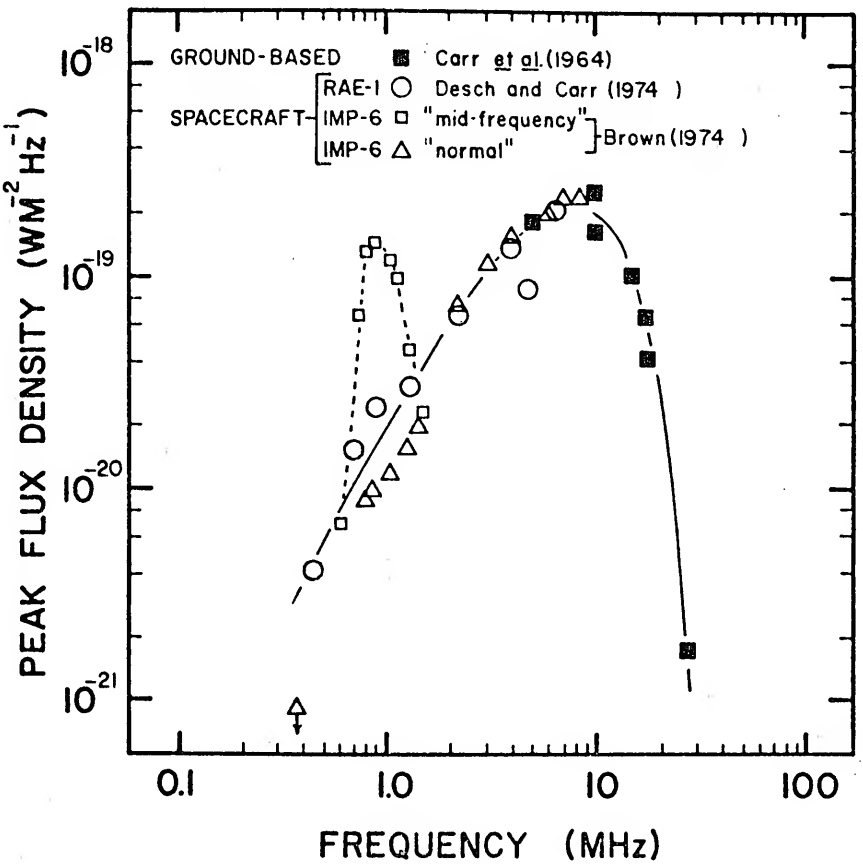

FIGURE VI-2. The Peak Flux Density Spectrum of Jovian Emission from Various Sources Is Illustrated Between 450 kHz and 27 MHz.

to occur in the neighborhood of 1 MHz. Concerning this latter observation, Carr and Desch have noted that none of the RAE-1 data exhibit such behavior and that the IMP-6 observations could be due to the fact that the observing frequencies are much more closely spaced in comparison with RAE-1.

The principal peak in the spectrum occurs at 8 MHz. The curve is down by a factor of 10 at 1 MHz and 21 MHz. The field strength in the Jovian magnetosphere where the most intense radiation occurs is thus about 3 Gauss if radiation is emitted close to the electron gyrofrequency, or somewhat less if radiation occurs at the upper hybrid frequency (Smith and Wu 1974). In either case, the fact that the peak in the spectrum occurs at one-fifth the upper cutoff frequency (40 MHz) suggests that the field strength at the location of the strongest emission is roughly one-fifth the strength of that at the planetary surface, and that this location is at about 1.7 radii from the center of the magnetic dipole (assuming an inverse cube variation of the field with distance).

Spacecraft observations have now permitted the delineation of the flux-density spectra, not only of Jupiter but also the earth (Kaiser and Stone 1975), Saturn (Brown 1975), and possibly also of Uranus (Brown 1976). The peak of each spectrum occurs at a different frequency, and yet the shapes of the individual spectra are all rather similar. In examining this information, Alexander (1976) has commented on the remarkable agreement

between the ratio of the spectral peak frequency of earth and Jupiter, and the corresponding ratio of their polar magnetic field strengths. Furthermore, if the spectral peak frequencies of Saturn and Uranus are understood to be representative of *their* polar magnetic field strengths, then the magnetic dipole moments of all four planets are obtained--the moments of Jupiter and earth are already known, those of Saturn and Uranus are predicted based upon their respective spectral behavior. One purpose of making such comparisons is in ultimately relating the magnetic dipole moment of each planet with its known angular momentum. Incredibly, in spite of the assumptions made concerning Uranus and Saturn, the relationship is quite linear, as illustrated in Figure VI-3 which is taken from Alexander. Although not a recognized source of radio emission, the planet Mercury is also included.

The possible implications of this simple but straightforward demonstration are startling. The uncomplicated interdependence between angular momentum, magnetic dipole moment, and spectral behavior suggests the existence of a unifying principle of magnetic dynamo mechanics threading four otherwise vastly dissimilar planetary bodies. With special regard to the subject matter of the present work, the association between the spectral behavior and magnetic moments of the planetary emitters further suggests the operation of similar emission mechanisms, at least insofar as the frequency at which the radiation takes place.

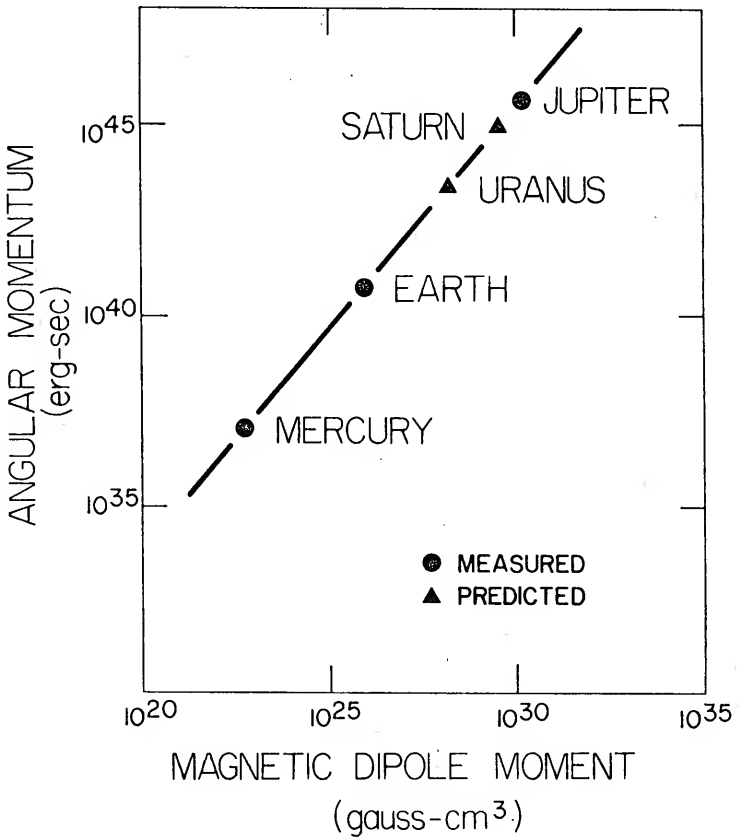

FIGURE VI-3. A Comparison of the Angular Moments and Magnetic Dipole Moments of the Three Known (Earth, Jupiter, Saturn) and One Possible (Uranus) Low-Frequency Radio Emitters. Mercury is included for comparison. (Adapted from Alexander 1976.)

VI-3. ROTATION-PHASE AND IO-PHASE MODULATIONS

In Chapter V we saw that the 26.3 MHz rotation phase profiles were clearly defined and had peaks at 140^{o} λ_{III} (Source B) and 270^{o} λ_{III} (Source A). Of equal importance was the fact that the "null" region (toward which Jupiter's south magnetic pole is tipped) was almost completely devoid of activity. It is understood that one cannot expect to observe the same rotation-phase morphology at lower frequencies. Many studies (*e.g.* Lebo 1964; McCulloch and Ellis 1966) have stressed the gradual evolution of the source regions in the λ_{III} coordinate as the observing frequency is changed. Besides showing that the sources undergo a shift in longitude, the studies have also demonstrated a general decline in the degree of rotation-phase control with decreasing frequency. For example, the rotation-phase profile obtained by Dulk and Clark (1966) at 10 MHz was nearly featureless except for a pronounced dip in the occurrence probability in the range $80^{o} < \lambda_{III} < 180^{o}$. This of course is almost precisely the System III longitude extent of Source B as seen at higher frequencies. The signature derived by Lebo at 10 MHz displayed a higher degree of rotation-phase control while retaining the anticorrelation with Source B seen by Dulk and Clark. It is notable that Lebo's observations were made with a relatively insensitive system compared with that of Dulk and Clark. This suggests that at the lower frequencies a significant correlation with rotation phase becomes apparent only when the more intense activity is

recorded. With respect to modulations in the γ_{Io} coordinate, we have already commented on the reduced extent of Io-control which has invariably been observed at lower decametric frequencies. In summary, various investigations have supported the notion that the rotation-phase and Io-phase modulations become considerably less pronounced as the frequency is reduced. With this rather sketchy development in mind, we proceed to examine the spacecraft-derived morphology.

In Figures VI-4 through VI-7 the occurrence probability of activity is plotted both as a function of the System III (1957.0) longitude and of Io phase at frequencies between 6550 and 450 kHz. The occurrence probabilities are calculated in the usual manner by dividing the amount of activity time by the observing time which occurs over a specified extent of Io or rotation phase. In both figures the histograms are divided into eighteen 20^{o}-wide zones. Unlike the procedure followed originally by Desch and Carr (1974), the histograms have neither been smoothed nor weighted by storm duration or intensity.

ROTATION-PHASE MODULATIONS

Comparing the λ_{III} histograms in Figures VI-4 through VI-7 with those derived at 26.3 MHz (Figure V-3), it is evident that the low-frequency rotation-phase modulation is rather indistinct; no source regions are readily apparent. It was thought at first that the random appearance of the System III profiles was

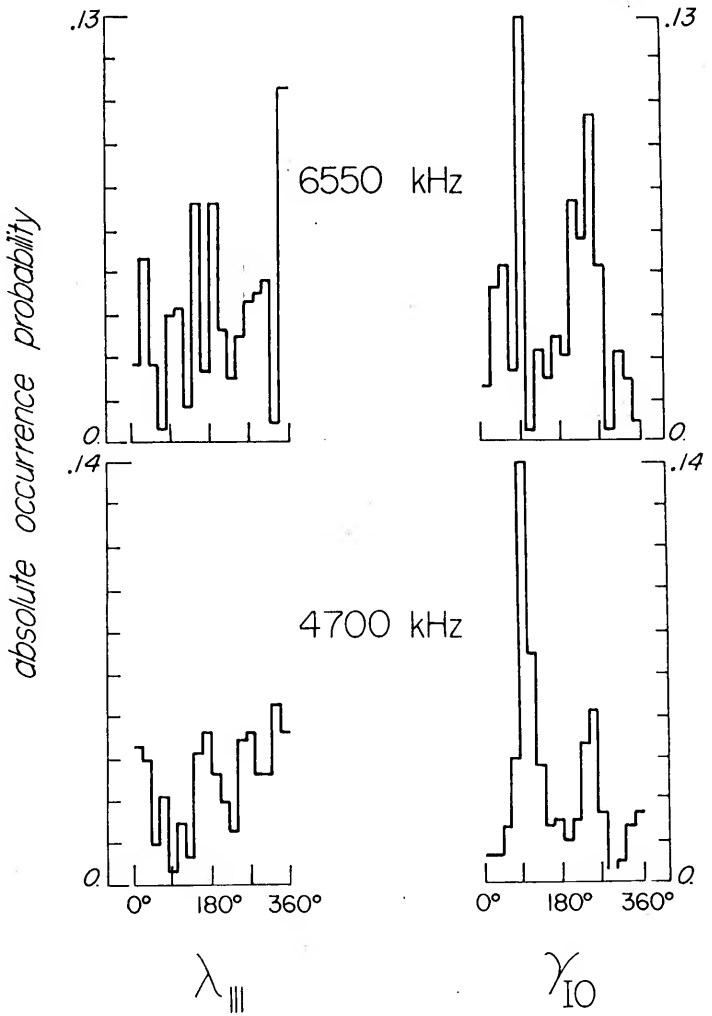

FIGURE VI-4. The Absolute Occurrence Probability of Jovian Emission Is Plotted As a Function of λ_{III} (1957.0) and γ_{Io} at 6550 and 4700 kHz. See Table VI-1 for dates.

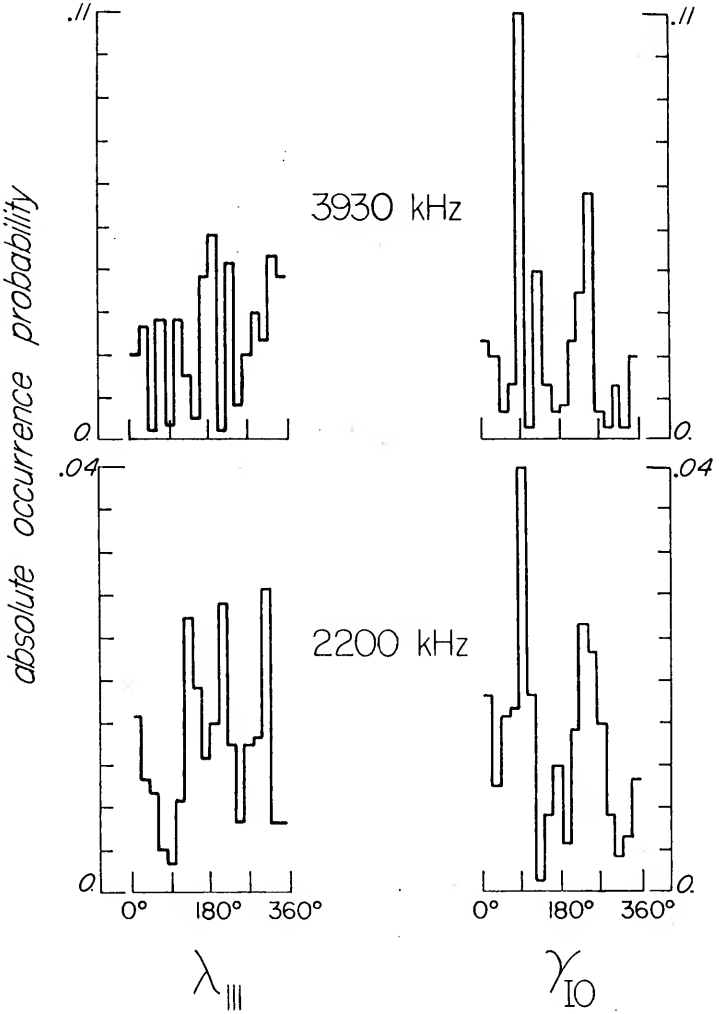

FIGURE VI-5. The Absolute Occurrence Probability of Jovian Emission Is Plotted As a Function of λ_{III} (1957.0) and γ_{Io} at 3930 and 2200 kHz. See Table VI-1 for dates.

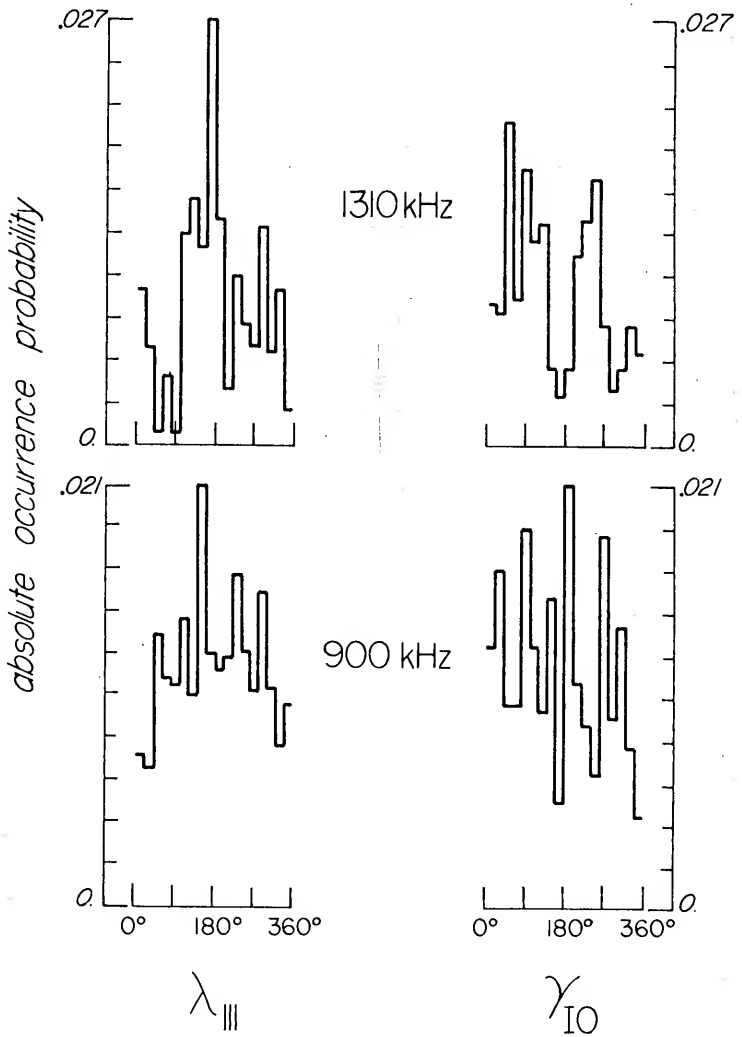

FIGURE VI-6. The Absolute Occurrence Probability of Jovian Emission Is Plotted As a Function of λ_{III} (1957.0) and γ_{Io} at 1310 and 900 kHz. See Table VI-1 for dates.

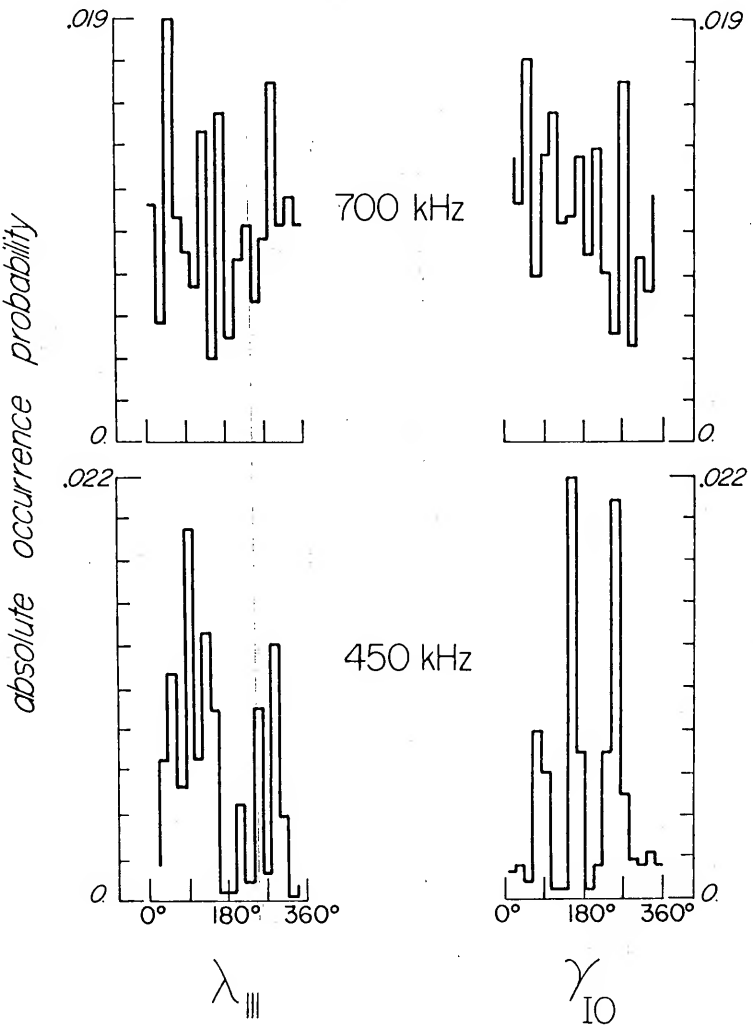

FIGURE VI-7. The Absolute Occurrence Probability of Jovian Emission Is Plotted As a Function of λ_{III} (1957.0) and γ_{Io} at 700 and 450 kHz. See Table VI-1 for dates.

due to the combined effects of inadequate sampling and slight contamination of the data by interference. Thus, in order to enhance the presence of any sources which might be present, Desch and Carr weighted the data according to the duration of the recorded activity and then smoothed the resultant histograms. This procedure emphasized the longitude regions associated with the more enduring (and hence more intense) activity. In particular, Desch and Carr noted a tendency for the emission at 2200 kHz and above to occur in association with the longitudes toward which Jupiter's north and south magnetic poles are tipped.[2] At 1310 kHz only emission associated with the north magnetic pole was apparent; below this frequency the System III morphology was less certain.

While the procedure followed by Desch and Carr of weighting and smoothing is statistically justified, it now appears that the original premise that the data were contaminated and inadequately sampled was quite incorrect. Subsequent examination of the modulation of the emission by Io, to be discussed presently, has shown that it is more likely that the data, at least above 900 kHz, is of reasonably high quality in a statistical sense. This implies that the generally observed lack of rotation-phase control reflects the true nature of the emission. That is, the unweighted and

---

[2] For the epoch of the observations (1969.3) the north and south magnetic poles were tipped toward 210^{o} and 30^{o} λ_{III} respectively (Mead 1974).

unsmoothed λ_{III} profiles appearing in Figures VI-4 and VI-5 are truly representative of the low-frequency behavior.

Confidence in discussing this morphology is greatest at the four frequencies where the highest quality data were recorded, namely at 6550, 4700, 3930, and 2200 kHz. At each frequency in Figures VI-4 and VI-5, the λ_{III} and γ_{Io} plots are drawn to the same absolute scale, thus permitting direct comparison between the degrees of modulation present in each coordinate. In every case the correlation of the activity with rotation phase is less than that with Io phase. This is particularly striking at 4700 kHz. The activity at each frequency appears to be almost randomly distributed throughout rotation phase, reminiscent of the low-intensity Io-phase signature seen at 26.3 MHz (Figure V-3). While not shown explicitly in this section (we defer until Section VI-4 the intensity-weighted morphology), it is only when duration or intensity weighting occurs that moderately defined source regions begin to appear. This was also the behavior we noted previously in comparing the results of Lebo and of Dulk and Clark at 10 MHz. One can only conclude that the trend toward a relinquishing of rotation-phase control, which was established first by studies conducted in the 10 to 15 MHz range, is further substantiated here.

At frequencies below 2200 kHz the situation is somewhat more confused. At 1310 kHz the rotation-phase modulation is more pronounced than the Io-phase modulation, with an enhancement

near 190^{o} λ_{III} apparent even without intensity weighting of the data. At 900, 700, and 450 kHz the activity lacks any obvious correlation with either rotation phase or Io phase. Of course it is difficult to draw any but the most tentative conclusions concerning this portion of the RAE-1 data. The total amount of activity identified as Jovian is small and subject to a higher probability of contamination as a result of intense terrestrial kilometric interference. Any inferences drawn from this study will therefore be based upon the higher frequency (>1310 kHz) morphology.

SATELLITE MODULATIONS

While the System III rotation-phase profiles are far from well defined and bear little resemblance to those observed at the higher decametric frequencies, the dependence on Io phase is strikingly clear. As is evident in Figures VI-4 and VI-5, Jupiter activity at all frequencies between 6550 and 2200 kHz is highly correlated with the phase of Io. In agreement with groundbased results at higher frequencies, the peak occurrence probabilities are near 90^{o} and 240^{o} γ_{Io} . Such a high degree of Io-control was not anticipated, however, based upon groundbased experience in the 10 to 15 MHz range. At 1310 kHz, while not as well defined as at 2200 kHz and above, the enhancements at 90^{o} and 240^{o} γ_{Io} persist. As we have noted, however, the activity at this frequency seems to be better correlated in the λ_{III} coordinate. Below 1310 kHz there does not appear to be any control by Io.

Before examining further the consequences of the Io correlation displayed here, a few comments are in order with regard to the quality of the data below 2200 kHz. It had appeared at one time, on the basis of the data which were first analyzed at 1310 kHz (26 Feb 69 to 12 May 69), that Io-control of the emission at this frequency had been supplanted by a fairly well defined Europa effect. The single broad peak in the occurrence probability was centered at 180^{o} to 200^{o} γ_{Eu} (departure of Europa from superior geocentric conjunction). Unaccountably, the data from the following year (6 Mar 70 to 9 Jun 70) did not show any correlation with Europa, although the data were considered to be of sufficient quality to show the effect. Thus it was with great interest that the 1310 kHz data derived from the extended period (13 Jan 69 to 27 Feb 69 and 13 May 69 to 21 May 69) were examined. Surprisingly, a marginal degree of Io correlation appeared, while Europa-control of the activity was entirely absent as it had been from the 1970 data. As the extended-period microfilms were read by a data technician other than the individual who had read the original data, it was decided that the 1310 kHz (1969) data set should be re-read in its entirety by the new technician. Special care was taken with regard to avoiding various upper-V channel phenomena which can masquerade as Jupiter activity (see Appendix B).

The result of this reanalysis, namely further evidence of Io-control, has been presented in Figure VI-5. The resulting

correlation with respect to Europa is displayed in Figure VI-8. The four major peaks in the histogram are simply artifacts which are expected as a result of the coupled orbital motions of Io and Europa. Thus, because the period of Europa is almost exactly twice that of Io, each correlation in Io phase will appear also as a correlation in Europa phase at two positions separated by 180^{o} γ_{Eu}. At the mean epoch of the observations (1969.25), the two positions of Europa which obtain at the γ_{Io} coordinates of interest are listed in Table VI-2. This relationship is also explicitly illustrated in Figure VI-8.

TABLE VI-2.

γ_{Io}	γ_{Eu} *(epoch 1969.25)*
90^{o}	168^{o}, 348^{o}
240^{o}	67^{o}, 247^{o}

It is evident from the foregoing that one may have difficulty in drawing reliable conclusions from what, at frequencies below 2200 kHz, is clearly a difficult body of data. In order to formulate a more reliable data set, additional observations are badly needed at hectometer wavelengths.

In summary, a high correlation of activity with Io phase appears conclusive at 6550, 4700, 3930, and 2200 kHz. This was the most startling result of the RAE-1 investigation, forcing a reinterpretation of the many groundbased investigations above 8 MHz which had indicated a pronounced relinquishing of Io-control with decreasing frequency (see *e.g.* Carr and Desch 1976). Strangely enough, though, a groundbased investigation carried out by McCulloch and Ellis (1966) at 4700 kHz indicated a high

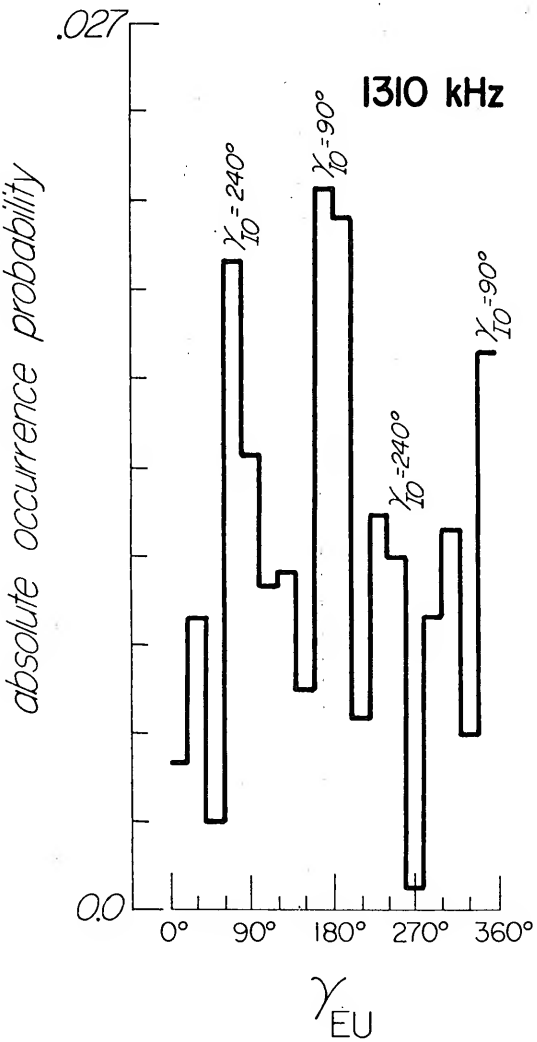

FIGURE VI-8. The Absolute Occurrence Probability of Jovian Emission is Plotted As a Function of γ_{Eu} at 1310 kHz. See Table VI-1 for dates.

degree of correlation with Io. The preferred positions were $120^{o} \pm 20^{o}$ and $250^{o} \pm 10^{o}$ γ_{Io} , quite representative of the normal Io modulation. This result has gone largely unnoticed as the authors originally attached a low confidence level to the data and the result was not included in subsequent theoretical works (*e.g.* McCulloch 1971). Their study, while limited to only 40 hours of effective monitoring (less than one Ioan period), was surprisingly accurate. There is thus at least one other investigation in this frequency range which supports the observations presented here.

In the next section a two-dimensional analysis of the 2200 to 6550 kHz data is presented, and the extent to which the RAE-1 results are consistent with the hypothesis of a flux-dependent Io effect will be discussed further.

VI-4. TWO-DIMENSIONAL ANALYSIS

In Figure VI-9 the observing (top) and activity (bottom) intervals at 6550, 4700, 3930, and 2200 kHz have been illustrated using the time-line format. Since the volume of data at any one frequency was rather small, the four most reliable RAE-1 channels have been combined in a single body of data. As opposed to merging the listening and activity times prior to plotting the data, the time-lines at each frequency have been independently superposed on the figure. Heavy lines were used for storms whose peak flux density was within a factor of five of the peak power spectrum of the emission (Figure VI-2). This of

FIGURE VI-9. Time-Line Presentation of Observing and activity intervals in the λ_{III} - γ_{Io} Plane. Data at 6550, 4700, 3930, and 2200 kHz have been merged. See text for explanation of heavy lines.

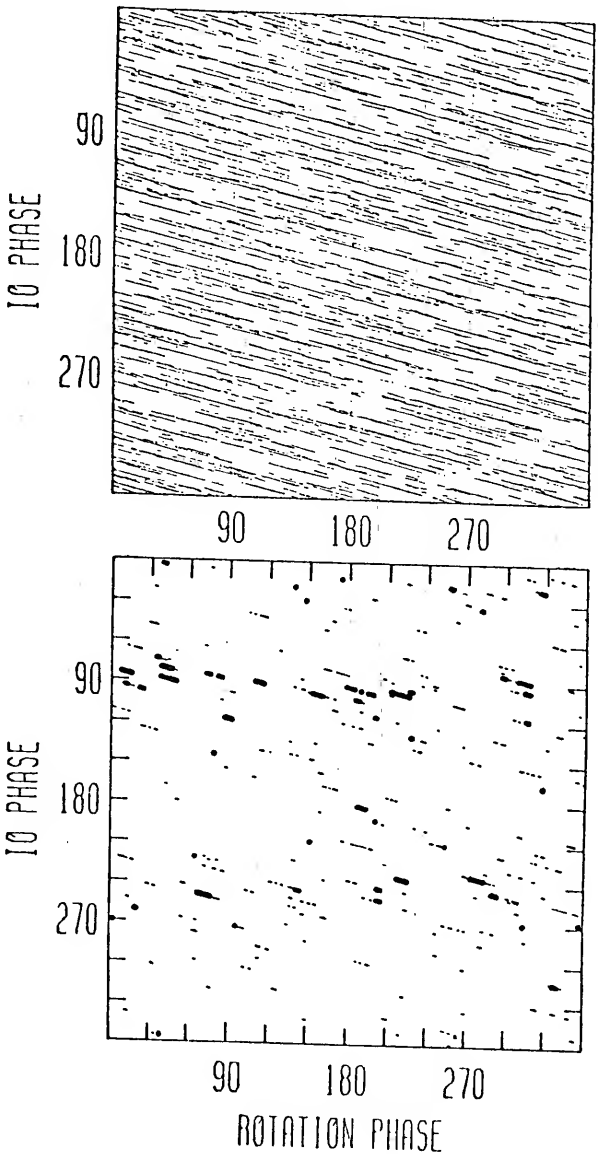
90
180
270
IO PHASE
90
180
270
90
180
270
IO PHASE
90
180
270
ROTATION PHASE

course enhances the appearance of the more intense activity relative to that which was measured to be weaker. Also, within the four-frequency data set itself, a selection criterion was applied to further improve its credibility. Thus, since the characteristic sporadic signature of Jovian emission is usually not apparent in the RAE-1 data when the storm duration is short, activity intervals not exceeding approximately 2 min were discarded.

Even with the data base increased through the merging of four channels of information, the resultant coverage of the $\lambda_{III} - \gamma_{Io}$ observing plane is somewhat less than adequate for doing any sort of detailed analysis. As a consequence also of the extremely small occurrence probabilities at each of the four frequencies, the activity plot appears rather sparse, lacking entirely the longitude source regions which are so strikingly apparent at the higher frequencies. It is possible, however, to draw some general conclusions regarding the activity which has been observed.

Recalling that the heavy lines indicate the higher flux density storms, the most obvious feature displayed in Figure VI-9 is the consistent tendency for the Io-related emission ($\gamma_{Io} \approx 90^{o}$ and 240^{o}) to be more intense than the remainder of the activity. Having already discussed the high degree of control which Io exerts over the radiation at these frequencies, it is probably not surprising to find that Io also enhances

the observed intensity of the emission. Experience from ground-based observations made at higher frequencies has shown this to be the case (Dulk and Clark 1966; Miller and Smith 1973). Also evident in the figure is a clear tendency for the emission as a whole to be concentrated in Io phase as opposed to rotation phase. It is particularly distinct in the case of the activity occurring near 90^{o} γ_{Io} . This behavior was to be expected, of course, based upon the individual λ_{III} and γ_{Io} results presented in the last section. One might also note a slight tendency for the stronger events in Figure VI-9 to concentrate near the longitudes toward which Jupiter's north (210^{o} λ_{III}) and south (30^{o} λ_{III}) magnetic poles are tipped.

In this chapter we have seen that the modulation of the activity in rotation phase is much less apparent than that in Io phase, and it is also less distinct than the rotation-phase control which obtains at the higher decametric frequencies. Therefore it may not be premature to conclude that the rotation-phase modulation of the emission vanishes at very low frequencies. Io-control may become the dominant feature. The rotation-phase modulation which is present, appearing near 210^{o} and 30^{o} λ_{III}, becomes evident only upon intensity-weighting of the activity. Also, as we have noted previously, a dependence of the λ_{III} modulation on flux density seems plausible.

This is of course quite the reverse of the situation noted in Chapter V regarding the 26.3 MHz morphology. Whereas the rotation

phase profiles at 26.3 MHz were quite pronounced and rather independent of the flux density, the RAE-1 morphology suggests an overall decrease in the dependence of activity on the rotation phase of the planet. This would also follow logically if one were to extrapolate to lower frequencies the negligible λ_{III} modulation observed by Dulk and Clark (1966) at 8.9 and 10 MHz. The full extent to which this is true will be determined when more sensitive observations than those possible in this study have been made.

The most conclusive aspect of the RAE-1 investigation, namely the surprising degree of Io control which has been observed, has important consequences *vis a vis* the supposed frequency-dependent nature of the Io effect. The selection-effect mechanism discussed in Chapter V which was developed to assist in understanding the 26.3 MHz results in particular, and the 10 to 40 MHz morphology in general, does not break down at all when applied to the RAE-1 results. On the contrary, the existence of significant amounts of low-frequency Io-related activity detected with a relatively low-gain system clearly reinforces the notion of a flux-dependent rather than a frequency-dependent Io effect. That a high degree of Io control should be evident at long decameter and even hectometer wavelengths prompts one to re-evaluate the 10 to 20 MHz region where the Io effect has been understood to wane appreciably. In the following chapter, then, the dependence of Io control on flux density will

be quantitatively assessed over a broad range of frequencies. In the process it will become apparent how the selection-effect phenomenon has resulted in the Io effect being improperly assigned a dependence upon frequency.

VII

THE DEPENDENCE OF IO-CONTROL ON FLUX DENSITY

Non semper ea sunt quae videntum.

--Phaedrus

WE HAVE BEEN CONFRONTED with two morphological features of the Jovian emission which were not anticipated on the basis of previous observational experience.

1. It was shown in Chapter V that significant amounts of *non*-Io related activity were present at a relatively high decametric frequency (26.3 MHz) and, furthermore, only the most intense emission appeared to be under Io's influence.

2. In Chapter VI the activity occurring at frequencies between 6500 and 2200 kHz was found to be highly correlated with the phase of Io. The preferred γ_{Io} coordinates were identical to those observed at higher frequencies.

Motivated by the results obtained at 26.3 MHz, it was reasoned that a selection effect and its consequences could

account for the well-documented observations concerning the dependence of Io control on frequency. Specifically, a framework was proposed in which the degree of Io modulation was a function not of the frequency, but of the flux density of the radiation. The degree of Io control apparent at any frequency is then governed solely by the intensity of the radiation which is sampled. It was further proposed that the operation of a selection effect has biased the sampling of the emission so that the proportion of low-intensity (non-Io-related) radiation which is recorded increases with decreasing frequency. In agreement with observations, the consequence of such a bias is a decline with decreasing frequency in the degree of Io control.

Although the RAE-1 observations offer critical support with regard to the above framework, it remains as yet to statistically confirm the elements of the proposed hypothesis over as broad a range of frequencies as possible. To this end, the dependence of Io-control on the flux density of the emission will be quantitatively assessed at 26.3, 18, and 10 MHz. Unfortunately, it was not possible to analyze the RAE-1 results in a similar fashion because of the small sample size and, more importantly, because of the relatively narrow range of intensities that were recorded. However, given that the high-intensity emission was well correlated with Io phase, it should be possible at the conclusion of the investigation to predict at what intensity level a significant decline in Io control will be observed.

VII-1. ANALYSIS OF THE 26.3 MHz RESULTS

In Chapter V the dependence of Io control on flux density was observed in a qualitative sense only. In particular, it was apparent from Figure V-3 that the activity occurring above a certain flux-density threshold was well correlated with the phase of Io, whereas the activity below this threshold appeared to be randomly distributed in Io phase. We require a quantitative measure of this behavior, however. A simple scheme is proposed to permit the calculation of the degree of Io control directly from a plot of occurrence probability versus Io phase. The following equation provides the needed formalism.

$$D = \frac{\sum_{i=60^{o}}^{110^{o}} A_i + \sum_{i=210^{o}}^{260^{o}} A_i}{\sum_{i=0^{o}}^{360^{o}} A_i} \qquad \text{(VII-1)}$$

where D = the degree of Io control and A_i = the amount of activity occurring at a particular Io phase γ_{Io}. The two terms in the numerator represent the contributions to the Io modulation from the Io-B ($60^{o} \leq \gamma_{Io} \leq 110^{o}$) and Io-A or Io-C ($210^{o} \leq \gamma_{Io} \leq 260^{o}$) sources. Clearly, if all of the activity occurs within the range of the recognized Io-related sources, then D = 1.0. At the opposite extreme, however, if the histogram is absolutely featureless, then D = 0.28. That is, when

there are equal amounts of activity at every value of γ_{Io}, then no modulation is present and D is proportional to $100^{o}/360^{o} = 0.28$.

In obtaining the desired relationship between flux density and Io control, the procedure has been to create a number of data sets, each set containing activity which occurs over a specified range of flux densities.[1] A histogram of each data set is constructed and D may be calculated from the histogram. Of course, the presentation of the data in the format of a histogram is not necessary for the calculation of D; it serves only as a convenience in illustrating the morphology. In practice, the calculation is performed by the computer which operates on the same data used in constructing the histogram. In this way the value obtained for D is easily verified from the plot. As an example we refer again to Figure V-3. Applying Equation VII-1 to the high-intensity γ_{Io} plot, we obtain $D\ (2 \cdot 10^4 < S(Jy) < 5 \cdot 10^6) = 0.79$. The low-intensity plot gives $D\ (50 < S(Jy) < 2 \cdot 10^4) = 0.35$. That is, in the former case 79% of the activity is said to be Io related, whereas in the latter case only 35% is Io related. These values are obviously in accord with what one might expect to obtain after examining the figure.

---

[1] Recalling the procedure followed in reducing the 26.3 MHz data, the flux density assigned to an uninterrupted activity interval was the peak flux density which occurred during that interval.

The results of the complete analysis are shown in Figure VII-1. The degree of Io control has been calculated for twenty-one subdivisions of the 26.3 MHz data. The upper and lower limits on the flux density of each subset are indicated in the figure. The actual data point (filled circle) has been placed at the average between the two limits. There is a certain amount of redundancy in that many of the data sets overlap; however, this has served as a check on the internal consistency of the results.

The behavior of D as a function of flux density apparent in Figure VII-1 confirms what we might have expected from the results presented in Figure V-3. The high-intensity data display good correlation with Io phase, but the reverse is true of the low-intensity storms. The degree of Io modulation reaches a value of 1.0 for storms exceeding 10^6 Jy, and there is a precipitous decline in D for activity below $2 \cdot 10^4$ Jy. At 10^4 Jy, D reaches a minimum of 0.28 (no modulation), then increases again slightly for values of S less than 10^4 Jy. The reason for this slight increase at very low intensities is not known; however, it is probably not statistically significant as the data sets were small in size relative to the higher intensity data.

The flux density where D = 0.5 will arbitrarily be designated the threshold $S_t(\upsilon)$ below which the activity is primarily non-Io related. S (26.3) is equal to $1.5 \cdot 10^4$ Jy. This

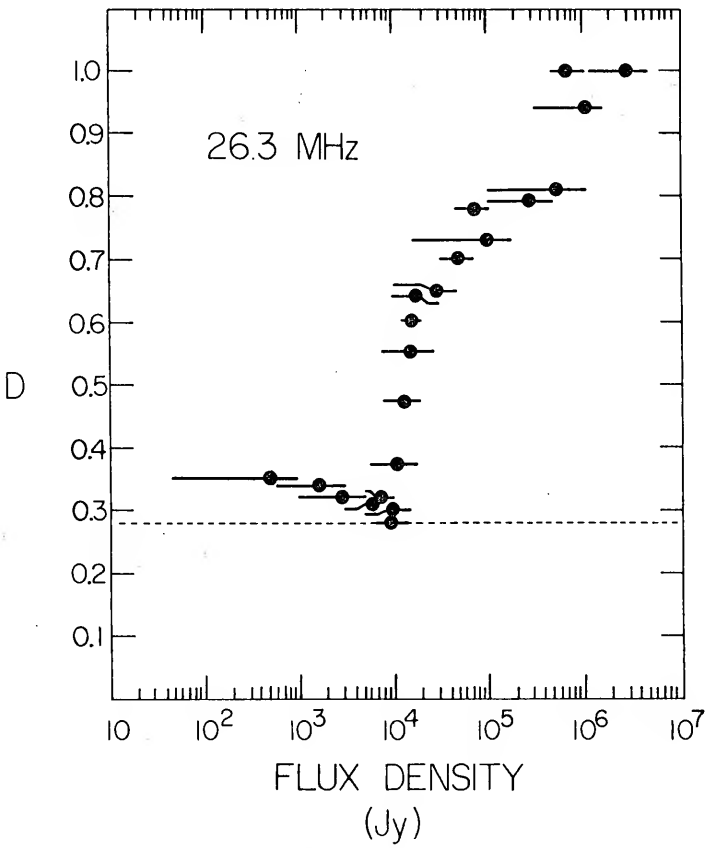

FIGURE VIII-1. The Degree of Io Control Is Plotted As a Function of the Peak Flux Density of Storms Occurring at 26.3 MHz.

parameter will be used to characterize the Io modulation at each frequency. Specifically, the degree of Io control which obtains for activity exceeding $S_t(\upsilon)$ will be labeled D_H and that not exceeding $S_t(\upsilon)$ will be labeled D_L. D_H and D_L have been calculated at 26.3 MHz to equal 0.77 and 0.33 respectively.

VIII-2. PREPARATION OF THE 18 AND 10 MHz DATA

The same procedure has been followed in analyzing data obtained at 18 and 10 MHz from the University of Florida and University of Chile radio observatories respectively. Both data sets had to be slightly reorganized, however, before being submitted to further analysis. In addition, the 10 MHz ("intermediate-deck") data lacked the flux density information essential to this investigation. The procedures followed in modifying the data format and in computing the flux density information are now outlined.

18 MHz

At 18 MHz the activity is normally reduced in 5-min intervals with a flux density assigned to each interval which contains activity (Register 1968). In order to make this format compatible with the 26.3 MHz data, uninterrupted intervals of activity were merged into single long periods and one flux density value was assigned to each. As was done at 26.3 MHz, the maximum flux density which occurred during the period was chosen to characterize the activity. This reorganization of the data format provides assurance that the results obtained at all the frequencies will be directly comparable.

10 MHz

At 10 MHz, besides merging activity intervals as above, it was also necessary to calculate the flux density of each interval from the calibration information provided on the raw data cards. Lebo (1964) has provided a detailed account of the method used in deriving the flux density from such data; the essential antenna-aperture information was provided by Brown (1963). The technique is similar to that described in Appendix A, with the exception that primary-standard noise-diode currents, instead of secondary-standard wide-band noise, were applied to the chart recordings. Also, in order to reduce the deflection of the Jupiter bursts so that they might remain on scale and be calibrated, an attenuator was inserted directly in front of the receiver during data recording. Even with this precaution, however, some of the most intense activity failed to remain on scale.

The 10 MHz data recorded at the Maipu Radioastronomical Observatory during the 1963/64 apparition were used in this study because the observing conditions were exceptional, and a considerable volume of activity was recorded. Unfortunately, the calibrations applied to the chart recordings were sometimes incorrect or were lacking entirely. Thus, as considerable effort was expended in editing the raw data, only this single apparition was processed. Table VII-1 summarizes the observing and activity

statistics of the 18 and 10 MHz data sets. The number of hours of observing and activity have been obtained from Register (1968).

TABLE VII-1. Overall Statistics at 18 and 10 MHz.

Frequency MHz	*Observatory*	*Dates*	*Observing Hours*	*Activity Hours*
18	Florida	7 May 64- 8 May 65	1630	191
18	Florida	15 Jul 65- 7 May 66	1550	176
18	Florida	2 Sep 66- 8 May 67	1100	124
10	Maipu, Chile	18 May 63-20 Jan 64	758	138

VII-3. ANALYSIS OF THE 18 AND 10 MHz RESULTS

Before presenting the results of the flux density behavior of D at these two frequencies, it is worthwhile to examine qualitatively the System III and Io-phase morphology at two different flux levels as was done at 26.3 MHz (Figure V-3).

In Figure VII-2 the 18 MHz activity at two different intensity levels is plotted both as a function of λ_{III} (1957.0) and γ_{Io} . As each flux density component contained nearly equal amounts of activity, the histograms in the γ_{Io} coordinate were plotted on the same absolute scale. The low-intensity data set consisted of all storms which did not exceed a threshold of $4 \cdot 10^5$ Jy, and the high-intensity data set was comprised of storms which did exceed this threshold. The value $4 \cdot 10^5$ Jy was chosen in anticipation of the results to be presented below. The value is in fact equal to S_t (18). As at 26.3 MHz,

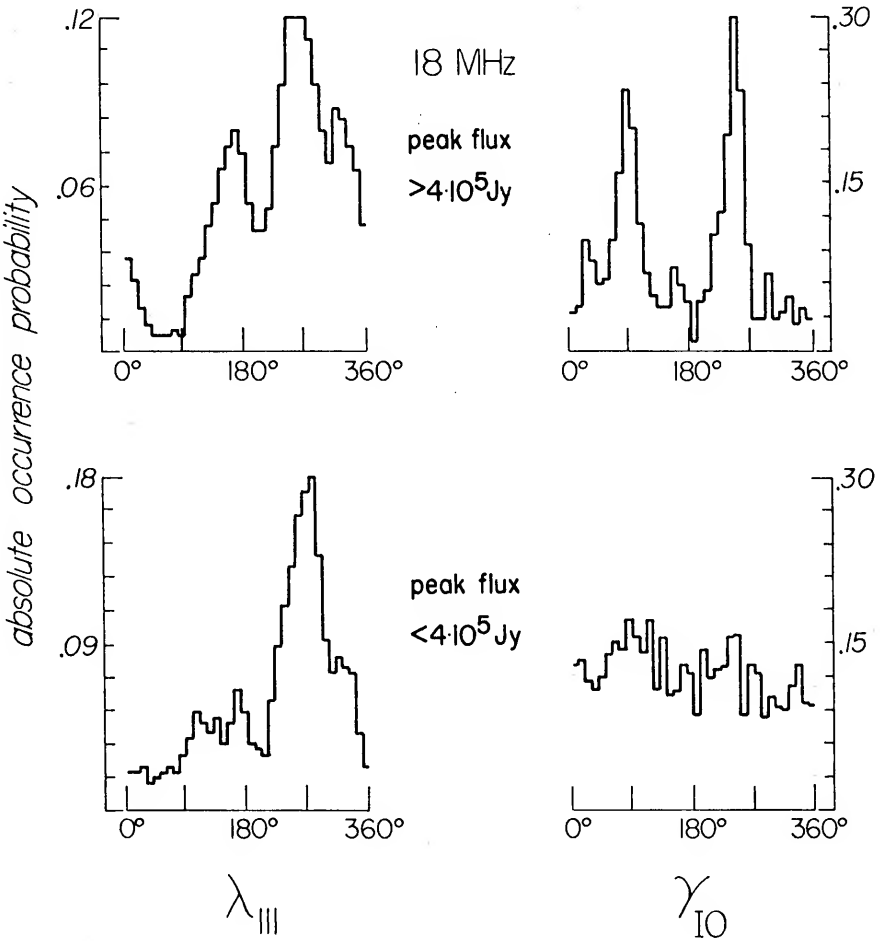

FIGURE VII-2. The Absolute Occurrence Probability of Activity Is Plotted as a Function of λ_{III} (1957.0) and γ_{Io} at 18 MHz. The high degree of Io control exhibited by the high-intensity component contrasts with the nearly featureless appearance of the weak activity in Io phase. The λ_{III} profiles, however, are similar at both intensity levels.

there are only minor differences apparent between the two System III longitude profiles. Sources A and B are plainly evident, with Source B less well defined in the low-intensity plot. The signatures of the two Io-phase components are vastly different, however. The high-intensity component is strongly correlated with Io phase ($D_H = 0.67$), but the low-intensity activity is almost uniformly distributed ($D_L = 0.39$).

The results of an identical analysis at 10 MHz are displayed in Figure VIII-3 where S (10) is equal to $4 \cdot 10^6$ Jy, as will become evident. Since the low-intensity component contains approximately three times as much activity as the high-intensity component, the histograms have been individually normalized; the absolute occurrence probabilities are indicated at the top of each ordinate grid. Recalling the discussion in Section VI-3 concerning the results of Lebo (1964) and of Dulk and Clark (1966), we may not be surprised to observe a difference between the signatures of the two components shown here. The low-intensity component, in particular, displays noticeably less correlation with rotation phase than the high-intensity data, and it is also significantly less modulated than that apparent at higher frequencies. In contrast, the modulation by Io is remarkably similar to the behavior evident at 18 and 26 MHz. At 10 MHz the high-intensity component yields a value $D_H = 0.72$, while the low-intensity component yields $D_L = 0.32$. In order to quantitatively compare the morphology at 18 and 10 MHz with that evident at

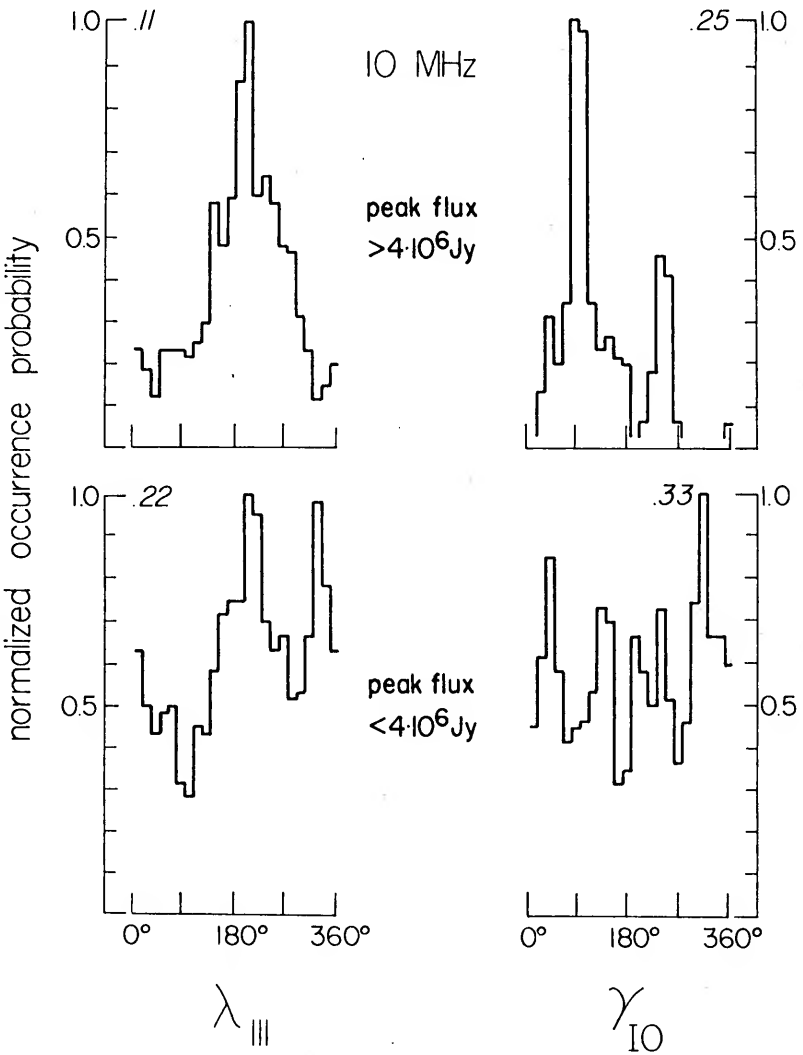

FIGURE VII-3. The Normalized Occurrence Probability of Activity Is Plotted as a Function of λ_{III} (1957.0) and γ_{Io} at 10 MHz. As compared with the well-modulated profiles at higher frequencies (*cf.* Figures V-3 and VII-2), the rotation-phase signature of the low-intensity component is poorly modulated. The modulation in the γ_{Io} coordinate is pronounced at high flux densities but absent at low flux levels, in agreement with the observations at 18 and 26 MHz.

26.3 MHz, it remains only to segment the data into smaller parts and to examine the behavior of D over the entire range of intensities.

The results are presented in Figures VII-4 and VII-5 at 18 and 10 MHz respectively. In general, the behavior of D as a function of intensity is quite similar to that observed at 26.3 MHz. The curves are shifted toward higher flux density, however, reflecting the fact that lower-frequency data is more intense. For example as we have mentioned, the threshold flux density $S_t(\upsilon)$ at 18 and 10 MHz is equal to $4 \cdot 10^5$ and $4 \cdot 10^6$ Jy respectively. At all three frequencies there is a very uniform increase in D as the peak flux density of the storms is increased. At 18 MHz, D never quite reaches the minimum value of 0.28. This is no doubt due to the fact that a relatively insignificant volume of low-intensity data has been sampled. At both 26.3 and 10 MHz the degree of Io modulation is observed to reach a minimum because the situation with regard to the low-intensity activity is different. In the former case, highly sensitive monitoring has assured the detection of very weak activity. In the latter case, although the monitoring was no more sensitive than that at 18 MHz, the peak intensity of the radiation is greater, thus increasing the relative volume of low-level activity which was recorded.

It is most important to note that at three widely spaced frequencies in the decameter range, any degree of Io modulation

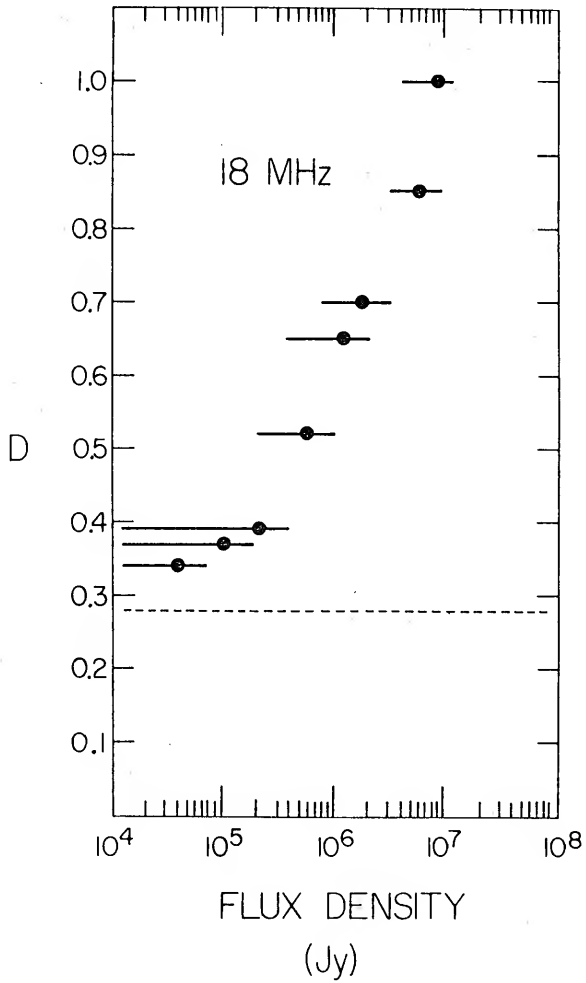

FIGURE VII-4. The Degree of Io-Control D Is Plotted as a Function of the Peak Flux Density of Storms Occurring at 18 MHz.

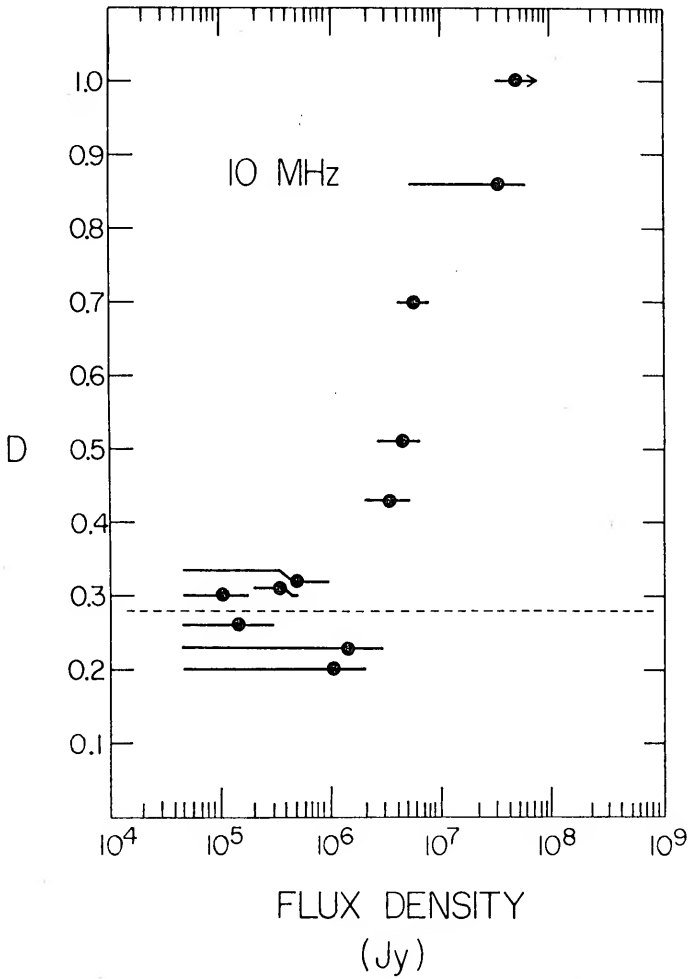

FIGURE VII-5. The Degree of Io-Control D Is Plotted as a Function of the Peak Flux Density of Storms Occurring at 10 MHz.

may be observed simply by specifying the range of flux densities within one's sample. The sole dependence of Io control on flux density is clearly and simply manifested. It remains only to demonstrate that the dependence of Io control on frequency is an artifact of a selection effect.

VII-4. THE SELECTION EFFECT AND THE FREQUENCY DEPENDENCE OF IO CONTROL

It has been shown that the degree of Io modulation apparent at three frequencies in the decameter range is a pronounced and smoothly varying function of the flux density of the emission. It is undoubtedly safe to infer further that this behavior obtains overall frequencies between 10 and 26 MHz. However, it would be premature at present to conclude that the same morphology applies outside this range, except to note that a high degree of Io control extends to frequencies well above 26 MHz (Duncan 1966) and, as we have seen, to frequencies as low as 2 MHz. For the present, then, we will confine our explorations of the consequences of a selection effect to the frequency range between approximately 10 and 30 MHz.

The selection effect we have spoken of is a result of two important elements of Jovian research. The first has already been mentioned in Sections I-3 and VI-2, namely, the steep nature of Jupiter's power spectrum. As with any selection effect, the second element is a result of the way in which the observations are

conducted. In the present case the employment of nearly uniformly sensitive radiometers constitutes the required factor. Both of these elements are illustrated in Figure VII-6. The peak power spectrum of the emission (solid circles) is from Carr *et al.* (1964) and from Desch and Carr (1974). The mean detection thresholds are taken from those reported by Alexander *et al.* (1975*a*) and Boyzan *et al.* (1972) (open squares and diamonds respectively). The error limits assigned to the detection thresholds are due to system variations which have occurred on a time scale of years. These include changes in the total system temperature (as a result of Jupiter's varying position with respect to the galactic background), instrumental changes, and variations between observatories. Although the variations at a single frequency may be large, it is clear that the radiometer sensitivities vary remarkably little as a function of frequency relative to the peak power spectrum. Hence the nature of the selection effect; the range of intensities available for detection near the spectral peak exceeds that available at the higher frequencies by over two orders of magnitude.

It is obvious at this stage how Io control has come to be interpreted as a frequency-dependent phenomenon. At the higher decametric frequencies only the most intense emission is recorded--precisely that portion which is Io modulated. Toward lower frequencies, that is toward the spectral peak, larger proportions of weaker, non-Io-related emission are capable of being recorded.

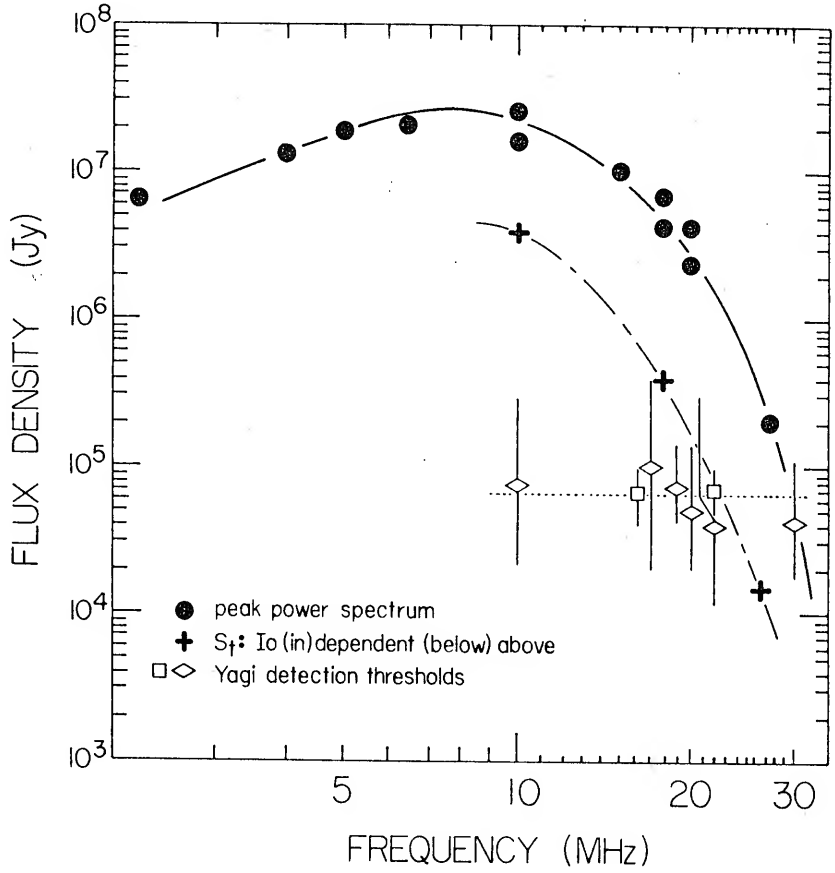

FIGURE VII-6. The Flux-Density Curve (Crosses) Separating Primarily Io-Related from non-Io-related activity Is Compared with Jupiter's Peak Power Spectrum (Solid Circles) and with the Detection Thresholds (Open Symbols) of Typical Yagi Radiometer Systems. A selection effect leading to the specious identification of a frequency-dependent Io modulation results from the ease with which non-Io activity is detected at low frequencies (υ < 22 MHz) relative to high frequencies.

The observed degree of Io control will then decrease as one approaches the spectral peak, since the data is increasingly diluted by this non-Io-related activity.

In order to further illustrate this situation, crosses have been added to Figure VII-6 to show at what flux density the degree of Io-control D is equal to 0.5. These are simply the $S_t(\upsilon)$ values derived in the previous section at 10, 18, and 26.3 MHz. Activity which exceeds $S_t(\upsilon)$ is strongly Io modulated, whereas activity which is weaker than $S_t(\upsilon)$ shows very little dependence on Io phase. In spite of the modest accuracy of the flux measurements at each frequency, it is remarkable how closely the curve joining the $S_t(\upsilon)$ values matches the shape of the peak flux-density curve.

The $S_t(\upsilon)$ curve intersects the radiometer-sensitivity line at about 22 MHz, indicating that data above this frequency should always display a high degree of Io control if recorded in the usual manner with low-gain systems. Below 22 MHz the proportion of activity not correlated with Io should increase markedly. These "predictions" are quite in agreement with the observations.

We conclude that the flux density of the emission is the principal factor controlling what degree of Io modulation is apparent. To first order at least, there is no dependence of Io control on frequency. The extent to which this morphology obtains outside the 10 to 30 MHz range must await the employment of more sensitive equipment. However, the observation of strong Io control in the high- and low-frequency domains is persuasive

evidence that Io modulation is completely independent of frequency. In the next section several theoretical models will be discussed in light of the developments presented here.

We turn briefly from the discussion of Io-related materials to note that the curve joining the $S_t(\upsilon)$ values in Figure VII-6 may be considered to represent the peak flux-density spectrum of the Io-*independent* component. Further, assuming that the non-Io curve faithfully follows the shape of the peak flux-density spectrum, we can expect to find 1310 to 6550 kHz non-Io activity at intensities not exceeding about 10% of the peak flux densities. The same comments apply of course to the emission occurring in the 30 to 40 MHz region.

Whether or not non-Io emission actually takes place above 30 MHz is unknown (see *e.g.* Goertz and Haschick 1972). This particular question has been addressed theoretically by Smith (1976), though, within the framework of the emission mechanism of Wu (1973). As seen by Smith, the post-Pioneer magnetic-field model of Jupiter (Acuna and Ness 1975) may preclude the possibility of higher frequency (>30 MHz) non-Io-related activity. Alternate mechanisms operating in a fundamentally different manner, such as those of Goldstein and Eviatar (1972) or Melrose (1976), do not explicitly rule out the possibility of such emission however. Observations made at threshold sensitivities as deduced from the extrapolation of the non-Io curve will aid in discriminating between competing mechanisms. We will explore the interesting

problem of the frequency limits of the non-Io emission in Chapter VIII.

VII-5. ROTATION- AND IO-PHASE BEHAVIOR AND CURRENT THEORETICAL MODELS

In this chapter the pronounced dependence of the Io-effect on flux density has been shown to account very nicely for the apparent decline in Io control observed at frequencies in the 10- to 20-MHz region. Evidence has been presented which strongly favors the concept of an Io morphology which is frequency invariant from at least 2 to 40 MHz. We have also seen, prior to this chapter, how the λ_{III} modulation of the activity is well defined at high frequencies but almost negligible at very low frequencies. With these new perspectives in mind, it is our intention to explore the possibility of inconsistencies between several of the current theoretical models and the above results. We will lean heavily on the post-Pioneer concept of the Jovian magnetosphere. However, before leaving behind the flux-density dependence developed in Sections VII-1 and VII-3, some clarification is in order concerning a problem in semantics which may have arisen.

We have consistently used the phrase "the dependence of Io-control on flux density." Although this terminology has not been inappropriately assigned thus far, it becomes physically unworkable in the present context. The observed behavior of D *versus* flux density should more appropriately be described as

the "dependence of flux density on γ_{Io} phase." That is, the rephrasing is accomplished through a simple reversal of the implied cause and effect. Stated in this way, it is clear that the high-intensity activity is a direct result of the sharp beaming properties of the Io-stimulated emission. Thus we are not surprised to observe high-intensity emission when γ_{Io} is near 90^{o} or 240^{o}, and relatively low-intensity emission otherwise. In the former case the radiation is beamed more directly at earth, and in the latter case, assuming the low-intensity activity is stimulated by Io, the radiation is beamed in another direction.[2] Beyond this it does not appear that any more need be said concerning the D versus flux-density behavior. This is not to imply that the study was unrewarding. Besides confirming the previously held suspicion that Io-related emission is approximately two orders of magnitude more intense than its non-Io counterpart (Warwick 1967), the investigation has been instrumental in exposing the frequency-invariant Io morphology.

---

[2] It is equally probable that the low-intensity activity, in manifesting no apparent dependence on Io phase, is generated in a manner similar to the terrestrial kilometric radiation, that is without the benefit of any satellite interaction. Unfortunately, it is impossible with the available evidence to distinguish between Io-stimulated emission not beamed toward the observer and true Io-independent activity which is inherently weak. Possible resolution of this problem is explored in Chapter VIII.

We turn now to the subject matter of this section, namely a discussion of several decametric theories in light of the statistical development presented concerning Io. In an excellent review of current decametric models, Smith (1976) has categorized the various theories according to the mechanism employed in coupling Io to the emission region near Jupiter. Of the three coupling mechanisms considered, two incorporate schemes which touch directly upon observational material that we have presented.

The first is the *sweeping model*, described in detail by Smith (1973; see also Wu 1973), in which a plasma instability is driven by a density-gradient-related drift current on the IFT (Io-threaded flux tube). The gradient in the particle density results from the sweeping-up of trapped, energetic particles by Io (Mead and Hess 1973). The instability is quenched by low-frequency turbulence which causes diffusion of the energetic particles back into the swept region. The refilling of the cavity, and hence the elimination of the density gradient, occurs on a time scale which is a function of the local cyclotron frequency. This frequency-dependent diffusion is the mechanism proposed to account specifically for the frequency dependence of Io-control.

The second mechanism to be considered is the *wave model* of Goertz (1973*b*, and references therein). Coupling is provided by Alfvenwaves which are triggered by Io's motion relative to the corotating magnetic field. The waves steepen into shocks

while propagating toward the surface of the planet where the decametric radiation takes place. The ionospheric depth to which the waves penetrate is a function of the frequency of the Alfven waves (1-3 Hz), which in turn depends upon the thermal plasma density at Io. As the plasma distribution is a function of Io's orbital position, a natural vehicle is provided to explain the variation in the peak frequency of decameter storms as a function of λ_{Io} .

Each of the above models is now examined in light of Pioneer 10 and 11 findings. Those aspects of the models are emphasized which bear directly upon the morphology that we have presented here.

THE SWEEPING MODEL

In proposing to explain the appearance of radiation statistically uncorrelated with Io, Smith (1973) calculated the spatial diffusion coefficient $D_{\perp}$ from an estimate of the non-thermal proton density N_p and energy E_p at L = 6 (L shell of Io) in Jupiter's magnetic equatorial plane. N_p and E_p were treated as free parameters, but they were delimited subject to the constraint that the characteristic diffusion time T_D across the boundary of the particle cavity not exceed 13 hr. (The time scale of 13 hr is the period of Io's orbital motion in the frame of Jupiter's corotating magnetic field.) The actual time required to eliminate the cavity is a function of location on

the L = 6 shell (and hence a function of gyrofrequency) because the unperturbed proton density is itself dependent upon magnetic latitude (Divine *et al.* 1971). If $T_D >> 13^h$ the cavity never completely refills, and the plasma instability is never quenched. On the other hand, if $T_D << 13^h$ then one would expect a high degree of correlation with Io, independent of frequency. As the model was developed prior to the Pioneer 10 and 11 missions to Jupiter (hence the relative freedom in choosing N_p and E_p), it is worthwhile examining to what extent the diffusion time is modified by the spacecraft-derived parameters.

The relevant Pioneer 11 values at the orbit of Io are listed in Table VII-2. Because of the highly inclined trajectory of the spacecraft, the observations pertain to a magnetic latitude of 42^o; however, the values at the magnetic equator should not be considerably different. For example, the 1.2-2.1 MeV proton counting rate at 7^o magnetic latitude as observed by Pioneer 10 exceeded the figure at 42^o by a factor of only 2 (Trainor *et al.* 1975).

Comparing these results with Smith's findings: for $T_D \approx 13$ hr the sweeping process requires $D_\perp = 0.003$ km^2 sec^{-1}, assuming a characteristic proton energy of 10 MeV. Smith pointed out that this condition is met for $N_p \geq 10^{-6}$ cm^{-3}. While there are no figures available for 10 MeV protons, we may surmise from

Table VII-2 that this density is probably not out of reach. For 5 MeV protons, however, N_p must exceed 10^{-3} cm^{-3}, a figure which is probably an order of magnitude too high. We may note a trend here that in general, to achieve a reasonable diffusion rate, the required densities become excessively large as E_p decreases.

Clearly, the analysis hinges upon the determination of exactly what proton energies are preferentially depleted from the IFT. Although the answer is not provided unambiguously by either set of Pioneer data, both Trainor *et al.* (1975) and Van Allen *et al.* (1975) noted that absorption features at the L = 6 shell were evident and displayed an energy dependence. Marked depletions in the counting rates were observed for three separate energy ranges: 1.2-2.1, 0.6-3.4, and 14.8-21.2 MeV. The most pronounced signature, however, appeared in the 1.2-2.1 and 0.6-3.4 MeV ranges where the omnidirectional proton flux just inside Io's orbit dropped to less than 1% of its value outside. The 14.8-21.2 MeV flux fell by only a factor of 3.6.[3] The implication is that the density gradient at the

---

[3] A dependence of the absorption depths on E_p might also be expected as a consequence of the more rapid diffusion expected at high particle energies (Smith 1973). However, as Pioneer 11 crossed the L = 6 shell less than one minute behind the instantaneous Io flux tube, the observed depletions cannot represent time-delayed effects. This was not the case with regard to the Pioneer 10 flyby.

TABLE VII-2. Energetic-Proton Observations at Io from Pioneer 11.

E_p MeV	Proton Flux cm^{-2} s^{-1}	N_p cm^{-3}	Reference
1.2 - 2.1	10^6	$6 \cdot 10^{-4}$	Trainor *et al.* (1975)
14.8 - 21.2	10^3	$2 \cdot 10^{-7}$	Trainor *et al.* (1975)
>80	10^3	$8 \cdot 10^{-8}$	Fillius *et al.* (1975)

walls of the IFT is comprised primarily of nonthermal protons possessing energies that are certainly less than 10 MeV and probably less than 5 MeV. It is instructive therefore to ask what T_D is equal to if we assume that the characteristic proton energy is only 2 MeV (for which $N_p = 6 \cdot 10^{-4}$ cm^{-3}). For this energy and density we find from Figures VII-5, VII-6, and VI-4 of Smith that $D \approx 0.008$ km^2 sec^{-1}, and the thickness at the boundary of the energetic-particle cavity is about 400 km. This leads to a characteristic diffusion time across the boundary of about $5 \cdot 10^3$ hr--well in excess of that required to cut off the instability on a time scale consistent with the Io morphology. It appears likely, then, that the cavity persists and is never completely filled in. Smith (1976) came to the same conclusion, namely that the model might explain the non-Io-emission morphology better than the Io morphology, but based his analysis on an examination of the azimuthal drift of the protons.

THE WAVE MODEL

Predictions based upon the wave model of Goertz are not necessarily inconsistent with the morphology we have presented. For example, according to the dynamics of the mechanism, the maximum frequency of the emission f_m is a pronounced function of λ_{Io} and reaches a peak of 40 MHz near 20^o and 200^o λ_{Io}. At other longitudes f_m is less than 40 MHz. As a result, since the radiation is beamed at an angle to the magnetic field which is close to 90^o (the coherent cyclotron instability is presumed), the high-frequency emission should be highly modulated in rotation phase. At frequencies below about 20 MHz, however, dependence on the λ_{III} coordinate will decrease. This is, of course, precisely the behavior we have obtained. Insofar as the Io-related emission is involved, then, the model is quite attractive, and in all fairness, one might conclude on this note. A subtle difficulty arises, though, in considering the non-Io-related emission, particularly at the higher decametric frequencies. In spite of the fact that the wave model attempts to treat only the Io-dependent component, we will pursue the issue further and consider its consequences for the non-Io activity.

We have noted (Figure V-3) that the rotation-phase morphology is quite similar with regard to both the Io and non-Io components at 26.3 MHz. If the wave model successfully explains the modulation in λ_{III} for the Io-controlled activity--as it does qualitatively at least--how then can the non-Io activity behave

in the same fashion? Any attempt to explain the Io-independent rotation-phase behavior solely within the framework of the wave model would surely result in some rather *ad hoc* corollaries to the theory. On the other hand, postulating that separate and distinct mechanisms for the Io and non-Io components can lead to the selfsame rotation-phase morphology appears equally untenable. It is worthwhile, then, to investigate this particular aspect of the wave model in light of the Pioneer 10 findings.

According to the dynamics of Alfven-wave propagation originating at Io, a significant modulation in the frequency υ_A of the waves requires a radical variation in either the magnetic field B_o or plasma density N_e at the source. Because B_o varies by only $\pm 4\%$ as a function of λ_{Io}, nearly all of the change in υ_A must be accounted for by fluctuations in N_e. As such, a model ionosphere and magnetosphere was derived by Goertz (1973a) which incorporates a magnetospheric plasma distribution which is highly concentrated in the planet's magnetic equatorial plane. N_e is predicted to vary between 0.10 and 1,000 cm^{-3} as the magnetic latitude of Io varies by $\pm 10^{o}$. Such an immoderate variation in N_e is probably not supported by the Pioneer results, however. For example, three independent experiments have led to the conclusion that N_e does not exceed 500 cm^{-3} and in fact is probably closer to 100 cm^{-3}. First, the S-band occultation experiment (Kliore *et al.* 1974) established an upper limit to the ambient

plasma density at Io of about 500 cm^{-3}. Second, in order to explain the azimuthal extent of the Io-associated hydrogen torus, McDonough (1975) required a thermal plasma density of about 100 cm^{-3} if the primary hydrogen sink is due to the charge-exchange mechanism. The third experiment, that of Frank *et al.* (1975), measured 100 eV proton densities of about 40 cm^{-3} at the orbit of Io. Notably, the inbound and outbound portions of the trajectory resulted in very similar values for N_e ($\approx$25 and 45 cm^{-3} respectively), even though the λ_{Io} coordinates varied by 102^{o}. The magnetospheric model of Goertz predicts N_e = 100 and 600 cm^{-3} respectively. Thus, assuming that the Pioneer 10 results are reliable, we should expect little if any significant variation in υ_A as a function of λ_{Io}. This forcibly eliminates the λ_{III} modulation predicted by the wave model, unless another way can be found to change the effective penetration depth of the Alven waves. The behavior of the Io-related activity in the λ_{III} coordinate thus remains unexplained by the wave model.

This leaves open the possibility, in fact the probability, that the λ_{III} modulation of the activity is introduced *after* the coupling and generation processes have occurred, that is during propagation from the inosophere. The obvious candidate to function as a proper modulating agent is the magnetic field of the planet. In fact, Alexander *et al.* (1975*b*) have obtained encouraging results in this regard by simultaneously considering the magnetic field geometry, ray reflection from the ionosphere,

and shadowing by the eastern and western limbs of the planet. It is not difficult to see intuitively that lower frequency emission, in agreement with observation, will be delimited by the planet's limb to a lesser degree than the higher frequency emission--assuming of course that the radiation takes place near the local electron gyrofrequency. Understandably, if the non-Io emission is to be explained by this geometrical model, then it too would have to originate near the local gyrofrequency and also near the eastern and/or western limb of the planet. This conclusion possibly provides a reasonable working hypothesis in developing a comprehensive non-Io emission mechanism.

In summary, it has not been our intention to unduly criticize the theories mentioned above. Rather, we wished only to extend the statistical analysis of the present work and show that the theoretical emission mechanisms relevant to the problem were not necessarily inconsistent with the observational morphology developed. We have accomplished this end by drawing upon the recent Pioneer 10 and 11 findings, thereby updating certain elements of the overall problem.

To reiterate:

The characteristic diffusion time appropriate to the sweeping mechanism may be much longer than that required to explain either the Io-modulated emission or, in particular, the observation of a statistical decline in Io control at lower frequencies. The model would appear better adapted to the phenomenology of the

non-Io-related emission (in this context, "non-Io" is used in a statistical sense only; see Chapter VIII), although an explanation of the rotation-phase modulation is still lacking.

With regard to the wave model, we have discussed how, because of a negligible variation in plasma density as a function of λ_{Io}, the frequency modulation of the Alfven waves at Io is severely restricted. Thus, although the attractive wave-model solution to the rotation-phase morphology is so sacrificed, a possibly untenable situation with respect to the similarity of the Io/non-Io morphology is also eliminated. Shadowing of the emission by the planet's limbs may provide a partial solution to the λ_{III} modulation of both the Io- and non-Io related activity.

VIII

THEORY AND EXPERIMENT: COMPLEMENTARY AREAS

Better is the completion of a
thing than its beginning thereof.

--Ecclesiastes 7:8

SINCE THE DISCOVERY OF THE DECAMETRIC EMISSION by Burke and Franklin in 1955, there has been little common ground between the theoretical and experimental elements of the phenomenon. This situation is rapidly changing, however, for a number of reasons. Principal among them, no doubt, are the Pioneer 10 and 11 findings by which meaningful constraints are finally being imposed on various plasma and field parameters used to describe the Jovian magnetosphere. We have already discussed (Section VII-5) several physical models in light of the Pioneer data. In addition, earth- and lunar-orbiting satellites (*e.g.* RAE-1), although not as impressively instrumented as the Pioneers, have nevertheless identified the low-frequency power spectra of earth, Jupiter, and Saturn. In doing so, the study of a new and unique area of comparative planetology has begun (*cf.* Section VI-2).

In what follows we take up the problem of the intersection of theory with observation, that is, those special areas where the domains of each seem to overlap. We will place particular emphasis on future areas of research. Some of the material to be discussed was inspired, naturally enough, by the investigation presented in this dissertation. The bulk of the subject matter, however, is a direct outgrowth of reflection upon several aspects of the decameter problem which have been discussed at departmental workshops and professional seminars over the past several years. In spite of the topical nature of the chapter--perhaps not in keeping with the single-theme philosophy of a work of this sort--we feel that the issue is important enough to be dealt with formally.

Four general areas are to be covered: (1) high-resolution dynamic spectra (drift rates, rise-times, fine structure), (2) the source size and location, (3) the frequency extent of the non-Io emission, and (4) correlations with solar activity. The salient features are summarized in Table VIII-2 which follows the discussion.

VIII-1. DYNAMIC SPECTRA

High-resolution dynamic spectra of the Io-related decametric emission probably offer the richest source of information concerning the dynamics of the emission process. There are three aspects of the phenomenology which may be discussed in the context of theoretical models: (a) the drift rates of the

millisecond (S) bursts, (b) the rise-times of the L and S bursts, and (c) the fine structure in the "bandlike" emission. Each of these elements will be discussed with special regard to various features which clearly need more extensive theoretical and experimental work.

DRIFT RATES

The uniform distribution of the S burst drift rates as a function of frequency (R versus υ) is often taken as evidence that the emission is due to $\gtrsim$10 keV electrons of a particular pitch-angle class radiating at the local electron gyrofrequency (Ellis 1974; Krausche 1975; Groth and Dowden 1975).[1] The uniformly varying drift rates are a consequence of the implicit assumption that the spontaneously radiating electrons conserve the first adiabatic invariant of the motion μ; that is, given initial conditions, the pitch angle α of each electron is uniquely defined at any point along a magnetic flux tube of intensity B. This may be expressed as

$$\mu = \frac{V^2 \sin^2 \alpha}{B} = \text{constant} \qquad \text{(VIII-1)}$$

where V = electron velocity.

---

[1] As of this writing, measurements have not been obtained at $\upsilon > 27$ MHz where the drift rates are predicted to change markedly with frequency. When these observations are made, the model will be put to a decisive test.

This basic assumption is open to question, however, because it is a commonly accepted hypothesis that the decametric emission is a consequence of an induced (as opposed to spontaneous) coherent plasma process. The strength of the argument rests upon the conclusion that the source brightness temperature is in the neighborhood of 10^{17} K (Dulk 1970), far exceeding that which could be explained on the basis of spontaneous emission alone. A wave-particle interaction (usually whistler wave-electron) is the sort of scheme commonly invoked to explain the phase coherence of the particles and the induced emission. However, it is well known (see *e.g.* Brice 1964) that the wave-particle interaction, resulting in the effective exchange of energy between particle and wave, violates the conditions under which the first adiabatic invariant holds; that is, the particle experiences magnetic and electric forces due to the wave, which vary on the order of the scale length of the particle motion. At resonance, the electric vector ε of the wave is in phase with the electron motion about the static magnetic field, and the particle undergoes a constant centripedal acceleration equal to $q\varepsilon/m_e$. As a result, when the transfer of energy is from wave to particle, Brice has shown that the particle pitch angle will increase.

It is impossible to determine with any certainty how severely the pitch angles will vary because the magnitude of ε is unknown. However, if we assume that terrestrial whistlers are typical, then we can expect the field intensity of the whistler wave to

vary over a range $10^{-6} \leq \varepsilon(vm^{-1}) \leq 4 \cdot 10^{-3}$ (Helliwell 1965).[2] The lower bound on ε is actually set by the receiver sensitivity, but for the sake of discussion we will adopt $10^{-6}\ vm^{-1}$ as a lower limit. One could now calculate the change in pitch angle $\Delta\alpha$ resulting from a wave-particle interaction which continues for a time Δt. Following Brice we find that

$$\Delta\alpha = \frac{1}{2 \sin 2\alpha} \frac{\Omega_e}{\omega} \frac{(q\varepsilon)^2}{Wm_e} \Delta t^2 \qquad \text{(VIII-2)}$$

where Ω_e = local electron gyrofrequency, ω = whistler wave frequency, W = particle energy, and $\Delta\alpha$ is expressed in radians. It is most convenient in what follows to express Equation VIII-2 in terms of a characteristic diffusion time t_d necessary to increase $\Delta\alpha$ by 57^o ($\Delta\alpha$ = 1 rad). Let us assume that an electron is in gyroresonance with a whistler wave emitted at Io ($\omega \approx \Omega_e$ = 60 kHz). In a manner consistent with the cyclotron theory, we set W = 10 keV, $\alpha = 20^o$, and let Ω_e = 30 MHz. When $\Delta\alpha$ = 1, $t = t_d$; Equation VIII-2 then becomes

$$t_d = \frac{1.2 \cdot 10^{-5}}{\varepsilon}$$

---

[2] For comparison, the field intensity of the electromagnetic wave which is radiated toward earth is estimated by Warwick (1970) to be approximately 1 vm^{-1}.

We have collected all parameters in mks units so that ε is in vm^{-1} and t_d is in seconds. Using the range of ε expressed previously, we finally obtain the results presented in the following table.

TABLE VIII-1.

ε vm^{-1}	t_d *sec*
10^{-6}	12
$4 \cdot 10^{-3}$	$3 \cdot 10^{-3}$

There is considerable latitude in the values derived for t_d, but they cover a most interesting time scale. Obviously the lower bound on t_d (3 msec) is unreasonably small because individual S bursts are observed to drift rather uniformly ($\dot{R} \approx 0$) from beginning to end of each event (Krausche 1975). Since the bursts last for about 50 to 80 msec, it follows that significant alterations in pitch angle must occur on a time scale $t_d \geq 1$ sec.

Primarily because of the uncertainties in ε, the limits quoted for t_d should not be regarded too seriously; rather, the calculation should be viewed in the spirit that pitch-angle diffusion may be a significant factor in accounting for the drift rates of the Jovian S bursts. The full extent to which resonance dynamics are important in stimulating the S bursts will only be determined when high-resolution spectra are made at widely separated frequencies simultaneously. The cumulative effects of successive wave-particle interactions along the IFT should then become apparent, and the consequences of pitch-angle diffusion may be compared with the theoretical drift-rate curve which assumes

that μ is conserved. Specifically, the observed $|R|$ should be less than that calculated using Equation VIII-1, and the departure should increase at the lower frequencies where the electron streams will have suffered the greatest number of interactions.

RISE-TIMES

The plasma instability which gives rise to the L or S bursts has associated with it a certain growth rate γ, the inverse of which, neglecting propagation effects, corresponds to the observed rise-time of the waveform. As such, the rise-time of the burst limits the number of mechanisms available to explain the observations. Growth rates have been evaluated under plasma conditions found in Jupiter's ionosphere in two cases: that of Melrose (1975) in the context of an acceleration model and that of Smith (1973) in the context of the sweeping model. Melrose found $10^4 \leq \gamma\ (\text{sec})^{-1} \leq 10^5$, whereas the sweeping model gives much smaller growth rates, $10^{-4} \leq \gamma\ (\text{sec})^{-1} \leq 1$. Commenting on this result, Smith (1976) noted that while the growth rates predicted by the sweeping mechanism are too small to account for the characteristically short time scales (10^{-5} sec) of the millisecond bursts, they are in accord with L burst time scales. Although the range of γ found by Melrose is consistent with the S burst rise times, the plasma parameters he used were not uniquely defined and considerable variation is possible.

We might point out further that the unusual class of bursts reported by Trapp (1971) had rise-times which require $\gamma \geq 3 \cdot 10^5$ sec^{-1}. No instability known to the author has been reported to have growth rates on this order.

FINE STRUCTURE

The "bandlike" emission exhibited by some of the millisecond activity (Figure I-1c) has been attributed by Flagg *et al.* (1976) to spatial discontinuities (density fluctuations) in the streaming electrons which give rise to the emission. In particular, the slowly oscillating *extinction band* (*Region 2* of Flagg *et al.*) is thought to arise from a density modulation imposed by a relatively stationary "active region" on the IFT. Hence, among the three elements of the emission process (coupling, generation, and propagation) which might be considered candidates, Flagg *et al.* ostensibly chose coupling-mechanism inhomogeneities to explain the observations, although the scheme is general enough to be interpreted as a combination coupling-generation model.

It is not inconceivable, however, that the observed fine structure is the result of frequency discontinuities which arise solely during the generation or propagation of the emission--processes which immediately succeed Jupiter-Io coupling. The coupling mechanism *per se* need not be involved. By way of example, Maeda (1975) has ventured an explanation for the extinction band evident in terrestrial VLF emissions which

relies upon anomalies in the generation process alone. Of course the VLF radiation is much lower in frequency than the decametric emission, by a factor of 10^4, and it endures for hours, as opposed to seconds; however, the extinction-band morphologies are remarkably similar, and in both cases the radiation takes place near the respective local electron gyrofrequencies. According to the model outlined by Maeda, a relatively broad spectrum of electrostatic waves is amplified or damped depending upon frequency. The damped wave spectrum constitutes the extinction band.

Although the growth-rate analysis of Maeda predicts an excessively broad absorption feature, much broader than could explain the very narrow-band nature of the extinction band, the qualitative agreement with observation is encouraging. Furthermore, some improvement might be expected if particle distributions are used which resemble delta functions in momentum space. Distributions of this sort are often used in modeling the decametric emission.

In summary, two elements of the bandlike emission problem are compelling: (1) Wave-particle interactions are suspected of triggering both the VLF and Jovian versions of the emission. (2) The overall phenomenology of the events is very similar. It is evident that the Jovian bandlike emission might lend itself very nicely to the sort of growth-rate analysis outlined by Maeda.

VIII-2. SOURCE SIZE AND LOCATION

The size of the Jovian source remains completely unresolved at interferometer baselines exceeding the radius of the earth (Lynch *et al.* 1976; Dulk 1970). Earth-moon baselines, providing resolutions down to 26 km at 18 MHz, will probably be required to resolve the source region. In view of the unlikelihood of such an experiment in the near future, inferences concerning the spatial extent of the emitting region must necessarily follow from observations of the dynamic spectra (Dulk 1967; Krausche *et al.* 1976).

VLBI experiments designed to locate the source region, however, may become feasible within the next few years. One system being proposed (T. D. Carr, personal communication) takes advantage of the fact that Jupiter will be sufficiently near the radio source 3C144 (Crab Nebula) to permit the determination of ionospheric propagation effects. Radiometers of greater sensitivity than those usually employed in low-frequency monitoring will be required; the 26.3-MHz array described in this dissertation will serve more than adequately at one end of the baseline. Another method (S. S. Shawhan, personal communication) will account for the same ionospheric effects through the crosspolarized reception and subsequent analysis of Jovian Faraday fringes. The fringes are produced during the reception of the linearly polarized signals when linearly polarized antennas are used.

Both experiments should be encouraged, and they should be executed simultaneously in order to substantiate the results.

In this regard the situation is ideal in that the two experiments are quite independent but are designed to operate at the same frequency (26.3 MHz).

VIII-3. FREQUENCY EXTENT OF THE NON-IO EMISSION

Two features of interest regarding the sweeping model of Wu and Smith are predictions concerning the low- and high-frequency limits, f_{mn} and f_{mx} respectively, of the non-Io related emission. In terms of the electron plasma frequency ω_e and the electron gyrofrequency Ω_e, the low-frequency cutoff results from the requirement that locally $\omega_e \gtrsim 0.03\ \Omega_e$, or equivalently V_A (Alven velocity) $\geq 0.7c$. At the foot of the IFT, V_A is less than 0.1c; however, V_A increases rapidly with distance from the planet. At some point, V_A may exceed the stated limit, but the calculation depends critically upon the thermal plasma-density distribution along the IFT. As this is lacking at present, f_{mn} cannot be predicted with any certainty.

Unlike f_{mn}, f_{mx} may be deduced fairly reliably simply from knowledge of the magnetic field strengths at the northern and southern feet of the IFT. As the sweeping mechanism relies upon a population of stably trapped particles, the maximum extent of the trapped radiation (and hence the plasma instability) lies between the conjugate mirror points, one of which will be located at the flux-tube foot having the *minimum* field intensity. Particles which are located between the opposite-hemisphere

mirror point and IFT foot are within the loss cone and are dumped into the atmosphere.

Examination of the paths of the IFT feet on a map of Jupiter's surface magnetic field (Alexander *et al.* 1975*b*) leads to the conclusion that $f_{mx} \gtrsim 29$ MHz. Since in the context of the sweeping model the radiation takes place at the upper hybrid frequency $\omega_H = \sqrt{(\omega_e^2 + \Omega_e^2)}$, one must have some knowledge of the plasma frequency. We have obtained ω_e from the peak thermal plasma density ($N_e = 3 \cdot 10^5$ cm^{-3}) in Jupiter's ionosphere, as deduced from S-band occultation by Fjeldbo *et al.* (1975). The choice of N_e is not critical, though; an order of magnitude error in the plasma-density profile results in a change in f_{mx} of only 3 MHz.

The observation by Goertz and Haschick (1972) that the Io-independent emission does not exceed 30 MHz would appear to lend considerable support to this aspect of the sweeping model. As we have noted in Section VII-4, however, the spectrum of the non-Io emission is such that it is simply not detectable above this frequency using conventional systems. Hence, the question as to whether non-Io activity occurs above 30 MHz is as yet unanswered. Nonetheless, we have shown that sufficiently sensitive monitoring can uncover large amounts of non-Io emission at high frequencies; at 26.3 MHz, 45% of the total activity was non-Io-related. The possibility of such emission at even higher frequencies seems quite plausible.

Clearly, f_{mn} and f_{mx} should be searched for in order to test the ability of the sweeping mechanism to generate decametric and hectometric (and kilometric?) radiation. Extrapolation of the Io-independent flux spectrum (Figure VII-6) into the high- and low-frequency regimes should provide a fairly reliable indication of what power levels to expect. The PRA experiment aboard the MJS-77 spacecraft will probably be capable of making the necessary observations, at least during the encounter phase of the mission.

VIII-4. CORRELATIONS WITH SOLAR ACTIVITY

There are generally two schools of thought regarding the Io independent component of the emission: the statistical school and the literal school. Members of the former hold that whereas the non-Io emission is *statistically* independent of Io, as clearly evidenced by the distribution of activity in the λ_{III} - γ_{Io} plane, the radiation is ultimately a consequence of Io's interaction with the Jovian magnetosphere. Although it seems difficult at first to envision a plausible scheme, the sweeping mechanism of Smith and Wu is a highly attractive model. The literal school, on the other hand, maintains that the radiation takes place independently of Io in a physical sense; it is implicit in the dynamics of the theories representative of this view (Chang 1963; Goldstein and Eviatar 1972; Houghton 1975 and personal communication; Melrose 1976) that the plasma

instability would proceed unaltered, even upon the (hypothetical) removal of Io from the system.

It is impossible with the observational evidence at hand to unequivocally support either the literal or statistical point of view, but extended analysis in various areas should begin to clarify the situation. By way of emphasis, we have just mentioned how determination of the frequency limits of the non-Io emission might confirm certain elements of the sweeping model. Conversely, evidence favoring the literal interpretation of the morphology would be provided by a convincing correlation between the non-Io emission and some parameter reflecting solar activity. Carr and Desch (1976) have reviewed the status of investigations into this area: there is no consensus of opinion because the solar correlation studies have yielded conflicting results. This unfortunate state of affairs has not developed for lack of industry though; the investigations have been vigorous and nearly exhaustive of the available observational resources. The difficulties lie, we believe, in the nature of the data sets, both solar and Jovian--difficulties which will not be overcome through simple refinements in data selection. The first completely credible correlation, or lack thereof, will probably be derived from analysis of the MJS-77 data. The uninterrupted Jupiter and solar wind data sets, the latter reflecting the velocity signatures at Jupiter when MJS is near encounter phase, will be unequaled in quality to any now available.

It is possible with information now available to anticipate the sort of directions a study such as the above would take. For example, Desch (1976) has used Pioneer 10 solar wind data to discover what interplanetary parameters are needed to completely determine a solution to the solar-Jovian correlation problem. A reliable daily index of Jupiter activity was obtained through the synthesis of multifrequency decameter data gathered by a global network of observatories; close examination of the solar wind velocity profile and the daily activity index revealed that pressure gradients at Jupiter may be necessary--but not sufficient--conditions for the stimulation of non-Io radiation. Interplanetary magnetic field (IMF) variations, as measured at 1 AU and extrapolated to 5 AU, seem to play an essential role; this tentative and very sketchy model is not very different from those developed to explain terrestrial magnetospheric substorms and related auroral activity (*cf.* Burch 1974). The implication is that attention should be paid to at least three parameters describing interplanetary conditions at Jupiter: solar wind velocity, IMF magnitude, and IMF direction. A correlation analysis using these three parameters should provide a definitive solution to the solar correlation problem. Hopefully, the gnawing question concerning the nature of the non-Io emission will then be answered.

TABLE VIII-2. Summary of Complementary Studies: Experimental and Theoretical.

Observational Feature	*FURTHER ANALYSIS REQUIRED* *Experimental*	*Theoretical*	*References*
Drift rates (S burst)	Simultaneous measurements at many frequencies	Effect of wave particle interactions	Brice (1964) and this work
Rise times (L and S bursts)	Differences among various types of L and S bursts	Growth rate analyses	Smith (1973), Melrose (1976)
Fine structure (bandlike emission)	Prevalence and morphology at frequencies other than 26 MHz	Effects of generation and propagation of emission on observed fine structure	Maeda (1975)
Frequency limits (non-Io)	Determine lower and upper frequency limits from PRA/MJS-77; distribution of N_e and B on IFT	Further development of (statistical) non-Io theory	Smith (1973)
Solar correlations	Monitor Jupiter and interplanetary parameters from MJS-77	Further development of (literal) non-Io theory	Chang (1963), Goldstein and Eviatar (1972), Houghton (1975), Melrose (1976)
Source size	Earth-moon VLBI	Direct bearing on all above	
Source location	"Reference-source" VLBI	Direct bearing on all above	
	"Faraday-fringe" VLBI	Direct bearing on all above	

EPILOGUE

THE SCOPE of the last chapter, in which I have considered the complementary domains of theory and experiment, has by no means been exhaustive, nor for that matter, has the material been covered in any great depth. Rather, my intention has been to provide several points of departure from which further progress in solving the Jupiter problem might be possible. In a certain sense, Chapter VIII has served as an epilogue for the entire work: an appeal for further study along similar lines, but of a less superficial nature than that presented herein. In this regard, a more lively exchange between the theoretical and experimental factions comprising the "Jupiter people" would be of lasting benefit.

APPENDICES

APPENDIX A

ARRAY CALIBRATION PROCEDURES

Both the Jupiter and calibration source records were manually calibrated by the system described in this appendix. The calibration procedures are designed to give reasonably accurate values for the absolute noise temperature T_n present at the input to the field preamplifier (refer to Figure A-1). In the absence of contributions from powerful radio sources, T_n is generally on the order of 600 to 1200 K, corresponding to the galactic background temperature after it has been attenuated by coaxial cables in the phasing networks of the array. The records were fully calibrated both before and after each observing session by applying at least three calibration steps at levels equal to and exceeding the background temperature. Additionally, single calibration steps, approximately equal to the background level, were applied to the calibration source records at 5- to 10-min intervals. This was done in order to subtract out baseline variations due to thermal drift in the field preamp. Reference to Figure A-1 will aid in understanding the following description of the noise standards and circuitry which were used in making the above measurements.

Calibration occurs when switches S_1 and S_2 are in positions 2 and 1 respectively. Antenna signals are recorded when both S_1

and S_2 are in position 1. In practice, antenna signals are recorded from three beams simultaneously; however, only one channel is shown here. Each record is calibrated by means of the Hewlett Packard 461A amplifier which acts as a secondary noise standard (sns). The calibrator signal, which is adjusted by means of the variable attenuator A_3 to bracket the source signal, is inserted at the input to the field preamp through A_1 (fixed attenuator on preamp input) and A_2 (350 m of coaxial cable). The sns is in turn calibrated against two Sylvania 5722 noise diodes connected in parallel, according to the scheme represented by the dotted lines (switch positions 2 and 3). A detailed account of the noise diode calibration may be found in Lebo (1964). The noise diode is generally considered (Brown 1973; Viner 1975) to function as a primary noise standard (pns), although the noise diodes used in this study have not been compared with National Bureau of Standards resistors. With A_3 equal to 34.8 db the output of the sns is equal to the output of the pns, indicating that the sns has an unattenuated (A_3 = 0 db) temperature T_O of $62.4 \cdot 10^6$ K. Knowledge of A_1 and A_2 (see Table A-1) then permits the direct calculation of T_n through the formula $T_n = pT_O$ where $T_O = 62.4 \cdot 10^6$ K, $p = 10^{-a}$, and $a = (A_1 + A_2 + A_3)/10$. A_3, of course, is adjusted so that the calibrator signal is in the range of the antenna signal as they appear on the chart recorder. When A_3 is equal to 23 db, the calibrator signal is approximately equal to the galactic background level (as of 16 May 74). A_1 and

A_2 have been modified at various times during the development of the system, and their values are tabulated below

TABLE A-1.

Date	A_1 db	A_2 db	Total db
1972 -26 Apr 73	25	17	42
27 Apr 73-15 May 74	25	10	35
16 May 74-present	20	6	26

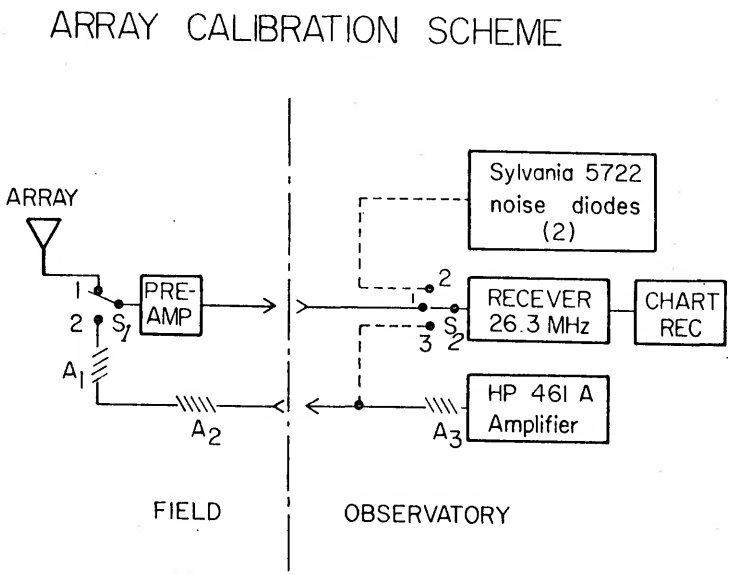

FIGURE A-1. Schematic representation of the Signal Detection (S_1 = S_2 = Position 1) and Calibration Scheme (S_1 = Position 2, S_2 = Position 1) Used at 26.3 MHz.

APPENDIX B

THE RAE-1 MICROFILM DATA: SOME SELECTED EXAMPLES

In this appendix we have assembled seven photographs illustrating twelve frames of the 16-mm microfilm library used in analyzing the RAE-1 data. The frames were selected primarily on the basis of the well-developed Jovian storms which appeared, but they also serve to illustrate several of the commonly encountered problems associated with the microfilm reduction. The following table summarizes the data frames to be illustrated and also tabulates the RAE-1 orbital (ϕ), rotation (λ_{III}), and Io (γ_{Io}) phases of the Jupiter activity appearing on each.

TABLE B-1.

Figure	*Date MMDDYY*	*Freq kHz*	ϕ	λ_{III} *(1957.0)*	γ_{Io}
B-1	022769	2200[a], 3930	99^o-108^o	38^o	80^o
B-2	022769	4700, 6550	99^o-108^o	38^o	80^o
B-3	031469	3930, 4700	92^o-108^o	190^o	182^o
B-4	031469	4700, 6550[b]	92^o-108^o	190^o	182^o
B-5	032469	2200, 3930	100^o-115^o	12^o	85^o
B-6	040269	3930, 4700	90^o-115^o	184^o	93^o
B-7	040269	4700, 6550	90^o-115^o	184^o	93^o

[a] Jupiter activity barely visible at 2200 kHz.

[b] Most of the Jupiter activity obscured by ionospheric breakthrough.

The Jupiter activity on each frame is recognizable by virtue of the enhancement in antenna temperature which the emission induces on the upper-V channel (top part of frame) relative to the usually "quiet" conditions on the lower-V channel (bottom part of frame). Table B-1 identifies the phase of each Jupiter event on each frame.

Ionospheric breakthrough (IB) dominates the channels above 2200 kHz, often exceeding the Jupiter activity by an order of magnitude or more. In Figure B-7, for example, IB occurs from about 15^{o} to 70^{o} ϕ. It is caused by station and lightning interference originating at or near the earth's surface, and it is thus always more intense at higher frequencies where the ionosphere is more transparent. Fortunately, IB is clearly distinguishable from Jupiter activity. As it originates from below the satellite, IB is always stronger on the lower-V channel.

Range changing (RC) was a source of difficulty which was not as easily disposed of as the IB problem. At the time of data transmission from satellite to ground station, measured voltages were converted to antenna temperature by means of three separate calibration curves. The particular curve employed depended upon the signal intensity. As the calibration curve for each range of intensities did not merge smoothly with the next range, it was possible, at certain temperature levels, for very small changes in intensity to appear as relatively large discontinuities in

antenna temperature. A good example is illustrated in Figure B-3 where RC extends from 140^{o} to $175^{o}\phi$ on both the 3930- and 4700-kHz channels. When it happens to appear as an enhancement on the upper V alone, it can usually be distinguished from a Jovian event by virtue of its characteristic "flat-topped" signature. Admittedly, there have been upper-V phenomena which did not lend themselves to simple classification as either sporadic (Jupiter) or flat-topped (RC). In these cases, the period in question was not counted as either observing or activity time.

Figures B1 through B7 follow; the appropriate rows of Table B-1 serve as figure captions.

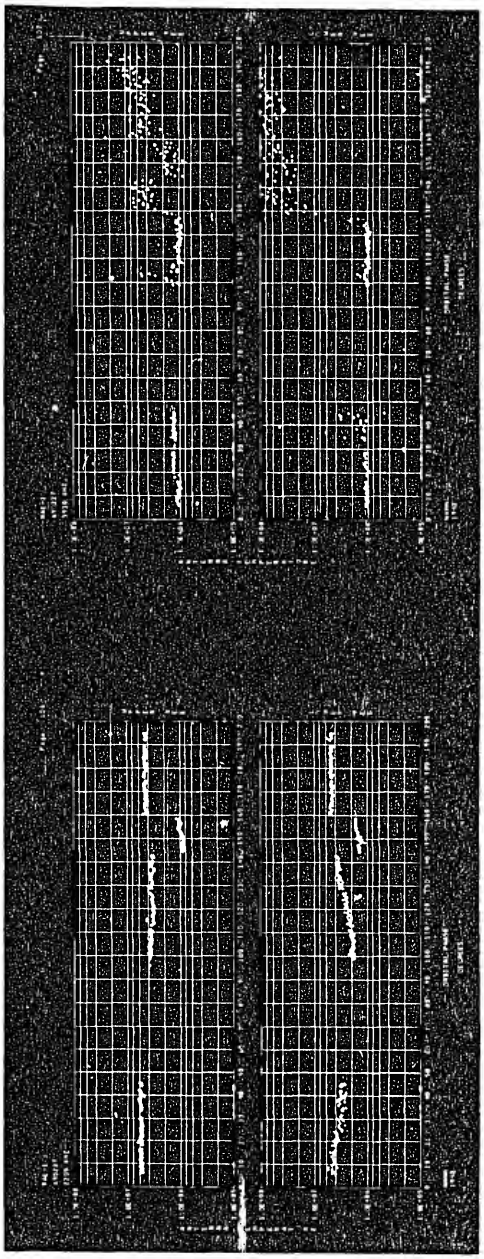

FIGURE B-1. See Table B-1.

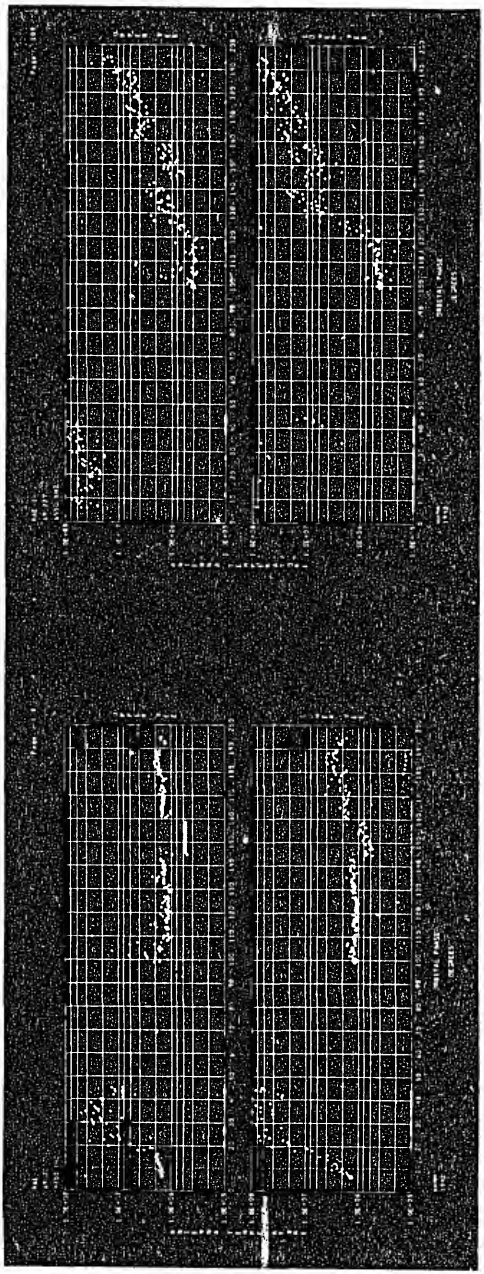

FIGURE B-2. See Table B-1.

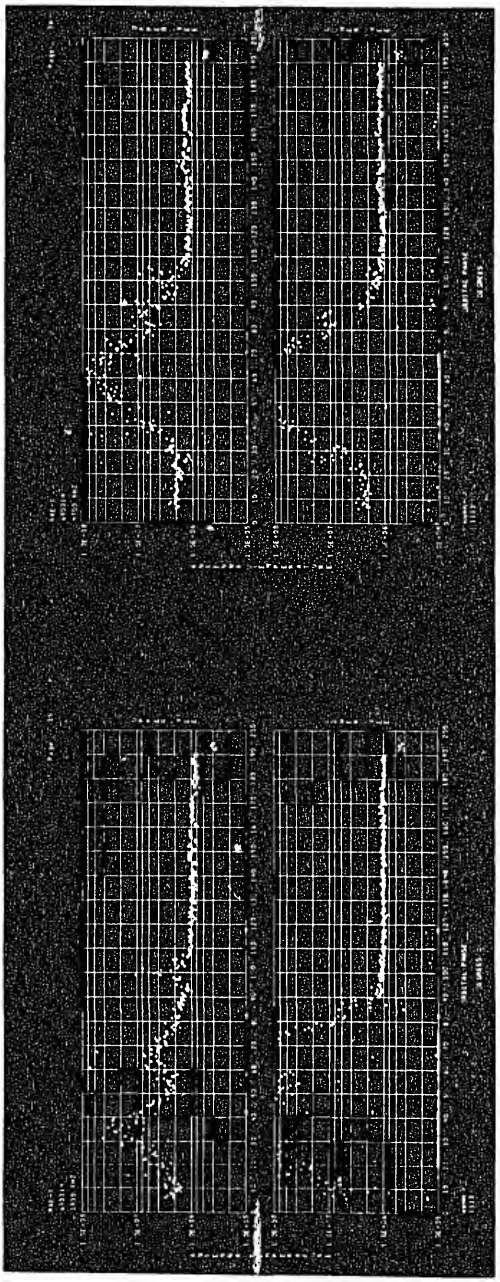

FIGURE B-3. See Table B-1.

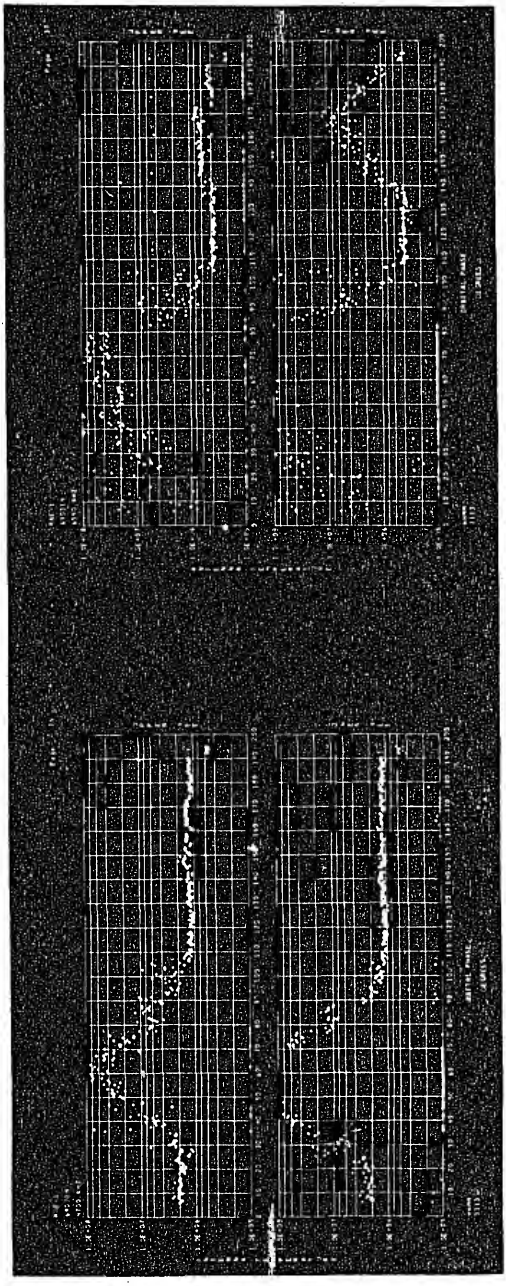

FIGURE B-4. See Table B-1.

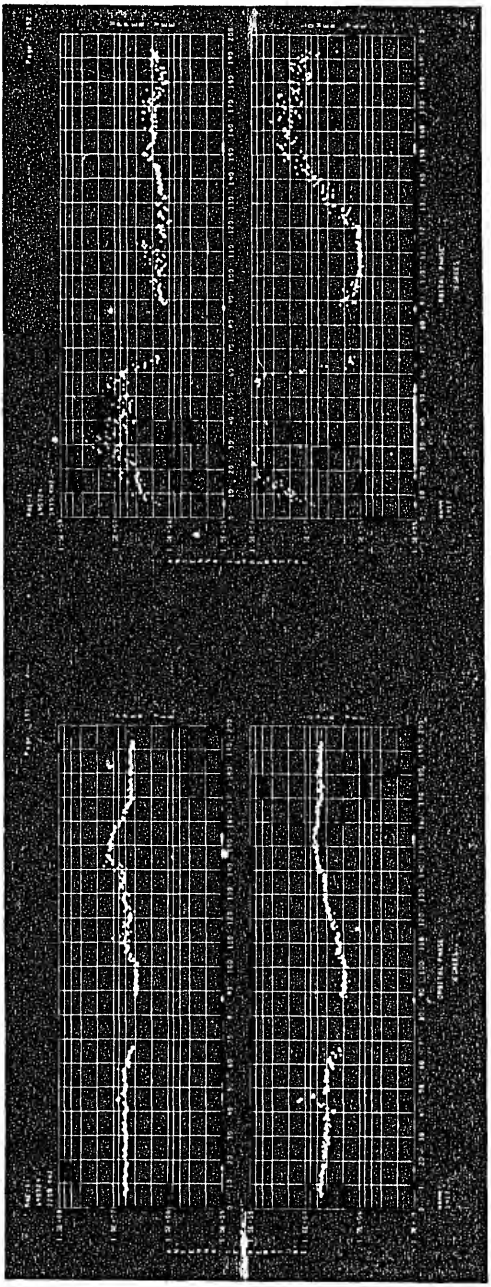

FIGURE B-5. See Table B-1.

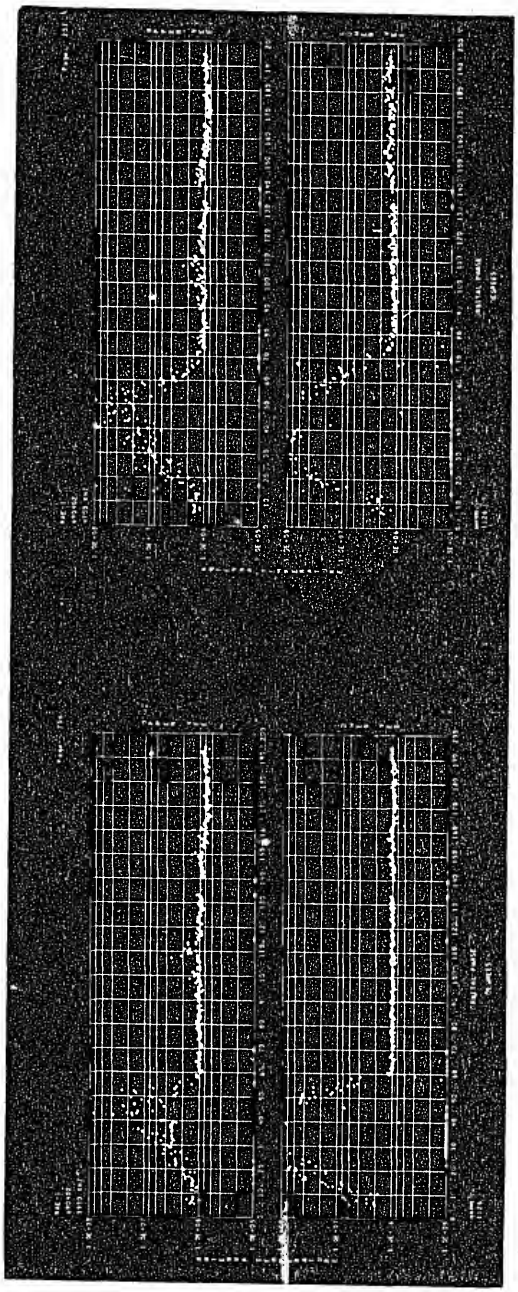

FIGURE B-6. See Table B-1.

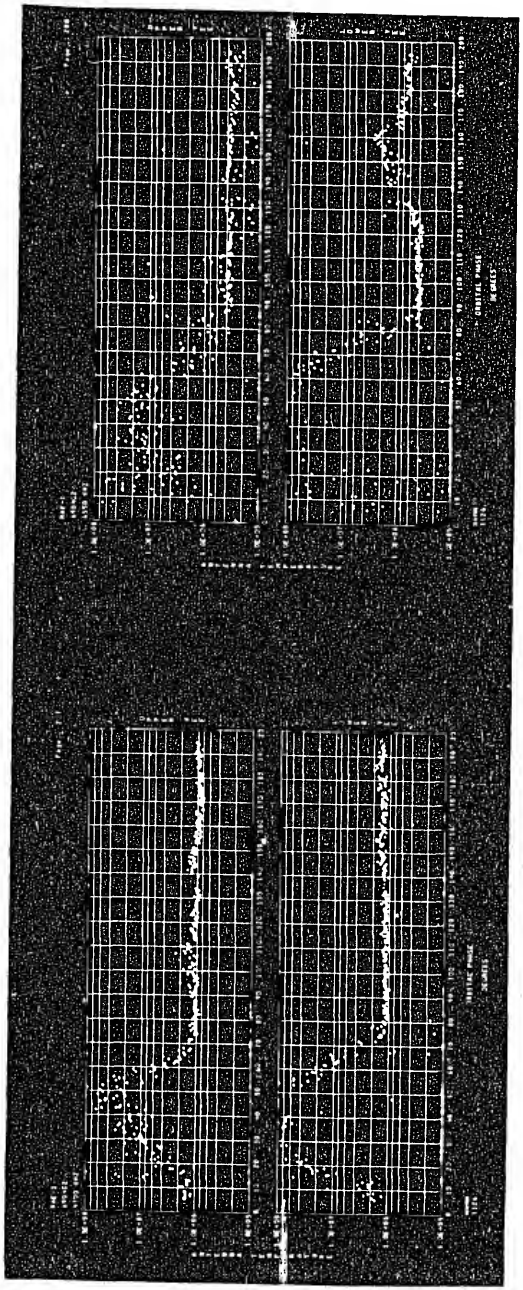

FIGURE B-7. See Table B-1.

REFERENCES

Acuna, M.H., and Ness, N.F. 1975, *Nature,* 253, 327.

Alexander, J.K. 1970, NASA-GSFC Report, X-693-70-267.

_____. 1976, *Sky and Telescope,* 51, 148.

_____, Brown, L.W., Clark, T.A., Stone, R.G., and Weber, R.R. 1969, *Ap.J. (Letters),* 157, L163.

Alexander, J.K., Kaiser, M.L., and Vaughan, S.S. 1975*a*, NASA-GSFC Report, X-693-75-48.

Alexander, J.K., and Novaco, J.C. 1974, *A.J.,* 79, 777.

Alexander, J.K., Smith, R.A., Kaiser, M.L., Acuna, M.H., and Thompsen, R.F. 1975*b*, NASA-GSFC Report, X-693-75-258.

Baars, J.W.M., Mezger, P.G., and Wendker, H. 1965, *Ap.J.,* 142, 122.

Bazelyan, L.L., Braude, S.Ya., Vaisberg, V.V., Krymkin, V.V., Men, A.V., and Sodin, L.G. 1965, *Soviet Astr.-AJ,* 9, 471.

Bigg, E.K. 1964, *Nature,* 203, 1008.

Bozyan, F.A., and Douglas, J.N. 1976, *Icarus,* in press.

_____, and Gopala Rao, U.V. 1972, University of Texas Report, Series II, 3, No. 8.

Braude, S.Ya., Lebedeva, O.M., Megn, A.V., Ryabov, B.P., and Zhouck, I.N. 1969, *Ap. Letters,* 5, 129.

Brice, N. 1964, *J. Geophys. Res.,* 69, 4515.

Bridle, A.H., and Purton, C.R. 1968, *A.J.,* 73, 717.

Brown, G.W. 1963, Master's thesis, University of Florida, Gainesville, Florida.

Brown, L.W. 1973, *Ap.J.*, 180, 359.

_____. 1974, *Ap.J. (Letters)*, 194, L159.

_____. 1975, *Ap.J. (Letters)*, 198, L89.

_____. 1976, *Ap.J. (Letters)*, in press.

Burch, J.L. 1974, *Rev. Geophys. and Space Phys.*, 12, 363.

Burke, B.F., and Franklin, K.L. 1955, *J. Geophys. Res.*, 60, 213.

Butler, J.L. 1966, in *Microwave Scanning Antennas*, Vol. III, ed. R.C. Hansen (New York: Academic Press), p. 217.

Carr, T.D. 1972, *Phys. Earth Planet. Interiors*, 6, 21.

_____, Brown, G.W., Smith, A.G., Bolhagen, H., May, J., and Levy, J. 1964, *Ap.J.*, 140, 778.

Carr, T.D., and Desch, M.D. 1976, in *Jupiter*, ed. T. Gehrels (Tucson: University of Arizona Press), in press.

Carr, T.D., and Gulkis, S. 1969, *Ann. Rev. Astr. and Ap.*, 7, 577.

Cavaliere, A., and Speranza, A. 1971, *Ap. Letters*, 10, 9.

Chang, D.B. 1963, *Ap.J.*, 138, 1231.

Conseil, L. 1972, Ph.D. thesis, Universite de Paris, Paris, France.

Desch, M.D. 1972, 26.3 MHz array reference manual, unpublished.

_____. 1976, manuscript in preparation.

_____, and Carr, T.D. 1974, *Ap.J. (Letters)*, 194, L57.

_____, and Levy, J. 1975, *Icarus*, 25, 12.

Divine, N., Beck, A.J., Haudenschild, C.A., Palluconi, F.D., and Schiffer, R.A. 1971, NASA-GSFC Report, SP-8069.

Dixon, R.S. 1970, *Ap.J. Suppl.*, 20, No. 180.

Douglas, J.N. 1961, Ph.D. thesis, Yale University, New Haven, Connecticut.

_____. 1964, *IEEE Trans Mil. Elec.*, MIL8, 173.

Douglas, J.N., and Smith, H.J. 1967, *Ap.J.*, 148, 885.

Dulk, G.A. 1965, Ph.D. thesis, University of Colorado, Boulder, Colorado.

_____. 1967, *Icarus*, 7, 173.

_____. 1970, *Ap.J.*, 159, 671.

_____, and Clark, T.A. 1966, *Ap.J.*, 145, 945.

Duncan, R.A. 1966, *Planet. Space Sci.*, 14, 1291.

Dungey, J.W. 1961, *Phys. Rev. Letters*, 6, 47.

Ellis, G.R.A. 1974, *Proc. Astr. Soc. Australia*, 2, 1.

Erickson, W.C., and Cronyn, W.M. 1965, 142, 1156.

Fainberg, J., and Stone, R.G. 1974, *Space Sci. Rev.*, 16, 145.

Fillius, R.W., McIlwain, C.E., and Mogro-Campero, A. 1975, *Science*, 188, 465.

Fjeldbo, G., Kliore, A., Seidel, B., Sweetnam, D., and Cain, D. 1975, *Astr. and Ap.*, 39, 91.

Flagg, R.S., Krausche, D.S., and Lebo, G.R. 1976, *Icarus*, in press.

Frank, L.A., Ackerson, K.L., Wolfe, J.H., and Mihalov, J.D. 1975, University of Iowa Report 75-5.

Goertz, C.K. 1973*a*, *Planet. Space Sci.*, 21, 1389.

_____. 1973*b*, *Planet. Space Sci.*, 21, 1431.

_____, and Haschick, A. 1972, *Nature*, 235, 91.

Goldreich, P., and Lynden-Bell, D. 1969, *Ap.J.*, 156, 59.

Goldstein, M.L., and Eviatar, A. 1972, *Ap.J.*, 175, 275.

Grigoreva, V.P., and Slysh, V.I. 1970, *Kosm. Issled.*, 8, 284.

Groth, M.J., and Dowden, R.L. 1975, *Nature*, 255, 382.

Guidice, D.A. 1966, *Nature*, 211, 57.

Guidice, D.A., and Castelli, J.P. 1968, AFCRL Report 68-0231.

Gulkis, S., and Carr, T.D. 1966, *Science,* 154, 257.

Gurnett, D.A. 1974, *J. Geophys. Res.,* 79, 4227.

Helliwell, R.A. 1965, *Whistlers and Related Ionospheric Phenomena* (Stanford: Stanford University Press).

Houghton, M.J. 1975, *Planet. Space Sci.,* 23, 409.

Hey, J.S. 1946, *Nature,* 157, 47.

Kaiser, M.L., and Alexander, J.K. 1972, *Ap. Letters,* 12, 215.

Kaiser, M.L., and Stone, R.G. 1975, *Science,* 189, 285.

Kennedy, D.J. 1969, Ph.D. thesis, University of Florida, Gainesville, Florida.

Kliore, A., Cain, D.L., Fjeldbo, G., Seidel, B.L., and Rasool, S.I. 1974, *Science,* 183, 323.

Kraus, J.D. 1950, *Antennas* (New York: McGraw-Hill).

_____. 1966, *Radio Astronomy* (New York: McGraw-Hill).

Krausche, D.S. 1975, Ph.D. thesis, University of Florida, Gainesville, Florida.

_____, Flagg, R.S., Lebo, G.R., and Smith, A.G. 1976, *Icarus,* in press.

Leacock, R.J. 1971, Ph.D. thesis, University of Florida, Gainesville, Florida.

Lebo, G.R. 1964, Ph.D. thesis, University of Florida, Gainesville, Florida.

Lecacheux, A. 1974, *Astr. and Ap.,* 37, 301.

Lodge, O. 1894, in *Electrician* (London), 4.

Lynch, M.A. 1972, Ph.D. thesis, University of Florida, Gainesville, Florida.

_____, Carr, T.D., and May, J. 1976, *Ap. J.,* in press.

McCulloch, P.M. 1971, *Planet. Space Sci.,* 19, 1297.

_____, and Ellis, G.R.A. 1966, *Planet. Space Sci.,* 14, 347.

McDonough, T.R. 1975, *Icarus*, 24, 400.

Maeda, K. 1975, NASA-GSFC Report, X-602-75-121.

Mead, G.D. 1974, *J. Geophys. Res.*, 79, 3514.

_____, and Hess, W.N. 1973, *J. Geophys. Res.*, 78, 2793.

Melrose, D.B. 1976, *Ap.J.*, in press.

Miller, H.R., and Smith, A.G. 1973, *Ap.J.*, 186, 687.

Miller, S.L. 1953, *Science*, 117, 528.

Neugebauer, M., and Snyder, C.W. 1962, *Science*, 138, 1095.

Register, H.I. 1968, Ph.D. thesis, University of Florida, Gainesville, Florida.

Riihimaa, J.J. 1970, *Astr. and Ap.*, 4, 180.

Roberts, J.A. 1965, *Radio Sci.*, 69D, 1543.

Roger, R.S., Costain, C.H., and Lacey, J.D. 1969, *A.J.*, 74, 366.

Sayre, E.P. 1974, AVCO-Systems Report, AVSD-0144-74-CR.

Shain, C.A. 1958, *Australian J. Phys.*, 11, 517.

Slysh, V.I. 1966, *Kosm. Issled.*, 6, 923.

Smith, E.J., Davis, L., Jones, D.E., Coleman, P.J., Colburn, D.S., Dyal, P., and Sonett, C.P. 1975, *Science*, 188, 451.

Smith, R.A. 1973, Ph.D. thesis, University of Maryland, College Park, Maryland.

_____. 1976, in *Jupiter*, ed. T. Gehrels (Tucson: University of Arizona Press), in press.

_____, and Wu, C.S. 1974, *Ap.J. (Letters)*, 190, L91.

Stone, R.G., Alexander, J.K., and Erickson, W.C. 1964, *Ap.J.*, 140, 374.

Thieman, J.R., Smith, A.G., and May, J. 1975, *Ap. Letters*, 16, 83.

Trainor, J.H., McDonald, F.B., Stilwell, D.E., Teegarden, B.J., and Weber, W.R. 1975, *Science,* 188, 462.

Trapp, B. 1971, Master's thesis, University of Florida, Gainesville, Florida

Van Allen, J.A., Ludwig, G.H., Ray, E.C., and McIlwain, C.E. 1958, *Jet Propulsion,* 28, 588.

Van Allen, J.A., Randall, B.A., Baker, D.N., Goertz, C.K., Sentman, D.D., Thomsen, M.F., and Flindt, H.R. 1975, *Science,* 188, 459.

Viner, M.R. 1975, Ph.D. thesis, University of Maryland, College Park, Maryland.

Warwick, J.W. 1963, *Ap.J.,* 137, 41.

_____. 1967, *Space Sci. Rev.,* 6, 841.

_____. 1970, NASA Contractor Report, CR-1685.

Weber, R.R., Alexander, J.K., and Stone, R.G. 1971, *Radio Sci.,* 6, 1085.

Weber, R.R., and Stone, R.G. 1970, *Nature,* 227, 591.

Wilson, R.G., Warwick, J.W., and Libby, W.F. 1968, *Nature,* 220, 1215.

Wu, C.S. 1973, *Ap.J.,* 186, 313.

BIOGRAPHICAL SKETCH

MICHAEL D. DESCH was born the oldest of six children on May 28, 1947, in Newark, New Jersey. He studied physics at Providence College, Providence, Rhode Island; the degree of Bachelor of Science was conferred Magna Cum Laude in June, 1969.

He began his graduate studies at the University of Florida, participating in various aspects of the radio astronomy program. His first few years were spent in the construction and testing of a 640-element dipole array while satisfying basic course requirements. This preliminary work led to an interest in and successful completion of a study involving the sporadic Jovian emission. The degree of Doctor of Philosophy was awarded by the University of Florida in August, 1976.

I certify that I have read this study and that in my opinion it conforms to acceptable standards of scholarly presentation and is fully adequate, in scope and quality, as a dissertation for the degree of Doctor of Philosophy.

Thomas D. Carr, Chairman
Professor of Physics
and Astronomy

I certify that I have read this study and that in my opinion it conforms to acceptable standards of scholarly presentation and is fully adequate, in scope and quality, as a dissertation for the degree of Doctor of Philosophy.

Alex G. Smith
Professor of Physics
and Astronomy

I certify that I have read this study and that in my opinion it conforms to acceptable standards of scholarly presentation and is fully adequate, in scope and quality, as a dissertation for the degree of Doctor of Philosophy.

Kwan-Yu Chen
Associate Professor of
Astronomy and Physical Sciences

I certify that I have read this study and that in my opinion it conforms to acceptable standards of scholarly presentation and is fully adequate, in scope and quality, as a dissertation for the degree of Doctor of Philosophy.

George R. Lebo
Assistant Professor of Astronomy

I certify that I have read this study and that in my opinion it conforms to acceptable standards of scholarly presentation and is fully adequate, in scope and quality, as a dissertation for the degree of Doctor of Philosophy.

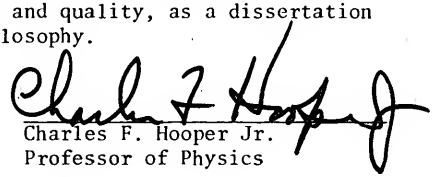

Charles F. Hooper Jr.
Professor of Physics

This dissertation was submitted to the Department of Physics and Astronomy in the College of Arts and Sciences and to the Graduate Council, and was accepted as partial fulfillment of the requirements for the degree of Doctor of Philosophy.

August, 1976

Harry H. Sisler, Dean
Graduate School